Hybrid Propelled Access to Space

Feasibility Study on a Hybrid Propulsion Concept for the Mk-III Spaceplane

Michiel Peeters

Delft University of Technology

TU Delft

Hybrid Propelled Access to Space

Feasibility Study on a Hybrid Propulsion Concept for the Mk-III Spaceplane

by

Michiel Peeters

to obtain the degree of Master of Science
at the Delft University of Technology,
to be defended publicly on Monday September 18, 2023 at 14:00.

Student number:	4824504	
Project duration:	March 13, 2023 – , September 18, 2023	
Thesis committee:	Dr. E. J. O. Schrama,	TU Delft, chairman
	Ir. M. C. Naeije,	TU Delft, supervisor
	Ir. B. T. C. Zandbergen,	TU Delft
	Ir. B. Oving,	Dawn Aerospace

An electronic version of this thesis is available at `http://repository.tudelft.nl/`.

Cover photo taken from an artist impression of Dawn Aerospace's Mk-II Aurora in-flight. [1]

[1] Artist impression of the Mk-II Aurora by Dawn Aerospace, `https://news.satnews.com/2020/12/08/suborbital-spaceplane-flight-okd-for-dawn-aerospace/`, (accessed March 15, 2023)

TU Delft

Preface

A little over five years ago I could barely imagine graduating and truth be told, I still barely can. It has been an incredible journey that went by way too fast, meeting numerous fantastic people and developing myself into a soon-to-be, competent engineer and a better person overall.

This thesis, which I started in March, I consider the pinnacle of my educational career in terms of the knowledge I gained, the work I put in and how it sparked my interest. I am incredibly grateful to Dawn Aerospace and especially Bertil and Philip for allowing me to do my thesis on such an interesting and relevant topic as the Mk-III.

As with all projects, things don't always go your way and you face difficulties and setbacks, however, my daily supervisor Marc Naeije always remained positive and believed in me, which boosted my mood after every single weekly meeting. A big thank you for this and for all of the feedback and advice you gave me, it has been a pleasure working as your thesis student. Also, from the university, I would like to thank Dominic Dirkx for his help when I was stuck with Tudat. As many students have said before me, I don't understand how you can help people so quickly and so well.

As I mentioned, I have met some incredible people during my studies here in Delft, especially those from Moeder Delftsche, they have brightened up my days in Delft so much. In particular Fabien, we started this adventure together, I am extremely happy I have gotten to know you this well, you were a fantastic study partner, DSE teammate and friend in general. Also a special mention for Niels, Oscar, Brecht, Arnaud, and Kasper, thanks for all the great memories in Delft!

I can't not mention the friends back home with whom I kept meeting up and made my life that much more fun, even though we studied in different cities and countries. Especially Lucas and Gilles, both of you have been there during the best periods of my life and have gotten me through the most difficult ones. I will always be thankful for being able to consider you among my best friends.

Finally, I would like to express my gratitude to my family. The support that my parents have given me over the past five years has been incredible, also financially. I can not say enough how thankful I am for the opportunities I have been given, and I hope that by completing this degree I have made them proud and taken my first step in repaying them for their unconditional support. Stientje, my little sister, I know it has not always been easy dealing with me teasing you all the time or doing my chores when I was at the end of my thesis. I am extremely lucky to have you as my sister, I could not have wished for a better one.

Michiel Peeters
Delft, September 2023

Summary

In an attempt to make access to space cheaper, easier and more sustainable, innovative launch systems are being developed by numerous enterprises. One of those companies is Dawn Aerospace, which is developing a semi-reusable, two-stage-to-orbit launch vehicle capable of horizontal take-off and landing at the same location. As with all present launch vehicles, the current design relies on rocket propulsion to propel both stages, however, in an endeavour to improve the performance even further, the usage of airbreathing engines on the first stage was suggested. The reason why airbreathing engines could improve the vehicle's performance is that they are first of all, more fuel efficient than rocket engines, having a higher specific impulse and secondly, they utilise oxidizer from the incoming airflow instead of carrying it onboard. Such a concept, however, has never seen flight and the feasibility of an airbreathing Mk-III design had to be studied to determine whether or not to invest further in this idea. This resulted in a research question to which the answer determines if this concept is worth studying further and is formulated as: *Would it be feasible to integrate airbreathing propulsion in the Dawn Mk-III, aiming to decrease the gross take-off mass whilst fulfilling the mission requirements?*

The first step towards providing a definite answer to the research question was identifying which airbreathing engine types exist, eliminating the obviously infeasible ones and analysing the remaining candidates further. Those were: turbine engines, ramjets, scramjets, dual-mode ramjets, turbine-based combined cycle engines and rocket-based combined cycle engines. To select the best one, an analytical hierarchy process was used to trade off the candidates according to four trade-off criteria: thrust-over-weight-ratio, specific impulse, technology readiness level and operational range. Herefrom, ramjet engines were deemed to provide the most potential for a feasible design, followed by turbine engines. These first two engine types were selected and a ramjet and turbine engine concept were designed. Three parts made up the design process, creating a vehicle mode, building a trajectory model with adequate guidance and integrating these two in an optimisation tool. The vehicle model was divided into the upper stage which has a conventional rocket configuration, without a fairing, and the first stage which is a scaled version of the Mk-II, carrying the upper stage inside. Both stages consist of a rocket propulsion, mass and geometry model. On top of that, the first stage also includes an airbreathing engine and aerodynamic model, the latter based on the aerodynamic coefficients of the Mk-II. For the trajectory model, the first and upper stages were also split, both guided by control nodes along the trajectory, implying desired flight path angles on the vehicles. The optimisation tool then attempted to find vehicle and trajectory designs that were able to meet all mission requirements whilst minimising the gross take-off weight through a differential evolution algorithm.
A baseline design was first established to serve as a reference and resulted in a first stage vehicle weighing 41571 kg, measuring 24.25 m in length and an upper stage weighing 6675 kg, measuring 5.84 m in length. After optimisation, the ramjet concept did not result in any feasible designs within the imposed constraints, the main cause being the disability to accelerate sufficiently during ramjet operation. However, when releasing the constraint put on the maximum allowable ramjet inlet area to half the fuselage cross-sectional area, which is noted as questionable, this changed and a feasible design was found that met all requirements. The resulting vehicle weighed 39242 kg, saving 5.6% in total mass compared to the baseline, although the dry mass had increased by 307 kg. The turbine engine concept suffered from the same problem as it was not able to accelerate sufficiently during the airbreathing phase, this was due to a lack of thrust of the selected engines and the increase in dry mass of nearly 40%. If a design was made to meet all requirements, it would weigh more than 55 tonnes, eliminating any benefit this concept could have had. A much lighter and more powerful turbine engine would have to be developed for this concept to come anywhere close to the baseline design performance.

The results of the optimised designs showed that within reasonable constraints and for the made assumptions, it is not feasible to integrate airbreathing engines on the Mk-III, nor for ramjets nor for turbine engines. Nevertheless, the potential of a ramjet concept was undeniable. If for an improved geometry, the aerodynamic drag of the vehicle could be decreased and less thrust would be required from the ramjets such that they can be reduced in size, the concept would definitely be able to reduce the gross take-off mass of the Mk-III compared to a fully rocket-powered version.

Nomenclature

Physical constants

Symbol	Definition	Value
g_0	Gravitational acceleration at sea level	9.81 [m/s^2]
$R*$	Universal gas constant	8.314 [$Jmol^{-1}K^{-1}$]
G	Universal gravitational constant	$6.67408 \cdot 10^{-11} [m^3 kg^{-1} s^{-2}]$

Abbreviations

Abbreviation	Definition
AHP	Analytical Hierarchy Process
CEA	Chemical Equilibrium Applications
EPS	Electrical Power System
ESA	European Space Agency
HASA	Hypersonic Aerospace Sizing Analysis
LEO	Low-Earth Orbit
LOX	Liquid Oxygen
MEOP	Maximum Expected Operating Pressure
mf	Modifying Factor
Mk-III	Mark-III
NASA	National Aeronautics and Space Administration
O/F	Oxidiser-over-Fuel ratio
RBCC	Rocket-Based Combined Cycle
RPA	Rocket Propulsion Analysis
RTLS	Return To Launch Site
SABRE	Synergetic Air-Breathing Rocket Engine
SO	Sub-Objective
SQ	Sub-Question
TBCC	Turbine-Based Combined Cycle
TPS	Thermal Protection System
TRE	Turbo-Ramjet-Engine
TRL	Technology readiness level
Tudat	Technical University Delft Astrodynamical Toolbox
T/W	Thrust-over-Weight ratio
ULF	Ultimate Load Factor
USD	United States Dollar

Symbols

Roman symbol	Definition	Unit
A	Area	[m^2]
a	Speed of sound	[m/s]
b_{span}	Span width	[m]
C	Coefficient	[-]
C_D	Drag coefficient	[-]
C_F	Thrust coefficient	[-]
C_L	Lift coefficient	[-]
C_P	Pressure coefficient	[-]
C_p	Specific heat at constant pressure	[J/kg K]
$c*$	Characteristic velocity	[m/s]
D	Diameter	[m]
	Drag	[N]
E_{sp}	Specific energy	[J/kg]
e	Eccentricity	[-]
F_t	Thrust force	[N]
f	fuel-to-air ratio	[-]
h	Altitude	[m]
I_{sp}	Specific impulse	[s]
K_c	Control gain factor	[-]
K_t	Tank mass correction factor	[-]
L	Lift force	[N]
l	Length	[m]
M	Mach number	[-]
M_m	Mean molar mass	[kg/mol]
m	Mass	[kg]
$\dot{m}$	Mass flow	[kg/s]
N_{eng}	Number of engines	[-]
n_{ult}	Ultimate load factor	[-]
p	Pressure	[Pa]
Q	Dynamic pressure	[Pa]
Q_R	Fuel heat of combustion	[J/kg]
q	Vehicle mass rate [kg/s]	
$\dot{q}$	Heat flux	[W$/$m^2]
R	Reynolds number	[-]
r	Distance from the Earth's centre of mass	[-]
	Total pressure ratio	[-]
S	Surface area	[m^2]
T	Temperature	[K]
t	Thickness	[m]
	Time	[s]
t/c	Thickness-over-chord ratio	[-]
U_{eq}	Equivalent exit velocity	[m/s]
u_e	Exit velocity	[m/s]
V	Velocity	[m^3]
	Volume	[m/s]
v	Velocity	[m/s]
W	Weight	[lbs]
W_a	Engine airflow	[lbs/s]

Greek symbol	Definition	Unit
α	Angle of attack	[deg]
α_T	Thermal accommodation coefficient	[-]
Γ	Vandenkerckhove function	[-]
γ	Specific heat ratio	[-]
	Flight path angle	[deg]
ΔV	Velocity increment	[m/s]
δ	Latitude	[deg]
ζ	Quality factor	[-]
η_r	Inlet ram recovery factor	[-]
η_c	Combustion efficiency	[-]
Λ	Sweep angle	[deg]
λ	Taper ratio	[-]
μ	Bank angle	[deg]
	Earth's gravitational parameter	[m^3/s^{-2}]
	Runway friction coefficient	[-]
ρ	Density	[kg/m^3]
σ	Stress	[Pa]
τ	Longitude	[deg]
ϕ	Installed engine loss coefficient	[-]
χ	Heading angle	[deg]

List of Figures

List of Tables

Contents

1

Introduction

Today's space industry and the commercialisation thereof aim to make space cheaper, more accessible and sustainable for the better of mankind. A crucial element in this is reaching space which involves launch vehicles which have always been one of the most cost-intensive mission segments. Numerous enterprises are active on this front, all having their vision of how to achieve a low-cost, accessible and sustainable launch system. One of these companies is Dawn Aerospace, located in the Netherlands and New Zealand which is currently developing an innovative launch system of its own that is intended to achieve the goals mentioned above. Their vision is to reduce costs and increase accessibility to space whilst improving sustainability by creating a semi-reusable launch vehicle capable of horizontal take-off and landing on conventional runways, using green propellants. This vehicle is called the Dawn Aerospace Mk-III and uses two stages, the first one being a spaceplane configuration, carrying an upper stage towards the required separation conditions, whereafter it performs a return manoeuvre and returns to the launch site. The upper stage, after separation, continues its trajectory to deliver the onboard payload which will be small satellites, in their target orbit. An intermediate phase in the development process has been the development of a sub-orbital vehicle, the Mk-II, illustrated in Figure 1.1. This vehicle has already seen multiple successful flights and is considered the first stage demonstrator of the Mk-III.

Figure 1.1: Dawn Mk-II Aurora in-flight [21].

The current version of the Mk-III, like most launch vehicles, relies on rocket propulsion to propel both stages, however, rocket engines are known for not being the most efficient engines available. In an attempt to improve the performance of the Mk-III, the idea was put forward to use a hybrid propulsion concept in the first stage by integrating airbreathing engines. These engines have much higher efficiencies than rocket engines, burning less fuel and not requiring any oxidiser to be taken on board because the oxygen in the air is used for that purpose. This saving in required oxidizer and fuel mass could lead to a reduced total vehicle mass. To explore this route of hybrid propulsion, a feasibility study is required to find out if it is worth investigating further, as

currently there has never been a vehicle made with the same characteristics. This feasibility study will be the main subject of this thesis and will aim to find out how much a hybrid concept would improve the performance of the Mk-III, if feasible at all, or which factors keep it from turning into reality.

1.1. Research objective and questions

From the goal of the thesis described above, a research objective can be formulated that summarises the aims of the research and guides the study in the right direction. What follows from this, is the research question and its sub-questions whose aim is to direct the research into finding the answers that are needed. Both the research objective and questions are listed below.

Research objective:
The objective of this research, is to investigate the feasibility and potentially increased performance, of an integrated air-breathing engine on the first stage of a horizontal take-off and horizontal landing, two-stage-to-orbit semi-reusable launch vehicle, more specifically the Mk-III, by selecting the best-performing air-breathing engine, creating a vehicle model and modelling the new concept in a trajectory analysis tool.

Research question
Would it be feasible to integrate airbreathing propulsion in the Dawn Mk-III, aiming to decrease the gross take-off mass whilst fulfilling the mission requirements?

- **SQ 1:** *What is the best type of airbreathing concept considering the requirements of the Mk-III?*
- **SQ 2:** *Can airbreathing propulsion be integrated into the Mk-III whilst meeting the original mission requirements?*
- **SQ 3:** *Will an airbreathing concept reduce the Mk-III take-off mass?*

1.2. Report outline

Within this report, one will find an attempt to answer the sub- and main research questions, starting in chapter 2 where firstly the available airbreathing engine types are identified, investigated and traded-off to one another through an analytical hierarchy process. This trade-off method provides the two best-performing airbreathing engines, considering the Mk-III mission requirements and both are proceeded with for further analysis. Once all results are obtained, the sensitivity of this trade-off is also analysed.

Having selected the best-performing airbreathing engine, a vehicle model is created in chapter 3 and includes a propulsion, geometry and mass model for the first and upper stages, whereas an aerodynamic model is only relevant for the first stage model. All of these disciplines come together and interact within the vehicle model. The propulsion model is further broken down into the rocket engine model, based on ideal rocket theory and the selected airbreathing engine models. Each of the models is validated independently by using data from reference engines and vehicles.

The created vehicle will follow a trajectory that is guided by a guidance law formulated for the first and upper stage mission segments. Those mission or trajectory segments are discussed in chapter 4 where for every segment the equations of motion which describe the vehicle's motion, are discussed, as well as how the guidance laws are implemented. In addition, it is explained how the airbreathing phases are incorporated in the first stage trajectory. To validate the trajectory model, a reference study is taken with a similar mission profile to that of the Mk-III, which included well documented vehicle and trajectory designs. This reference study is used as input for the trajectory model and the outcomes are then compared to the results found in the reference study.

In chapter 5 the tools are described to numerically model both the vehicle and trajectory models with an emphasis on the latter. Here the TU Delft Astrodynamic Toolbox is introduced in which the modelling is done, as well as the selected propagation and integration methods. Thereafter, the selected optimisation method used to optimise the trajectory and vehicle design, is presented alongside the principles behind it. Finally, the specific optimisation problems of all concepts are discussed.

Up until chapter 5 all of the building blocks have been presented, after connecting those, the actual results are generated which are presented in chapter 6 where first a baseline design, using rocket propulsion only is

established. From this baseline design the results of the two airbreathing concepts are discussed and compared to the baseline. This chapter is concluded by a summarising section on all of the findings and drawn conclusions which serves as the basis for answering the research questions introduced above.

As an additional form of validation, a sensitivity analysis is conducted in chapter 7, in the form of a on-at-a-time approach, where single design variables are varied and the impacts on the trajectory results are analysed.

Finally, the thesis is concluded by briefly recapping what has been done during the research, before formulating an answer to each research sub-question. Those sub-questions are combined and used to provide a definitive answer to the primary research question. A final section presents recommendations for further studies conducted on this topic, where improvements could be made or what would be interesting to investigate further.

2

Propulsion Concept Selection

Numerous airbreathing engine types have been developed or are under development, each serving their own purpose with their characteristics. From these, it is essential to select the most suited type of engine given the Mk-III requirements and mission profile, whilst taking into account the preferences of Dawn Aerospace. This will be achieved through a trade-off where the performances of concepts are scored with respect to a set of criteria. The overall concept scores are then compared to end up with a winning concept, being the most suited engine for this application. The selection process starts by identifying and defining the candidates, as well as the trade-off criteria. Consequentially, the performance of the concepts regarding those criteria is determined. Hereafter, the preferred trade-off method and tool is introduced, which is used to determine the relative weighting of the criteria, score the concept performance, select a winning concept and perform a sensitivity analysis on the weighting factors.

2.1. Propulsion concepts

The concepts considered for use on the Mk-III, are based on the literature research done by Peeters [30], which already eliminated the obviously unsuitable candidates being turboprop, turbofan and pulse detonation engines. Turboprops were immediately eliminated because of their limited performance at higher velocities and pulse detonation engines because of their limited development. The concepts which will be taken further in the trade-off are described below.

- **Turbine engine** operating from take-off until a velocity is reached at which its performance in terms of thrust production and specific impulse has degraded until rocket propulsion is preferred and the rocket engine is turned on, which propels the first stage further until separation. Both a turbojet and a low-bypass turbofan are considered, a high-bypass turbofan would add too much mass.
- **Ramjet** operation after the vehicle has been accelerated by the rocket engine to a velocity at which meaningful thrust can be produced by the ramjet until a velocity is reached at which the ramjet performance deteriorates and the rocket engine takes over again.
- **Scramjet** operation after the vehicle has been accelerated by the rocket engine to a velocity at which meaningful thrust can be produced by the scramjet until a velocity is reached at which the scramjet performance deteriorates and the rocket engine takes over.
- **Dual-mode ramjet** operation, after the vehicle has been accelerated by the rocket engine to a velocity at which meaningful thrust can be produced by the ramjet until a velocity is reached at which the scramjet provides increased performance. Then, the scramjet is operated until its performance deteriorates and the rocket engine takes over again.
- **TBCC TRE engine** operation from take-off, where the turbine engine segment initially accelerates the vehicle to sufficient velocities for the ramjet to take over. Once the ramjet's performance has deteriorated due to increased velocity and decreased air density, the rocket engine takes over and accelerates the vehicle to separation conditions.
- **RBCC engine** operation from take-off, all the way to separation, meaning that the rocket engines currently envisioned for the Mk-III would not be needed and the first stage is fully propelled by the RBCC engine phases: ejector jet, ramjet, scramjet and rocket engine.

2.2. Trade-off criteria

Essential when determining what ”the best” concept is, are the trade-off criteria, these criteria determine what is considered ”the best” and are arguably the most important in a trade-off. In consultation with Dawn Aerospace, four trade-off criteria were determined in order to end up with the best possible engine for use on the Mk-III first stage, with the resources available at the company. The four criteria, with a rationale for why these criteria were chosen, are given below.

- **Technology readiness level** represents how mature a technology is and can be quantified by a TRL score of 1 to 9. This criteria embodies both the development time and cost, it would take to develop a working, proven and validated system, therefore it was decided not to include a separate criterion on cost or time because it would be heavily connected to the TRL and the trade-off could become skewed.
- **Specific impulse** indicates how efficiently, the engine concept is able to transfer propellant mass into thrust to accelerate the vehicle. A high specific impulse, over a wide range of operations is desired.
- **Range of operations** is the velocity (and altitude) range along which the engine concept is able to produce meaningful thrust and not have a specific impulse decrease below that of a liquid rocket engine.
- **Thrust-over-weight ratio** is the maximum thrust produced by the engine divided by its weight. A high T/W would mean that an engine is able to provide a lot of thrust whilst not leading to a high mass penalty, which is obviously preferred. Note that all of the engine concepts mentioned above are able to provide high levels of thrust, sufficient for horizontal take-off, hence, thrust in itself is not taken as a criterion.

2.3. Concept performance

2.3.1. Technology readiness level

The performance of the defined concepts in terms of technology readiness level is determined by simply taking the TRL scale as presented by ESA [36], who define levels from 1 to 9 as shown in Figure 2.1. Each of the concepts is given a level, based on the gathered literature in [30] on what has been developed in the past, which engines have seen successful flight and which are operated on a regular basis. The first concept, a turbine engine has a TRL of 9, as it has seen successful operations during several decades and can be considered as flight proven during numerous successful missions. Ramjets, although simpler in theory than turbines, have not seen as many successful flights as turbines and are not commonly used on aircraft, whereas they are often used on missiles. Nevertheless, ramjet-powered vehicles have operated successfully in the past but require some final developments which is why they are awarded a TRL of 8. Scramjets are the more advanced version of ramjets, they have powered experimental vehicles such as the X43-A and the X51 successfully for 10s of seconds, but not for larger amounts of time, still requiring development progress to be made, hence, they have a TRL of 7. Dual-mode engines which combine ramjet and scramjet operations, have never flown, both the ram and scram segments have been flight proven before but not together in one engine, therefore a TRL of 5 is given. The TBCC concept also exists of two already existing engine types, but contrary to the dual-mode engine, a TBCC engine has been flown in the form of the P&W J58 engine which operated like a TBCC as discussed in [30]. In addition, the technologies required for this engine, are less advanced than those needed when a scramjet is involved, hence a TRL of 7 is given. Finally, RBCC engines, similar to dual-mode engines, have separately proven phases of operations, but have never been put into one engine. The most developed RBCC engine, the SABRE engine discussed in the preceding literature study [30], currently has a TRL level of 5 according to a progress report [41]. This value will be the TRL given to the RBCC engine concept in general.

2.3.2. Range of operations

The range of operations of all types of engine concepts is based on the literature collected on them in the preceding literature study to this report [30]. State-of-the-art turbine engines are currently able to achieve a maximum operation velocity of Mach 2.4, although some literature even suggests a velocity of Mach 3. To be conservative, an operating range between stand still and Mach 2.4 is taken for turbine engines. Ramjets on the other hand, cannot produce thrust from standstill, they require an initial velocity of around Mach 0.5 to start producing any meaningful thrust, maximum efficiency however, is only achieved between Mach 3 and Mach 6, after which performance starts to decrease. Using the same operating principles as ramjets but with supersonic combustion, scramjets start operating from around Mach 5 up until Mach numbers above 15. In theory, at least, the maximum velocity at which it has operated until now is Mach 9.5. A dual-mode ramjet would combine both ramjet and scramjet operations, achieving a range of operation between Mach 0.5 to

ISO Technology Readiness Level Summary	
TRL	**Level Description**
1	Basic principles observed and reported
2	Technology concept and/or application formulated
3	Analytical and experimental critical function and/or characteristic proof-of-concept
4	Component and/or breadboard functional verification in laboratory environment
5	Component and/or breadboard critical function verification in relevant environment
6	Model demonstrating the critical functions of the element in a relevant environment
7	Model demonstrating the element performance for the operational environment
8	Actual system completed and accepted for flight ("flight qualified")
9	Actual system "flight proven" through successful mission operations

Figure 2.1: Technology readiness levels explained as defined by ESA [36].

above 15. The TBCC or turbo-ramjet engine combines a turbine engine and ramjet operation, meaning that it can start operating, efficiently, from a standstill up to Mach 6. Lastly, since RBCC engines use rocket propulsion, it is able to operate from a standstill up to extremely high Mach numbers, even beyond those of scramjets.

It is also important to know what the expected maximum velocity at which the first stage is expected to fly will be, such that it can be evaluated which engine type best covers the velocity profile of the first stage. After some discussions with Dawn Aerospace and researching the literature of other two-stage-to-orbit launch vehicles, it is assumed that the first stage shall operate from a standstill to a maximum velocity of around Mach 6, at which staging shall occur. Ideally, the selected engine is able to cover as much of this velocity range as possible, at high efficiency.

2.3.3. Specific impulse

The specific impulse of the concepts are obtained from the graph shown in Figure 2.2, where an average is taken along the applicable range of operations of each engine type. For engine concepts with multiple combined types, a weighted average is taken of the separate engine types, taking into account the expected velocity range during which each type shall be active. Turbine engines are estimated to have an I_{sp} between 1700 s and 3700 s at Mach 0 and between 1500 s and 2700 s at Mach 2.4. Taking the average of both ranges and then taking the average of those two values gives an average I_{sp} of around 2400 s along its entire operating range. Ramjets have a smaller I_{sp} compared to turbine engines, between 1100 s and 1900 s, an average is taken of 1500 s. Scramjets have an I_{sp} of 1000 s on average. Arriving at the combined engine types, the dual-mode ramjet engine has a weighted average I_{sp} of 1409.09 s accounting for ramjet operation from Mach 0.5 until Mach 5, followed by scramjet operation from Mach 5 until Mach 6. The specific impulse of the TBCC engine is computed by taking the weighted average of the turbine engine I_{sp} from Mach 0 to Mach 2.4 and the ramjet I_{sp} from Mach 2.4 until Mach 6 which results in an I_{sp} of 1860 s. Finally, the RBCC engine is assumed to operate in ejector mode from a standstill until Mach 1, when transitions to ramjet mode until Mach 5, after which it transitions into scramjet mode until Mach 6. Assuming an ejector rocket I_{sp} of 350 s, this gives an average specific impulse of 1225 s.

2.3.4. Thrust-over-weight ratio

Turbine engines commonly have a T/W in the range of 6 to 8, with multiple sources providing a value in between this range. The P&W F119 low-bypass turbine engine has a reported T/W of 7.95, Mehta and Bowles provide a T/W of 6.65 whereas Lord, Macmartin and Tillman provide the most recent trend that shows T/W values between 7 and 8 [28][24][47]. Thrust-over-weight ratios of the other engine types are not as easily obtained, and values differ a lot based on the source in literature, therefore an average is taken from reported values. Ramjets are characterised by a high T/W of 15 and above [14], in order to remain conservative, a value of 15

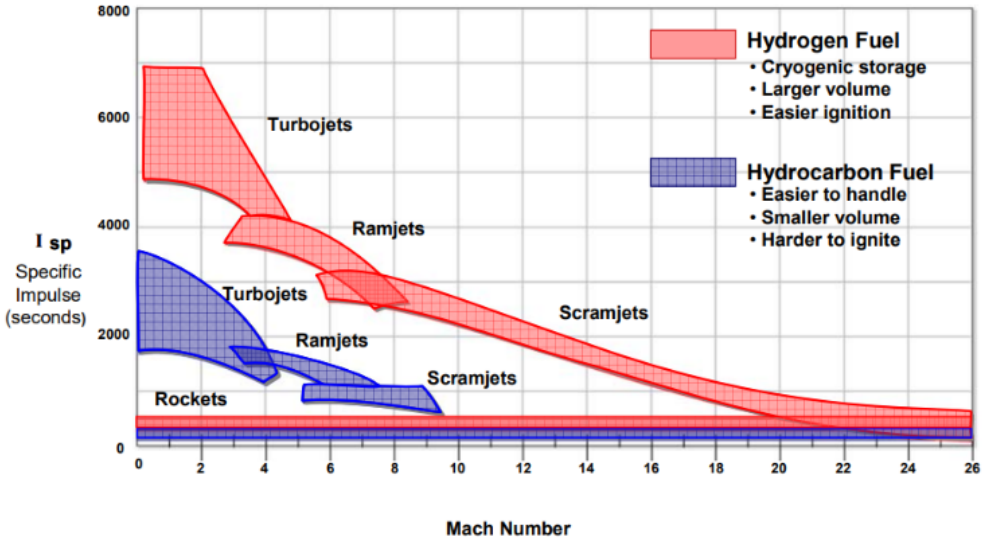

Figure 2.2: Comparison of engine performance in terms of the specific impulse for a range of Mach numbers [25].

Table 2.1: Engine concept performance metrics

	turbine engines	Ramjets	Scramjets	Dual-mode	TBCC	RBCC
TRL	9	9	7	5	7	5
I_{sp}	2400 s	1500 s	1000 s	1409 s	1860 s	1250 s
Operation range overlap	40%	91.67%	16.67%	91.67%	100%	100%
T/W	7	15	4	9.5	6	22

shall be assumed as the minimum value. Scramjets, produce less thrust than ramjets and are overall heavier than ramjets due to increased thermal loads. They are reported to have rather poor T/W values in the order of 2 to 5, of which an average of 3.5 is taken [31][33]. The T/W of a dual-mode ramjet is assumed to be equal to the average T/W of a ramjet and scramjet combined, as no literature could be found on this. TBCC's on the other hand, have more literature available on their estimated T/W values. The most common T/W ratios found, were in between 4 and 5, although obtained from papers in the 60's and 90's [43][40]. A more recent study conducted in 2005, found an installed T/W value of 6, although it is believed that this number has increased by now, no literature could be found to confirm this. Therefore, a T/W of 6 will be taken for the TBCC concept. For RBCC's the expected T/W seems to be much higher, mainly due to the rocket-powered phases included in the engine operations. Bradford, Olds and Wallace present a wide range of expected T/W values from 10 to 35 [9]. Bulman and Siebenhaar on the other hand give a specific expected value of 22, which happens to be in the middle of the previously given range of values and will be assumed as the T/W value for the RBCC engine concept. An overview of the performance of all concepts with respect to all criteria is provided in Table 2.1 where it should be noted that the operation range overlap is computed by dividing the range of operations of each engine type, by the maximum velocity range of the first stage discussed in Section 2.3.2, being from Mach 0 to Mach 6. For example, the range of operations of a turbine engine is from Mach 0 to Mach 2.4, which means that it can cover 40% of the entire expected flight regime.

2.4. Analytical hierarchy process

Having defined the concepts, the criteria and the concept performances with respect to those criteria, the trade-off can be done. The selected trade-off method is the AHP, which is thoroughly discussed in the literature review prior to this report [30]. For the mathematical theory and exact workings of this method, the reader is referred to that literature review. Briefly summarised, this method uses pair-wise comparisons of the importance of trade-off criteria to determine the criteria weighting and uses a pair-wise comparison of concept performance in the form of "Concept A performs X times better than concept B with respect to criteria Z", to determine the score of all concepts. An Excel-based tool was made available by Dutch Space of which a screenshot is shown in Figure 2.3, together with a user manual [4]. In Figure 2.3, the concepts are given as

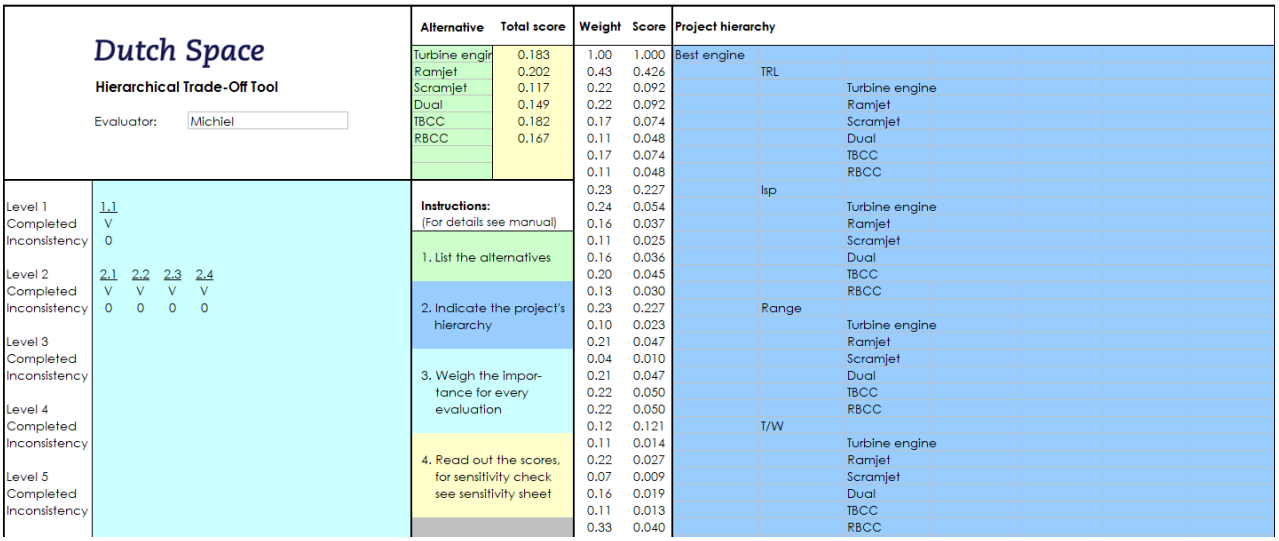

Figure 2.3: Screenshot of the AHP tool provided by Dutch Space [4].

input in the upper green column, and the project hierarchy is put in the blue right-hand side of the sheet. This project hierarchy starts at the goal of the trade-off, down to the criteria and subsequently the concepts. The light-blue segment on the left side shows the evaluation of the criteria weighting on level 1 and the evaluation of the concept performances, on level 2. A consistency between 0 and 0.1 means that the evaluation has an acceptable consistency and is done correctly.

2.4.1. Weighting of criteria

As mentioned, the criteria weighting is done by comparing criteria importance in pairs, using a subjective scale, ranging from 9 to 1 to 9 as presented in Figure 2.4. The meaning behind these scores is explained in Figure A.1 in Appendix A. The scoring is done based on a discussion with Dawn Aerospace, and logical reasoning. Dawn Aerospace clearly communicated that the TRL of the concept is the most important criterion as this is highly related to development cost and especially time, they do not want to spend ten's of millions of euros to develop a propulsion system which will be ready for its first test flight in 2030. Secondly, the range of operations is given an equal score as I_{sp} because a highly efficient engine, which is only able to operate briefly will most likely offer less mass savings than a little less efficient engine, which is able to cover the entire flight profile. Ideally, the engine should have a high specific impulse, over the entire flight profile of the first stage. Both of these criteria are considered to be slightly more important than T/W as the savings in oxidiser mass shall offset the added vehicle empty mass due to a heavier engine, and all engines considered are able to provide sufficient thrust for this flight profile and vehicle mass category. Nevertheless, T/W is still an important engine parameter which is why I_{sp} and range are only given a slight preference. TRL versus T/W is a larger difference, with TRL being strongly favoured mainly due to the input of Dawn Aerospace. The AHP tool automatically calculates the resulting weighting factors of these criteria, which are shown in the "*Weight*" column at the rows of TRL, I_{sp}, Range and T/W in the project hierarchy, being 0.43, 0.23, 0.23 and 0.12, respectively.

2.4.2. Concept comparison

The concepts are compared by taking the performance with respect to a criterion, and then dividing it by the performance of another criterion, or the other way around, such that a number equal to, or above one is obtained. Using an objective scoring scheme now, an **x** is put in the column corresponding to the value closest to the obtained number. The performance comparison sheet for the TRL level is shown in Figure 2.5. For example, the TRL of turbine engines is compared to that of RBCC engines and the TRL of turbine engines is divided by the TRL of RBCC engines, resulting in 1.8. Since 1.8 is closest to 2, an **x** is put in the column underneath 2, on the side of turbine engines. The other evaluation sheets can be found in Appendix A.

With respect to Best engine rate the importance of each pair by putting an x in the appropriate field.

Scale (S/O/C): S

Complete, Inconsistency=0

9	8	7	6	5	4	3	2	1	2	3	4	5	6	7	8	9	
T/W											x						Range
T/W											x						Isp
Range									x								Isp
T/W														x			TRL
Range											x						TRL
Isp											x						TRL

Figure 2.4: Pair-wise comparison of criteria importance.

With respect to TRL rate the importance of each pair by putting an x in the appropriate field.

Scale (S/O/C): O

Complete, Inconsistency=0

9	5	3	2	1.5	1.2	1.1	1.03	1	1.03	1.1	1.2	1.5	2	3	5	9	
RBCC												x					TBCC
RBCC								x									Dual
TBCC				x													Dual
RBCC												x					Scramjet
TBCC								x									Scramjet
Dual												x					Scramjet
RBCC													x				Ramjet
TBCC											x						Ramjet
Dual													x				Ramjet
Scramjet											x						Ramjet
RBCC													x				Turbojet
TBCC											x						Turbojet
Dual													x				Turbojet
Scramjet											x						Turbojet
Ramjet								x									Turbojet

Figure 2.5: Screenshot of the concept evaluation with respect to TRL.

Table 2.2: Trade-off results and concept ranking

Rank	Concept	Score
1	Ramjet	0.202
2	Turbine engine	0.183
3	TBCC	0.182
4	RBCC	0.167
5	Dual-mode	0.149
6	Scramjet	0.117

2.4.3. Results

The main results from the trade-off are shown in Figure 2.3, in the yellow, "*Total score*" column, where the ramjet concept receives the highest score followed by the turbine engine and TBCC concepts which have an almost identical score, an overview of the ranking is given in Table 2.2. In Figure 2.3, two columns to the right underneath "*Score*", one can see the individual scores of the concepts with respect to each criterion and identify the weak points of all concepts. It is clear that the scramjet is an unacceptable concept, mainly due to the limited velocity range it covers, as well as having the lowest specific impulse and T/W of all concepts. The dual-mode and RBCC concepts do perform not as badly as the scramjet but are still far from the top, predominantly due to their low TRL. From this trade-off, it can be concluded that the ramjet concept is the one to be investigated further and selected as a propulsion concept to use on the first Mk-III stage, showing the most potential at this point in time. However, the turbine engine concept is taken along as second best option for further analysis as well and its performance can be compared to the ramjet concept.

2.4.4. Sensitivity analysis

In addition to the trade-off itself, the AHP tool also has a dedicated sheet for performing a sensitivity analysis where weights of one or more criteria can easily be changed by entering a new weighting factor in the middle column in Figure 2.6. The new scores are indicated next tomes the yellow bar on the left side of the sheet. The sensitivity of the trade-off to the weighting factors was investigated by analysing the trade-off results for 10 different weighting combinations. Firstly, each of the four weighting factors was separately decreased to 25% of its original value, creating four cases. This was followed by doubling the four weighting factors, creating another four cases. Finally, the weighting factor of every criterion was halved and one other weighting factor was doubled separately. This created an additional 12 different cases of doubled and halved criteria. From the resulting 20 different cases, the ramjet came on top 14 times. Only when decreasing the TRL weighting to 25% of its original value, the RBCC engine was ranked first. Five times, the turbine engine was ranked first, mainly when increasing the I_{sp} weighting factor or when reducing the range of operations weighting factor to 25% of its original value. It did however fall out of the top three concepts eight times, whereas the TBCC concept only fell out twice. From this sensitivity analysis, it can be concluded that the trade-off is rather robust, and the ramjet is indeed the best concept according to these criteria. In addition, the TBCC concept is a steady performer, doing well for whichever set of weighting factors and the turbine engine concept performs the best when TRL or I_{sp} are important and the range of operations is not.

Figure 2.6: Sensitivity analysis case 1 with 25% of the original TRL weighting factor.

3

Vehicle Model

The Mk-III vehicle model consists of propulsion models for both rocket and airbreathing engines, mass and geometry models and an aerodynamic model. Each of these models shall be treated separately within this chapter but are all combined into one single vehicle model. As can be seen in Figure 3.1, the propulsion models output thrust levels, mass flows and engine sizes for both the first and upper stages. These parameters are used by the vehicle geometry and mass models to scale the first stage geometry, size the upper stage and determine the masses of both. Finally, the aerodynamic model is responsible for providing aerodynamic coefficients of the vehicle for a given Mach number and angle of attack for the first stage geometry. Each sub-model is immediately validated by comparison to data of reference engines of vehicles.

3.1. Rocket propulsion model

Modelling the rocket engines is done based on ideal rocket theory as presented by Zandbergen [6], in combination with design choices made by Dawn Aerospace and by Haex [17]. These design choices include the number of engines on both stages, the oxidiser over fuel ratio and the chamber pressure. The first step for the first stage is to find a rocket engine design which is able to produce the required amount of sea level thrust as specified by the input design variable, finding the propellant mass flow and the exit and throat areas. Then, this mass flow and engine geometry are assumed to be constant throughout the trajectory, which allows for the thrust to be computed at all atmospheric conditions. For the upper stage, only the first part is required since it is assumed that the upper stage flies in vacuum conditions and the ambient conditions do not change along the trajectory. Also note that for the first stage, the sea level thrust produced by a single engine is a design variable whereas for the upper stage, the vacuum engine thrust is defined by Dawn Aerospace at 30 kN.

Given that a combination of kerosene and hydrogen peroxide is used as propellant, the chemical chamber conditions can be computed by free software called Rocket Propulsion Analysis Lite (RPA Lite), which only requires the chamber pressure, oxidiser-over-fuel ratio (O/F) and the selected propellants. This software provides the temperature, mean molar mass and specific heat ratio in the combustion chamber assuming chemical equilibrium. These characteristics are then used to compute the characteristic velocity as defined in Equation 3.1 with the Vandenkerckhove function found through Equation 3.2 where R, M_w, T_c and γ_c are thee universal gas constant, mean molar mass, chamber temperature and specific heat ratio respectively.

$$c^* = \frac{1}{\Gamma}\sqrt{\frac{R}{M_w}T_c} \tag{3.1}$$

$$\Gamma = \sqrt{\gamma_c\left(\frac{1+\gamma_c}{2}\right)^{\frac{1+\gamma_c}{1-\gamma_c}}} \tag{3.2}$$

Using a second definition of the characteristic velocity and the fact that the propellant mass flow is a design variable, the throat area is computed as in Equation 3.3. The throat area is then used to find the thrust coefficient by solving Equation 3.4.

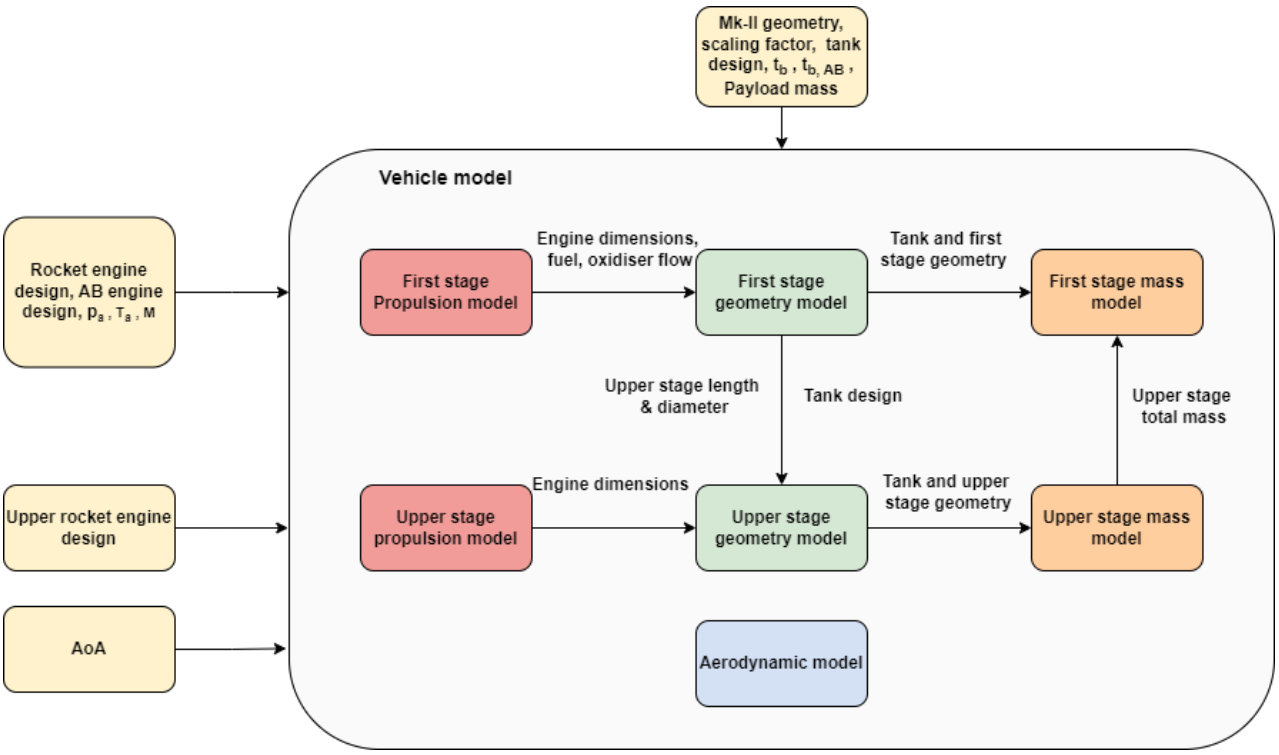

Figure 3.1: Vehicle model flow chart including in- and outputs for every module.

$$c^* = \frac{p_c A_t}{\dot{m}} \qquad A_t = \frac{c^* \dot{m}}{p_c} \tag{3.3}$$

$$C_F = \frac{F_t}{p_c A_t} \tag{3.4}$$

Similar to the characteristic velocity, the thrust coefficient also has an alternative formulation. This formulation shown in Equation 3.5 can be used to find the pressure ratio by substituting the area ratio according to Equation 3.6 and then iteratively solving the equation for the pressure ratio. The second most right fraction in Equation 3.5 resembles the atmospheric pressure over the chamber pressure, introducing the environmental conditions in the rocket performance computations.

$$C_F = \Gamma \sqrt{\frac{2\gamma}{\gamma - 1}\left(1 - \left(\frac{p_e}{p_c}\right)^{\frac{\gamma-1}{\gamma}}\right)} + \left(\frac{p_e}{p_c} - \frac{p_a}{p_c}\right)\frac{A_e}{A_t} \tag{3.5}$$

$$\epsilon = \frac{A_e}{A_t} = \frac{\Gamma}{\sqrt{\frac{2\gamma}{\gamma-1}\left(\frac{p_e}{p_c}\right)^{\frac{2}{\gamma}}\left(1 - \left(\frac{p_e}{p_c}\right)^{\frac{\gamma-1}{\gamma}}\right)}} \tag{3.6}$$

Once the pressure ratio has been found, the area ratio is computed by inserting the pressure ratio in Equation 3.6. Since the throat is already known, the exit area is also found. The specific impulse is then computed as the remaining performance parameter via Equation 3.7.

$$I_{sp} = \frac{c^* C_F}{g_0} \tag{3.7}$$

As mentioned, the propellant mass flow is a design variable which leads to different engine dimensions and performance parameters when it varies. There are multiple combinations of propellant mass flow and engine dimensions that are able to provide the specified sea-level thrust. Aiming to design the most efficient engine, the combination with the smallest mass flow is selected and used to compute the thrust along the trajectory of the first stage. For the upper stage, the latter is not necessary as mentioned, because of the assumption

Table 3.1: Overview of the design variables, in- and output parameters of the first stage rocket engine model.

Rocket engine model	
Design variables:	$F_{t,sl}, \dot{m}$
Environment input:	p_a
Input parameters:	$p_c, T_c, O/F, M_m, \gamma_c, \zeta_F$
Model output:	$F_t, I_{sp}, \dot{m}_f, \dot{m}_{ox}, A_e$

that it operates in vacuum conditions and the prescribed thrust level remains constant.

To compute the provided thrust in varying environmental conditions, the atmospheric pressure is defined as an environmental variable instead of sea level pressure. The propellant mass flow, engine exit and throat area, remain the same, as do the engine design choices introduced earlier. As a consequence, only the atmospheric over chamber pressure is different which leads to a different thrust coefficient as can be seen in Equation 3.5. With the new thrust coefficient, a new thrust and specific impulse at different atmospheric conditions, are computed through Equation 3.8 and Equation 3.7 respectively. An overview of the parameters used in this model is shown in Table 3.1, where for the upper stage rocket model, $F_{t,sl}$ would be replaced by F_t and the latter would not be defined as a model output.

$$F_t = \dot{m} C_F c^* \tag{3.8}$$

3.1.1. Rocket propulsion model validation

Because this model is based on ideal rocket theory, there are some simplifications and assumptions made that lead to inaccuracies compared to the real world. To ensure that the rocket propulsion model is accurate, or at least accurate enough, it is validated by using data from existing rocket engines as input and comparing the model outputs to real-world data. By doing this, a thrust quality factor can also be determined which aims to minimise the differences in thrust values between the model and the real world, improving the accuracy.

Ideally, the validation engines use the same propellant types as the engine on the Mk-III, however, only one engine, the Gamma 8 by Bristol Siddely, could be found which had sufficient data available that uses both kerosene and hydrogen peroxide as propellants. Since one reference engine is not enough, four other engines were selected which also use kerosene as fuel, but have liquid oxygen as oxidiser instead. The five engines with data are tabulated in Table 3.2 where one can immediately see the close resemblance between the model results and actual performance. This includes large rocket engines such as the Merlin 1D and the H-1B but also smaller rocket engines like the Rutherford and RD-58M rocket engine. Do note that the quality factors shown in the table are only meant to indicate the close resemblance of each individual engine.
Improving the model's accuracy further, a thrust quality factor is applied as in Equation 3.9 [6]. This quality factor is determined by computing the relative mean error, absolute mean error and the sample standard deviation of the model compared to the validation data with varying applied quality factors. From this procedure, a quality factor of 0.95 minimised these metrics, resulting in the errors and sample standard deviation presented in Table 3.3. Literature on quality factors confirms that this is a sensible result as 0.95 falls within the range defined by Sutton and Biblarz spanning from 0.92 to 1.00 [16]. Considering the rather small discrepancies and the thrust quality factor which has a realistic value, the rocket propulsion model can be considered validated for use in the vehicle model.

$$F_{t,real} = F_{t,ideal} \zeta_F \tag{3.9}$$

3.2. Airbreathing propulsion models

Models of the airbreathing engines, the ramjet and turbojet, are governed by different principles than the rocket model. Air is now taken in from the atmosphere and compressed, after which it is mixed with fuel, ignited and combusted and then accelerated through a nozzle, generating thrust. Still, this process differs significantly for the ramjet and turbine engines. The prior does not use any rotating components and relies on the forward airspeed and ram effect to compress the air. Turbine engines on the other hand utilise a compressor powered

Table 3.2: Rocket engine validation data of four Kerosene/LOX engines and one Kerosene/Hydrogen peroxide engine. *(*) derived value*

Merlin 1D				Rutherford			
Validation data (input)		Quality factors		Validation data (input)		Quality factors	
$\dot{m}[kg/s]$	236.6	$\zeta_{F,sl}$	0.946	$\dot{m}[kg/s]$	7.176*	$\zeta_{F,sl}$	0.920
$D_e[m^2]$	1.071	$\zeta_{I_{sp},sl}$	0.947	$D_e[m^2]$	0.205*	$\zeta_{I_{sp},sl}$	0.920
$p_c[MPa]$	9.72	$\zeta_{F,vac}$	0.949	$p_c[MPa]$	5*	$\zeta_{F,vac}$	0.931
O/F [-]	2.34	$\zeta_{I_{sp},vac}$	0.949	O/F [-]	2.3*	$\zeta_{I_{sp},vac}$	0.931
Validation data (output)		Model results		Validation data (output)		Model results	
$F_{t,sl}[kN]$	654.33	$F_{t,sl}[kN]$	691.39	$F_{t,sl}[kN]$	18.00	$F_{t,sl}[kN]$	19.57
$I_{sp,sl}[s]$	282	$I_{sp,sl}[s]$	298	$I_{sp,sl}[s]$	256	$I_{sp,sl}[s]$	278
$F_{t,vac}[kN]$	742.41	$F_{t,vac}[kN]$	782.68	$F_{t,vac}[kN]$	21.33	$F_{t,vac}[kN]$	22.91
$I_{sp,vac}[s]$	320	$I_{sp,vac}[s]$	337	$I_{sp,vac}[s]$	303	$I_{sp,vac}[s]$	324
Rocketdyne H-1B				RD-58M			
Validation data (input)		Quality factors		Validation data (input)		Quality factors	
$\dot{m}[kg/s]$	353.44*	$\zeta_{F,sl}$	0.951	$\dot{m}[kg/s]$	23.88*	$\zeta_{F,sl}$	-
$D_e[m^2]$	1.494	$\zeta_{I_{sp},sl}$	0.954	$D_e[m^2]$	1.151	$\zeta_{I_{sp},sl}$	-
$p_c[MPa]$	4.826	$\zeta_{F,vac}$	0.907	$p_c[MPa]$	7.747	$\zeta_{F,vac}$	0.965
O/F [-]	2.23	$\zeta_{I_{sp},vac}$	0.909	O/F [-]	2.4	$\zeta_{I_{sp},vac}$	0.965
Validation data (output)		Model results		Validation data (output)		Model results	
$F_{t,sl}[kN]$	911.88	$F_{t,sl}[kN]$	958.81	$F_{t,sl}[kN]$	-	$F_{t,sl}[kN]$	-
$I_{sp,sl}[s]$	263	$I_{sp,sl}[s]$	276	$I_{sp,sl}[s]$	-	$I_{sp,sl}[s]$	-
$F_{t,vac}[kN]$	1030.25	$F_{t,vac}[kN]$	1136.44	$F_{t,vac}[kN]$	83.4	$F_{t,vac}[kN]$	86.41
$I_{sp,vac}[s]$	297	$I_{sp,vac}[s]$	327	$I_{sp,vac}[s]$	356	$I_{sp,vac}[s]$	369
Gamma 8 (98% pure hydrogen peroxide)							
Validation data (input)		Quality factors		Validation data (output)		Model results	
$\dot{m}[kg/s]$	90.32*	$\zeta_{F,sl}$	0.990	$F_{t,sl}[kN]$	222.4	$F_{t,sl}[kN]$	224.60
$D_e[m^2]$	0.395*	$\zeta_{I_{sp},sl}$	0.990	$I_{sp,sl}[s]$	251	$I_{sp,sl}[s]$	253
$p_c[MPa]$	4.74	$\zeta_{F,vac}$	0.991	$F_{t,vac}[kN]$	234.8	$F_{t,vac}[kN]$	237.02
O/F [-]	8.2	$\zeta_{I_{sp},vac}$	0.991	$I_{sp,vac}[s]$	265	$I_{sp,vac}[s]$	268

Table 3.3: Sample standard deviation, absolute and relative mean error for a thrust quality factor of 0.95.

	$F_{t,sl}$	$I_{sp,sl}$	$F_{t,vac}$	$I_{sp,vac}$
Relative mean error	0.079%	-0.319%	0.024%	-0.393%
Absolute mean error	12.58 kN	3.53 s	7.52 kN	5.42 s
Sample standard deviation	25.27 kN	6.01 s	9.56 kN	8.17 s

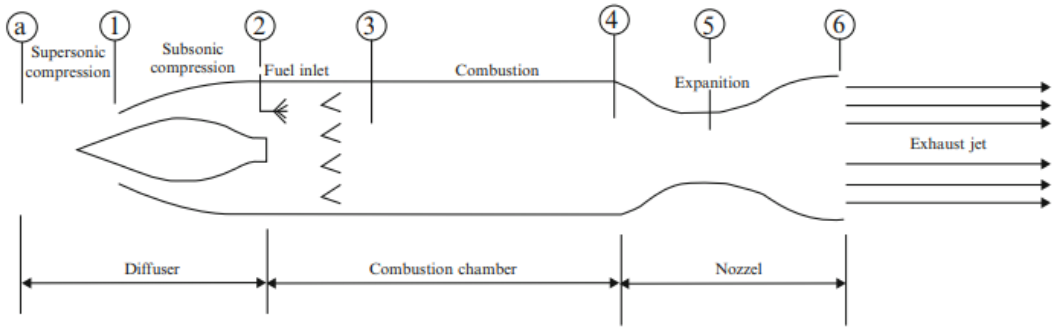

Figure 3.2: Schematic of a ramjet engine with seven important locations [32].

by a turbine to compress air. Both processes will be explained in more detail below as well as how both engines are modelled.

3.2.1. Ramjet model

Introduction to ramjet propulsion

Before jumping straight into the ramjet model, a brief introduction is given to the workings of ramjet engines via the schematic as shown in Figure 3.2. Here, seven locations are defined, starting with location **a**, which is the free stream corresponding to free stream or ambient conditions. Location **1** corresponds to the inlet of the engine, also the inlet of the diffuser, location **2** is the exit of the diffuser, **3** is the entrance of the combustion chamber, **4** the exit of the combustion chamber or the nozzle inlet, **5** the nozzle throat and finally **6** the exit of the nozzle or engine as a whole. The phenomena that occur between these locations are described in the list below as taken from the work of El-Sayed [32].

a-1: Between the free stream conditions and the inlet of the engine, diffusion already occurs and the airflow is slowed down by a small amount.

1-2: In the engine inlet, air is slowed down further to subsonic speeds and compressed via shock waves which can be one normal shock, or multiple oblique shocks followed by a normal shock.

2-3: After leaving the intake, the air enters the combustion chamber and is sprayed with fuel in the form of droplets to achieve a well-mixed flow in a short period of time. This mixture is then ignited and proceeds through the combustion chamber.

3-4: Here, the mixture is fully combusted and has increased in temperature to 1600 - 3000 K

4-5: Once fully combusted (in the ideal case), the hot gas mixture is being expanded through a converging nozzle up until the throat.

5-6: The flow is further expanded through the diverging section of the nozzle until the engine exit where it leaves the engine at a higher velocity than at free stream conditions, generating thrust.

The thermodynamic cycle of a ramjet engine is classified as a Brayton cycle which, in the ideal case, consists of an isentropic compression, followed by combustion at constant pressure. Then, air is expanded isentropically before finally, heat is rejected at constant pressure in the atmosphere [32]. A visual representation of how such an ideal cycle looks like in a T-s diagram is given in Figure 3.3a. In reality, however, it is extremely difficult to have isentropic compression and expansion, as well as constant pressure combustion, therefore the compression and expansion in the inlet and nozzle respectively, are adiabatic processes instead of isentropic. Also, pressure losses in the combustion chamber should be accounted for, a graph of these modified processes is shown in Figure 3.3b. With this knowledge, a basic ramjet model can be built which uses the ramjet inlet area and combustion chamber temperature as design parameters and outputs the thrust force, specific impulse and fuel consumption.

3.2.2. Ramjet modelling

The ramjet model is based on a non-ideal cycle model as presented by El-Sayed [32], and accounts for pressure losses in the intake, combustion chamber and nozzle. Still, some assumptions have to be made which are the following:

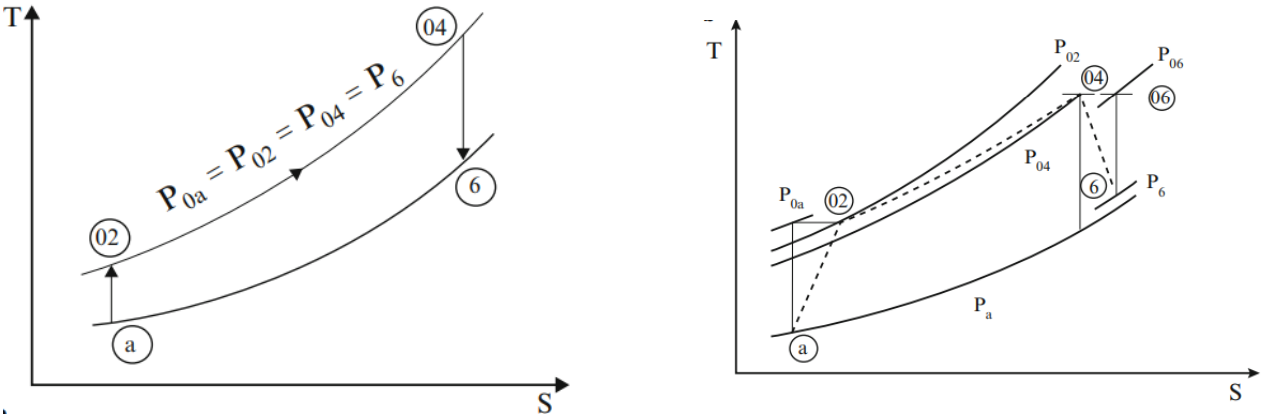

(a) Ideal Brayton cycle of a ramjet

(b) Real Brayton cycle of a ramjet

Figure 3.3: T-s diagrams of an ideal and real Brayton cycle of a ramjet engine [32].

- The compression and expansion of the airflow in the diffuser and nozzle are considered adiabatic, hence no heat leaves the airflow, nor is it added.
- The air and gas flow are assumed to be calorically perfect gasses, the specific heat ratio and gas constant remain constant.
- Inside the combustion chamber, losses occur which are accounted for by including combustion efficiency.
- It is assumed that the flow is fully expanded at location **6** such that the exit pressure is equal to the ambient pressure.

The goal of the model, is to find the thrust, alongside the fuel consumption for a ramjet design which is based on design variables and certain design choices. A good place to start is the general thrust equation shown in Equation 3.10, which is already transformed such that it introduces the parameter f, being the fuel-to-air ratio. An expression should be found for the exit velocity u_e and for f, the intake air mass flow $\dot{m}_a$ can be computed by multiplying the free stream velocity, density and the inlet area and u is simply the velocity at which the vehicle is flying at.

$$F_t = \left(\dot{m}_e u_e - \dot{m}_a u_a\right) + (p_e - p_a)A_e \rightarrow \frac{F}{\dot{m}_a} = \left[(1+f)u_e - u_a\right] + (p_e - p_a)\frac{A_e}{\dot{m}_a} \tag{3.10}$$

First, the stagnation pressure ratios across the three main components are defined as in Equation 3.11 and can be combined into a formulation for the overall engine pressure ratio. The total pressure ratio across the diffuser is computed by Equation 3.12 where $r_{d,max}$ is taken from literature for a supersonic intake embedded in the airframe, depending on the level of technology [27].

$$r_d = \frac{p_{02}}{p_{0a}}, \qquad r_c = \frac{p_{04}}{p_{02}}, \qquad r_n = \frac{p_{06}}{p_{04}}, \qquad \frac{p_{06}}{p_{0a}} = r_d r_c r_n \tag{3.11}$$

$$r_d = r_{d,max}\eta_r \qquad \eta_r = \begin{cases} 1 & : \text{M < 1} \\ 1 - 0.075(M_a - 1)^{1.35} & : \text{1 < M < 5} \\ \dfrac{800}{M_a^4 + 935} & : \text{5 < M} \end{cases} \tag{3.12}$$

Next, the expression for the free stream total pressure ratio is modified as in Equation 3.13 and the formulation of the exit total pressure ratio is changed such that an expression is obtained for the exit Mach number.

$$\frac{p_{0a}}{p_a} = \left(1 + \frac{\gamma - 1}{2}M_a^2\right)^{\frac{\gamma}{\gamma-1}} \rightarrow \left(\frac{p_a}{p_{0a}}\right)^{\frac{\gamma-1}{\gamma}}\left(1 + \frac{\gamma - 1}{2}M_a^2\right) = 1 \tag{3.13}$$

$$\frac{p_{06}}{p_6} = \left(1 + \frac{\gamma - 1}{2}M_e^2\right)^{\frac{\gamma}{\gamma-1}} \rightarrow M_e^2 = \frac{2}{\gamma - 1}\left[\left(\frac{p_{06}}{p_6}\right)^{\frac{\gamma-1}{\gamma}} - 1\right] \tag{3.14}$$

Because Equation 3.13 is equal to one, it can be multiplied with the terms between brackets in Equation 3.14, resulting in Equation 3.15. By taking the two pressure ratios together, $\frac{p_{06}}{p_{0a}}$ can be replaced by the expression on the far right side of Equation 3.11 which is done in Equation 3.16.

$$M_e^2 = \left(\frac{2}{\gamma-1}\right)\left[\left(1+\frac{\gamma-1}{2}M_a^2\right)\left(\frac{p_a}{p_{0a}}\right)^{\frac{\gamma-1}{\gamma}}\left(\frac{p_{06}}{p_6}\right)^{\frac{\gamma-1}{\gamma}}-1\right] \tag{3.15}$$

$$M_e^2 = \left(\frac{2}{\gamma-1}\right)\left[\left(1+\frac{\gamma-1}{2}M_a^2\right)\left(r_d r_c r_n \frac{p_a}{p_6}\right)^{\frac{\gamma-1}{\gamma}}-1\right] \tag{3.16}$$

Now, the parameter m is defined as in Equation 3.17, which can be put in Equation 3.16 leading to left hand side of Equation 3.18. This allows for another definition of the parameter m, shown on the right-hand side.

$$m = \left(1+\frac{\gamma-1}{2}M_a^2\right)\left(r_d r_c r_n \frac{p_a}{p_6}\right)^{\frac{\gamma-1}{\gamma}} \tag{3.17}$$

$$M_e^2 = \left(\frac{2}{\gamma-1}\right)(m-1) \rightarrow m = \left(1+\frac{\gamma-1}{2}M_e^2\right) \tag{3.18}$$

The exit velocity is equal to the exit Mach number, times the speed of sound at the nozzle exit, which is written and modified in Equation 3.19 such that the stagnation temperature ratio $\frac{T_{04}}{T_6}$ is introduced.

$$u_e = M_e\sqrt{\gamma R T_6} = M_e\sqrt{\gamma R T_{04}\frac{T_6}{T_{04}}} \tag{3.19}$$

Assuming adiabatic expansion, as mentioned above, no heat is lost between location **4** and **6**, therefore, the stagnation temperature ratio can be written as in Equation 3.20. Entering this expression in Equation 3.19 results in the left-hand side of Equation 3.21 which can be further modified and simplified by using the parameter m which is solely dependent on the diffuser, combustion chamber and nozzle losses together with the free stream Mach number and ambient over exit pressure ratio which is reduced to one because of the assumption of ideal expansion. The chamber total temperature T_{04} depends on the structural limits of the combustion chamber and is taken as a design variable.

$$\frac{T_{06}}{T_6} = \frac{T_{04}}{T_6} = 1+\frac{\gamma-1}{2}M_e^2 \tag{3.20}$$

$$u_e = M_e\sqrt{\gamma R\frac{T_{04}}{1+\frac{\gamma-1}{2}M_e^2}} = \sqrt{\frac{2\gamma R T_{04}(m-1)}{(\gamma-1)m}} \tag{3.21}$$

Still, a formulation for the fuel-to-air ratio is required. This formulation can be found based on the chamber's total temperature, the heat of combustion of the fuel, and total ambient temperature, assuming that the compression between the free stream and location **2** is adiabatic and the combustion efficiency. For the reasoning behind Equation 3.22, the reader is referred to Fundamentals of Aircraft and Rocket Propulsion by El-Sayed [32].

$$f = \frac{C_{p,4}T_{04} - C_{p,2}T_{0a}}{\eta_b Q_R - C_{p,4}T_{04}} \tag{3.22}$$

Finally, the equation for thrust can be written as in Equation 3.23 where every parameter is known or can be computed based on design variables being the engine inlet area and combustion chamber total pressure, common component characteristics being r_d, r_c, r_d and η_b, propellant characteristics being $\gamma, R, Q_R, C_{p,2}$ and $C_{p,4}$, and environmental inputs being the free stream velocity, - Mach number and free stream air density. An overview of all variables and parameters of the ramjet model is given in Table 3.4.

$$\frac{F_t}{\dot{m}_a} = (1+f)\sqrt{\frac{2\gamma R T_{04}(m-1)}{(\gamma-1)m}} - M_a\sqrt{\gamma R T_a} + \frac{p_e A_e}{\dot{m}_a}\left(1-\frac{p_a}{p_e}\right) \tag{3.23}$$

Table 3.4: Overview of ramjet model design variables, in- and output parameters.

Ramjet model	
Design variables:	T_{04}, A_i
Environment input:	p_a, M_a, u_a, ρ_a
Input parameters:	$r_d, r_c, r_n, \gamma, R, C_p, \eta_c, Q_R$
Model output:	$F_t, \dot{m}_f, \dot{m}_a, f, A_e, u_e$

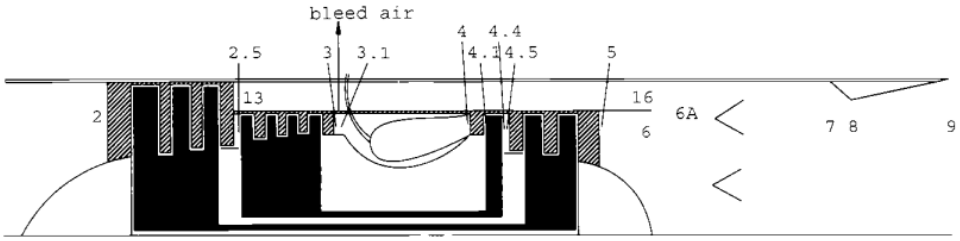

Figure 3.4: Schematic of a general turbine engine including location numbering [27].

3.2.3. Ramjet validation

Similar to the rocket propulsion model, the ramjet model requires validation to see if the assumptions made do not lead to unrealistic results and that no errors were made along the way. This is again done by comparing the performance of reference engines to model results based on input data of those engines. Because ramjets are often used for military purposes, there is not much data available for the public, let alone complete data. Only two engines were found of which enough data could be found: The Wright XRJ47 and the Marquardt RJ43-MA. Although two reference engines are not much to validate a model one, the Marquardt ramjet has flight test data available at multiple altitudes and chamber temperatures, four data points were selected, two at 50000 ft and two at 60000 ft. The validation data can be found in Table 3.5, where for r_d, r_c and r_n, values are taken from literature and η_b were taken from the specifications of each engine or measurement. Note that the free stream velocity and temperature are not added in this table, but they can be computed via the ambient pressure, density and the free stream Mach number which are stated in the table.

Looking at the results in Table 3.5, the mode overestimates the amount of thrust that can be generated by the engines and underestimates the fuel flow that is needed to achieve these thrust levels. as can be seen from the relative mean error in Table 3.6. Similar to the rocket engine model, a thrust correction factor can be applied, which aims to minimise the errors and standard deviation. In addition, a correction factor is applied to the fuel mass flow calculations, also to minimise errors and deviations. The right-hand side of Table 3.6 shows the minimised standard deviation, relative and absolute mean errors for a thrust correction factor of 0.925 and a fuel mass flow correction factor of 1.38. Note that the three parameters are not exactly minimised, only the relative mean errors are minimised but the other two are near-minimum. After applying these correction factors, the ramjet model can be considered as validated as the results only differ from reality by less than 1% as shown by the relative mean error.

3.2.4. Turbine engine model

A turbine engine is much more complicated than a ramjet as it includes rotating components actively compressing and expanding air. A schematic of a typical turbine engine can be seen in Figure 3.4 of which the indicated locations are explained in Table 3.7. Not all locations are included here, the ones which are not relevant to the turbine engine description are left out. Note that the description is fully based on the work of Mattingly for a general turbine engine meaning that components such as a fan or afterburner can be excluded if desired. For a more in-depth analysis of airbreathing aircraft engine design, the reader is kindly referred to Mattingly his work in [27].
The incoming air at free-stream conditions enters the engine through the inlet entry until it encounters the fan entry or the low-pressure compressor. In the case of the prior a portion of the air bypasses the core and another portion enters the high-pressure compressor. Here the pressure is increased further until the air enters the combustion chamber, where it is mixed with fuel and combusted. The high-temperature gas then

Table 3.5: Ramjet model validation data [44][45].

Wright XRJ47				Marquardt RJ43-MA			
Validation data (input)		Quality factors		Validation data		Quality factors	
$A_i[m^2]$	0.41	$\zeta_F[-]$	0.970	$A_i[m^2]$	0.1597	$\zeta_F[-]$	0.876
$T_{04}[K]$	1887	$\zeta_m[-]$	1.234	$T_{04}[K]$	2017	$\zeta_m[-]$	1.221
$p_a[Pa]$	5071			$p_a[Pa]$	11597		
$M_a[-]$	2.75			$M_a[-]$	2.7		
$\rho_a[kg/m^3]$	0.082			$\rho_a[kg/m^3]$	0.186		
$r_{d,max}[-]$	0.90			$r_{d,max}[-]$	0.90		
$r_c[-]$	0.97			$r_c[-]$	0.97		
$r_n[-]$	0.96			$r_n[-]$	0.96		
$\eta_b[-]$	0.83			$\eta_b[-]$	0.92		
Validation data (output)		Model results		Validation data (output)		Model results	
$F_t[kN]$	16.87	$F_t[kN]$	17.39	$F_t[kN]$	16.13	$F_t[kN]$	18.40
$\dot{m}_f[kg/s]$	1.329	$\dot{m}_f[kg/s]$	1.077	$\dot{m}_f[kg/s]$	1.255	$\dot{m}_f[kg/s]$	1.028
Marquardt RJ43-MA				Marquardt RJ43-MA			
Validation data		Quality factors		Validation data		Quality factors	
$A_i[m^2]$	0.1597	$\zeta_F[-]$	0.830	$A_i[m^2]$	0.1597	$\zeta_F[-]$	0.928
$T_{04}[K]$	1791	$\zeta_m[-]$	1.20	$T_{04}[K]$	2171	$\zeta_m[-]$	1.402
$p_a[Pa]$	7172			$p_a[Pa]$	11597		
$M_a[-]$	2.7			$M_a[-]$	2.7		
$\rho_a[kg/m^3]$	0.115			$\rho_a[kg/m^3]$	0.186		
$r_{d,max}[-]$	0.90			$r_{d,max}[-]$	0.90		
$r_c[-]$	0.97			$r_c[-]$	0.97		
$r_n[-]$	0.96			$r_n[-]$	0.96		
$\eta_b[-]$	0.89			$\eta_b[-]$	0.92		
Validation data (output)		Model results		Validation data (output)		Model results	
$F_t[kN]$	7.34	$F_t[kN]$	8.84	$F_t[kN]$	18.67	$F_t[kN]$	20.12
$\dot{m}_f[kg/s]$	0.607	$\dot{m}_f[kg/s]$	0.506	$\dot{m}_f[kg/s]$	1.604	$\dot{m}_f[kg/s]$	1.144
Marquardt RJ43-MA							
Validation data (input)						Quality factors	
$A_i[m^2]$	0.1597	$r_{d,max}[-]$	0.90			$\zeta_F[-]$	0.999
$T_{04}[K]$	2163	$r_c[-]$	0.97			$\zeta_m[-]$	1.825
$p_a[Pa]$	7172	$r_n[-]$	0.96	Validation data (output)		Model results	
$M_a[-]$	2.7	$\eta_b[-]$	0.92	$F_t[kN]$	11.05	$F_t[kN]$	11.05
$\rho_a[kg/m^3]$	0.115			$\dot{m}_f[kg/s]$	1.173	$\dot{m}_f[kg/s]$	0.643

Table 3.6: Sample standard deviation, absolute and relative mean error of the ramjet model compared to validation data.

	F_t	$\dot{m}_f$	$F_t(corrected)$	$\dot{m}_f(corrected)$
Relative mean error	7.91%	-37.60%	0.44%	0.27%
Absolute mean error	1.15 kN	0.314 kg/s	0.680 kN	0.145 kg/s
Sample standard deviation	1.57 kN	0.024 kg/s	0.837 kN	0.0013 kg/s

Table 3.7: Location numbering of a general turbine engine as taken and slightly modified from the work of Mattingly [27].

Location	Location
0	Far upstream, free-stream
1	Inlet entry
2	Inlet exit, fan entry
13	Fan exit
2.5	Low-pressure compressor exit, high-pressure compressor entry
3	High-pressure compressor exit
3.1	Burner entry
4	Burner exit, high-pressure turbine entry
4.5	High-pressure turbine exit, low-pressure turbine entry
5	Low-pressure turbine exit
6	Core stream mixer entry
16	Fan bypass stream mixer entry
6A	Mixer exit, afterburner entry
7	Afterburner exit, exhaust nozzle entry
8	Exhaust nozzle throat
9	Exhaust nozzle exit

enters the high-pressure turbine and is expanded, which powers the high-pressure compressor. Hereafter, the gas passes another turbine, which powers the fan. Before flowing to the afterburner combustion chamber, the bypassed airflow is mixed with the core flow via the mixer. In the combustion chamber, the flow is again mixed with injected fuel and combusted. The mixture with increased temperature is then accelerated through the nozzle throat until the nozzle exit at which point it has attained a higher velocity than the free stream, generating the thrust of the turbine engine.

As previously stated, a turbine engine is much more complicated than a ramjet. Using a simple parametric cycle analysis the so-called design-point performance of a turbine engine can be relatively well estimated, that is, however, only one point in the flight envelope where the engine has to operate. At all other points, off-design if you will, the engine will behave differently than on this design point [27]. This, in combination with the fact that designing a turbine engine in detail is simply outside the scope of this project has resulted in the choice to use a readily validated engine simulation software called Gas turbine Simulation Program. GSP is developed and maintained by the NLR, in corporation with TU Delft, and allows for off-design performance analysis of gas turbine engines. The available version for students already includes engine models of some existing turbine engines such as the GE J85-GE-15 afterburning turbojet and the F100-PW-229 afterburning low-bypass turbofan. After some discussions with Dawn Aerospace, the choice was made to use this F100-PW-229 engine as a first estimate for the turbine engine concept on the Mk-III. This has several reasons, the first being the availability of data on this engine. Secondly, this engine is able to produce a very high thrust and even more so with afterburners operational and has an uninstalled thrust-over-weight ratio of 7.8. It is recognised that this engine may lead to a less-than-optimal design, at this stage of the project it is considered a fair assumption and design choice to make.

Using GSP and the already configured model of the F100-PW-229, simulations are made for all combinations of altitude between 0 and 20km and Mach numbers between 0 and 2.2. These upper limits are what seem to be the limits of the engine's operational envelope, performance near these limits has decreased so much that the engines are not expected to operate in a useful way at these conditions anyway. Simulations are run for both an inoperative afterburner as well as for an operating afterburner. Either a constant turbine inlet temperature can be selected or a constant fuel mass flow. The prior was deemed to make the most sense performance-wise hence, the maximum turbine inlet temperature of the selected engine was taken and has a value of 1755 K [27]. For the afterburner, the same choice was made and a maximum combustion temperature of 2033 K was found [27]. During simulations at lower Mach numbers and higher altitudes, however, some problems were encountered for the operative afterburner case where the specified afterburner temperature could not be reached and reverse flow would be created if attempting to do so. For these cases, the afterburner temperature was decreased via trial-and-error until the simulation ran smoothly again.
The main results of interest, are the generated thrust and fuel mass flow at different altitudes and Mach numbers. These results are extracted and put into a data sheet in Excel which tabulates the data for any Mach

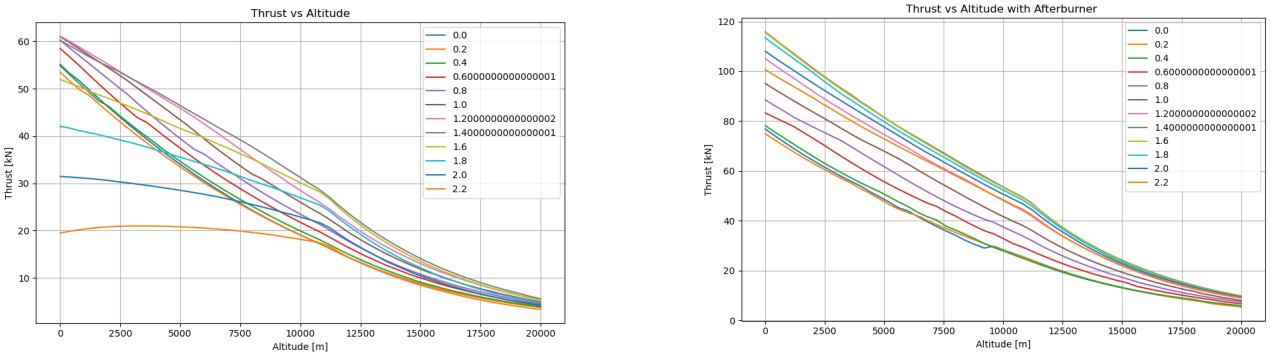

(a) Afterburner off **(b)** Afterburner on

Figure 3.5: Thrust plotted against altitude for all Mach numbers for the F100-PW-229 low-bypass turbofan, generated with GSP.

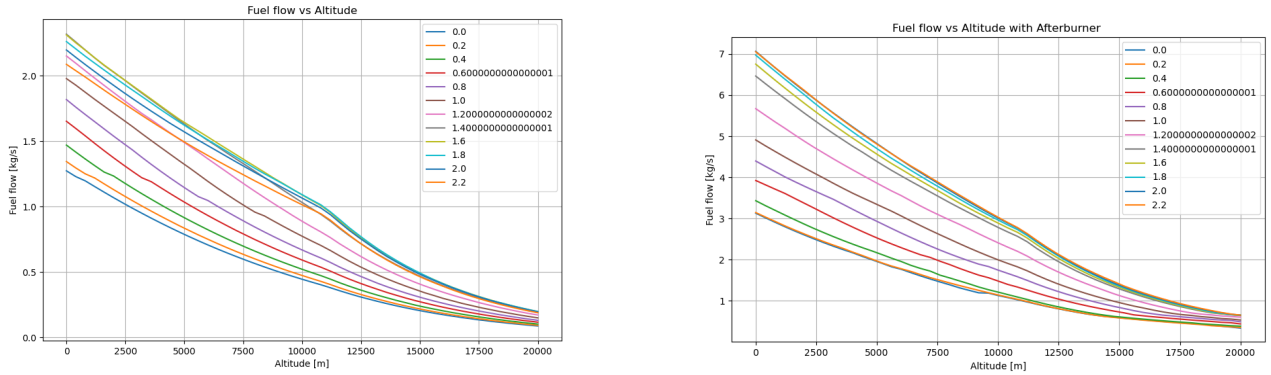

(a) Afterburner off **(b)** Afterburner on

Figure 3.6: Fuel flow plotted against altitude for all Mach numbers for the F100-PW-229 low-bypass turbofan, generated with GSP.

number and altitude combination. These tables are loaded in the Python-based model, which then creates matrices of them such that a look-up table is generated. Because the altitude spacing of the simulation is still 400 m and the Mach number spacing of data points is 0.2, the data is first interpolated to achieve more accurate data for any given input altitude and Mach number. Therefore a two-dimensional interpolation function of the open-access scipy library is used which interpolates the Mach number data with a new spacing of 0.1 and the altitude data with a spacing of 100 m. Using the interpolated set of data, the model determines the closest Mach number and data point to any input Mach number and altitude combination (within the allowable range). For this point, the fuel mass flow and thrust are then returned, depending on whether the afterburner is operational or not. In Figure 3.5 and Figure 3.6 the thrust and mass flows versus altitude, for different Mach numbers, with and without afterburner are plotted, based on the simulation data generated by GSP for the F100-PW-229 low-bypass turbofan. Both figures show the expected behaviour of a decrease in thrust and fuel mass flow with increasing altitude.

3.2.5. Turbine engine validation

The GSP software is an already validated tool which means that GSP of itself should not be validated. What should be validated still, is that simulations have been performed correctly and the generated data is accurate. For this, the estimated maximum thrust and corresponding TSFC were compared to tabulated data of the engine in the literature. The maximum produced force found in the literature was found to be 129 kN in literature, whereas the maximum found thrust from the GSP software was 116 kN, showing a discrepancy of roughly 10% which was considered acceptable. In addition, the shape of the graphs shown above was compared to graphs of other turbine engines to validate the behaviour of the engine model, here the same curve shapes were found as those obtained from the GSP software as can be seen when comparing the thrust versus altitude graphs to Figure 3.7.

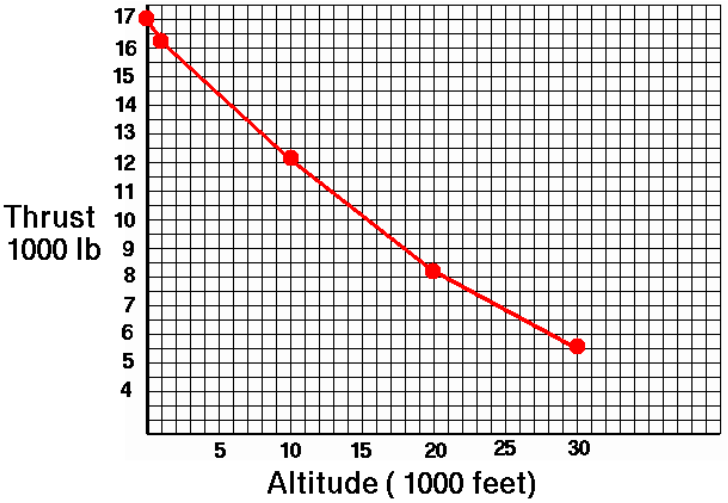

Figure 3.7: Effect of altitude on thrust output [8].

3.2.6. Installed thrust

Despite the models themselves being accurate, they consider only the engine and not the induced drag caused by installing the engine on an airframe which reduces the effective thrust [27]. Until now, all computed thrust values are for the uninstalled case, meaning that the installed thrust must still be computed. The inlet and nozzle are the largest contributors to the additional external drag and their contribution can be expressed in terms of a fraction of the uninstalled thrust as in Equation 3.24. If an expression or value can be found for ϕ_{inlet} and ϕ_{nozzle} then the installed thrust can be obtained quite easily.

$$T = F_t - \phi_{inlet} F_t - \phi_{nozzle} F_t \tag{3.24}$$

The approach of Mattingly to these losses is to assume a worst-case scenario being full boundary layer separation. For this, he provides common values for ϕ_{inlet} at subsonic free stream conditions in the form of graphs, of which an averaged value of 0.2 is taken. In addition, a relation is given to compute ϕ_{inlet} for supersonic conditions as shown in Equation 3.25 [27]. The area ratio $\frac{A_1}{A_0}$ stated here is assumed to be 1.2. Regarding the nozzle, the additional drag is caused by external boundary layer separation at the exit and again a common value for this loss is provided being 0.03 which is taken for both sub- and supersonic velocities[27]. Using the loss coefficients, the uninstalled thrust is modified by the airbreathing propulsion models to an installed thrust value.

$$\phi_{inlet} = \frac{\left(\frac{A_1}{A_0} - 1\right)\left(M_0 - \left(\frac{2}{\gamma+1} + \frac{\gamma-1}{\gamma+1} M_0^2\right)^{\frac{1}{2}}\right.}{\left(\frac{F}{\dot{m}_0 a_0}\right)} \tag{3.25}$$

3.3. Geometry and mass models

Both the geometry and mass of the vehicle that is being designed, highly influence its performance, the latter is also a performance parameter of its own as seen from the research question. Both stages have very different configurations, the first having a plane-like configuration and the upper stage being a conventional rocket. Therefore, the geometry and mass models are very different and are separately discussed in this section.

3.3.1. First stage geometry model

The first stage external geometry, is based on the geometry of the predecessor of the Mk-III, the Mk-II Aurora, and is scaled up by a scaling factor. A text file was provided by Dawn Aerospace which included the dimensions of the wing planform, fuselage and vertical tail such that the same geometrical shape can be constructed for the Mk-III and scaled to the required vehicle size.

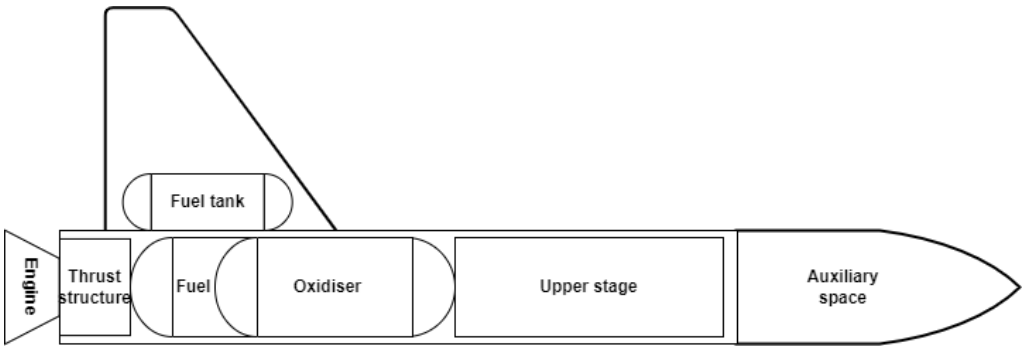

Figure 3.8: Sketch of the first stage interior design

Inside the vehicle, a part of the engine should be housed, as well as the propellant tanks and the upper stage vehicle as shown in Figure 3.8, where only one of the two wings is drawn to not make the figure unnecessarily large.
From the sketch it can be seen that the cylindrical part of the first stage fuselage houses a part of the engine and the thrust structure, the fuel if not all of the required fuel can be stored in the wings, the oxidiser tank which has a common bulkhead design with the fuel tank and the upper stage rocket. This can be expressed as in Equation 3.26 where subscripts 1 and 2 refer to the first and upper stages respectively. Note, that the whole engine length is taken, neglecting the fact that a part can extend out of the fuselage. This is done to account for the thrust structure length which may be larger than the remaining engine length inside the fuselage.

$$l_{cyl,1} = l_{tank,ox_1} + l_{tank,f_1} + l_{engine} + l_2 \tag{3.26}$$

Given that the rocket propellant mass flow, O/F and the airbreathing engine fuel mass flow, are provided by the propulsion model, that the rocket and airbreathing burn times are design variables and that the tank diameter is taken as the fuselage diameter minus 10 cm, the propellant tank sizes can be computed. Equation 3.27 and Equation 3.28 show how the required propellant and tank volumes are computed, accounting for 5% ullage volume.

$$V_{ox_1} = \frac{O/F}{O/F+1}\frac{\dot{m}_{rocket,1}N_{eng}t_{b,rocket}}{\rho_{ox}} \qquad V_{f_1} = \frac{\dot{m}_{rocket,1}N_{eng}t_{b,rocket}}{(O/F+1)\rho_{fuel}} + \frac{\dot{m}_{ab}N_{eng,ab}t_{b,ab}}{\rho_{fuel}} \tag{3.27}$$

$$V_{t,ox_1} = 1.05V_{ox,1} \qquad V_{t,f_1} = 1.05V_{f_1} \tag{3.28}$$

Next, the required tank dimensions are computed to hold these volumes, using the assumption that the tanks are thin-walled structures. This is done first by checking if the required propellant can be stored inside a spherical tank, which is the most mass-efficient tank shape, by computing the volume of a spherical tank with the tank diameter as mentioned above, and verifying if V_{t,ox_1} or V_{t,f_1} is smaller than this value. If yes, then the diameter is computed as required to hold one or both of the volumes. If not, the fuel and oxidiser tank diameters remain as specified before and the dimensions of the cylindrical, common bulkhead tanks are computed via Equation 3.29 and Equation 3.30 based on the tank dimension definition in Figure 3.9. If only one of the tanks can be spherical, the other tank is modelled as a basic cylindrical tank.

$$l_{t,ox_1} = \frac{V_{t,ox_1} - \frac{\pi}{6}D_{t,ox_1}^3}{\frac{\pi}{4}D_{t,ox_1}^2} + D_{t,ox_1} \qquad l_{t,f_1} = \frac{V_{t,f_1}}{\frac{\pi}{4}D_{t,f_1}^2} + \frac{D_{t,f_1}}{2} \tag{3.29}$$

$$l_{cyl,ox_1} = l_{t,ox_1} - D_{t,ox_1} \qquad l_{cyl,f_1} = l_{t,f_1} - \frac{D_{t,f_1}}{2} \tag{3.30}$$

The thicknesses of the tanks are computed based on an assumed maximum expected operating pressure of 5 bar, common for pump-fed systems. The tanks are assumed to be made from carbon-epoxy material which has an ultimate strength of 603 MPa and a minimum manufacturing thickness of 1 mm which must be adhered to. In addition, a factor of safety for the ultimate strength of 1.7 is found in the literature to be a common value for composite shell structures [6]. In Equation 3.31 the tank wall thicknesses are computed for the spherical sections. Because the loads are twice as high in the cylindrical part, the thickness here is taken as double the

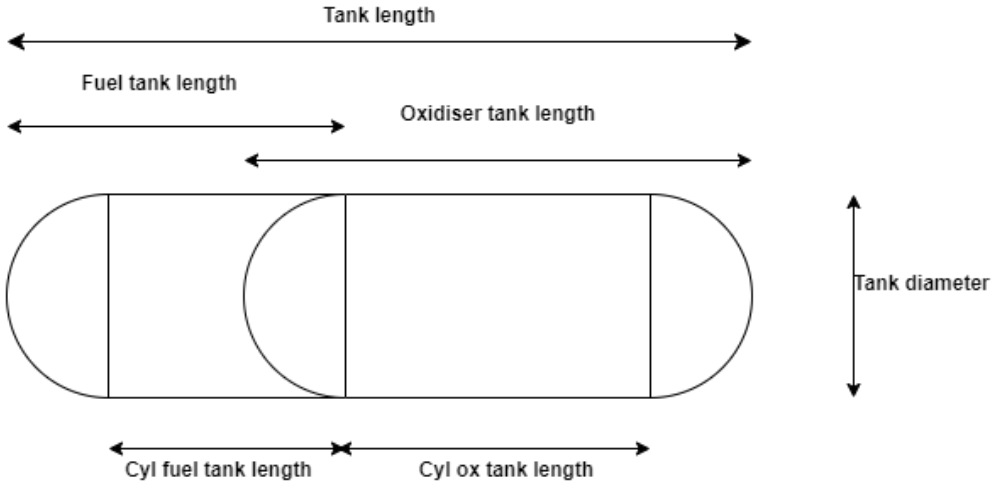

Figure 3.9: Definition of the tank dimensions in a common bulkhead design

spherical cap thickness. If a computed thickness is below 1 mm, then that wall thickness is automatically set to 1 mm, ensuring that the tanks can actually be manufactured.

$$t_{t,ox_1} = \frac{p_t D_{t,ox_1}}{4\sigma_{ult}} SF \qquad t_{t,f_1} = \frac{p_t D_{t,f_1}}{4\sigma_{ult}} SF \tag{3.31}$$

Finally, the engine length is computed using a statistical relationship that is based on the rocket's thrust as in Equation 3.32 which is valid for engines from 0.5 kN until 8000 kN [6].

$$l_{eng} = 0.1362 F_{rocket}^{0.2279} \tag{3.32}$$

Having computed all the lengths of the components which must be housed in the cylindrical section of the first stage, the available length for the upper stage can be found by changing Equation 3.26 into Equation 3.33 where half of the tank diameter is subtracted from the fuel tank length because of the overlap in tank dimension definition as can be seen from Figure 3.9. Note that l_{t,ox_1} or $(l_{t,f_1} - D_{t,f_1}/2)$ would be changed by D_{t,ox_1} or D_{t,f_1} respectively if one or both of the propellant tanks would be spherically shaped.

$$l_2 = l_{cyl,1} - l_{t,ox_1} - \left(l_{t,f_1} - \frac{D_{t,f_1}}{2} \right) - l_{eng} \tag{3.33}$$

3.3.2. First stage mass model

Knowing the first stage external and internal geometry, the mass can be determined using a weight estimation method called the Hypersonic Aerospace Sizing Analysis method (HASA) which is commonly used for sizing of winged, hypersonic vehicles such as launch vehicles or hypersonic transports and is a validated method developed by NASA. This method decomposes the total vehicle mass into structural, subsystem, propulsion system, payload and propellant mass of which each can be further decomposed into component masses except for the propellant and payload mass. The reader must be aware that all of the mass estimating relations are in imperial units unless stated otherwise, of course, pounds will be converted to kilograms before any of the masses is used as input to another module.

The structural weight is divided into body weight, tail weight (only vertical tail for the Mk-III), thermal protection system weight, landing gear weight, and thrust structure weight. The body weight includes the entire fuselage and is computed as in Equation 3.34 where a modifying factor is introduced which will be used in multiple relations and accounts for technological developments and material choices. The maximum dynamic pressure is taken as the upper limit of the range provided by Van Kesteren, being 90 kPa [22]. To find the ultimate load factor, the limit lateral acceleration is divided by g_0 and multiplied by 1.5 as prescribed in regulations [38]. Lastly, the body wetted area is found by adding twice the planform areas of the wings and vertical tail, the area of the cylindrical fuselage part and the area of the nose cone.

$$W_b = 0.341 m f \sigma \qquad \sigma = \left[\left(\frac{l_1 ULF}{D_{be}} \right)^{0.15} Q_{max}^{0.16} S_{b,tot}^{1.05} \right] \tag{3.34}$$

To compute the wing weight as in Equation 3.36, the empty weight is required as input, which is defined as in Equation 3.35. Here, the propellant mass is already known based on the propellant mass flows provided by the propulsion model and the burn times as design variables. The gross take-off weight on the other hand is not known yet, and is required as input for other component mass calculations as well. To solve this, an iterative loop is created that uses a first estimate provided by Dawn Aerospace to compute the component masses and keeps updating the gross take-off weight until convergence. All other mass estimating relations are rather straightforward, except for the thermal protection mass, which uses an areal density of the protection material. In previous work, ten Houte de Lange selected titanium as the best TPS material to use on the Mk-III, which has an areal density of 5.29 kg/m^2 for a layer of sufficient thickness to withstand most encountered aerothermal loads [20].

$$W_{empt} = W_{GTOW} - W_{propellant} \tag{3.35}$$

$$W_w = 0.2958 m f \left[\left(\frac{W_{empt} ULF}{1000} \right)^{0.52} S_{ref}^{0.7} A^{0.47} \left(\frac{1+\lambda}{t/c} \right) \left(0.3 + \frac{0.7}{\cos \Lambda_{1/2}} \right) \right]^{1.017} \tag{3.36}$$

$$W_{fin,v} = 5 (S_{fin,v})^{1.09} \qquad W_{tps} = W_{ins} (S_{tb} + S_{ref}) \tag{3.37}$$

$$W_{gear} = 0.00916 W_{GTOW}^{1.124} \tag{3.38}$$

$$W_{thr} = \begin{cases} 0.0025 F_{t,rkt} & \text{: Rocket} \\ 0.00625 F_{t,ab} + 69 & \text{: Airbreathing} \end{cases} \tag{3.39}$$

Having computed all structural component masses using the relations above, the structural weight is found.

$$W_{str} = W_b + W_w + W_{fin,v} + W_{tps} + W_{gear} + W_{thr} \tag{3.40}$$

Two parts are present in the propulsion system mass, the engine mass and the propellant tank mass. The prior is computed depending on the type of propulsion used and the number of engines as seen in Equation 3.41 and Equation 3.42.

$$W_{tbj} = 1375 kg \qquad W_{rj} = 0.01 T_{tot,rj} \tag{3.41}$$

$$W_{rkt} = 0.00766 T_{tot,rkt} + 0.00033 T_{tot,rkt} \epsilon^{0.5} + 130 N_{eng,rkt} \tag{3.42}$$

Tank dimensions were already computed in the previous section and are now used to compute the mass of the propellant tanks. For this, the shell mass method was followed presented by Zandbergen [6] where the propellant tanks are assumed to be thin shell structures of which the shell mass is computed. Then, this mass is multiplied by a correction factor to account for add-ons. The shell volumes are computed as in Equation 3.43 when using common bulkhead cylindrical tanks and Equation 3.44 when using spherical tanks. By multiplying these volumes by the density of the tank material, carbon-epoxy in this case, the shell masses are found.

$$V_{shell,ox_1} = 4\pi \left(\frac{D_{t,ox_1}}{2}\right)^2 t_{t,ox_1} + \pi D_{t,ox_1} l_{cyl,ox_1} t_{cyl,ox_1} \qquad V_{shell,f_1} = \frac{4}{2}\pi \left(\frac{D_{t,f_1}}{2}\right)^2 t_{t,f_1} + \pi D_{t,f_1} l_{cyl,f_1} t_{cyl,f_1} \tag{3.43}$$

$$V_{shell,ox_1} = 4\pi \left(\frac{D_{t,ox_1}}{2}\right)^2 t_{t,ox_1} \qquad V_{shell,f_1} = 4\pi \left(\frac{D_{t,f_1}}{2}\right)^2 t_{t,f_1} \tag{3.44}$$

$$m_{shell,ox} = V_{shell,ox} \rho_{t,m} \qquad m_{shell,f} = V_{shell,f} \rho_{t,m} \tag{3.45}$$

A shell mass correction factor of 1.85 is then proposed, which is the average of two ranges provided by Zandbergen [6], resulting in the total tank mass as stated in Equation 3.46. Notice that the tank mass is

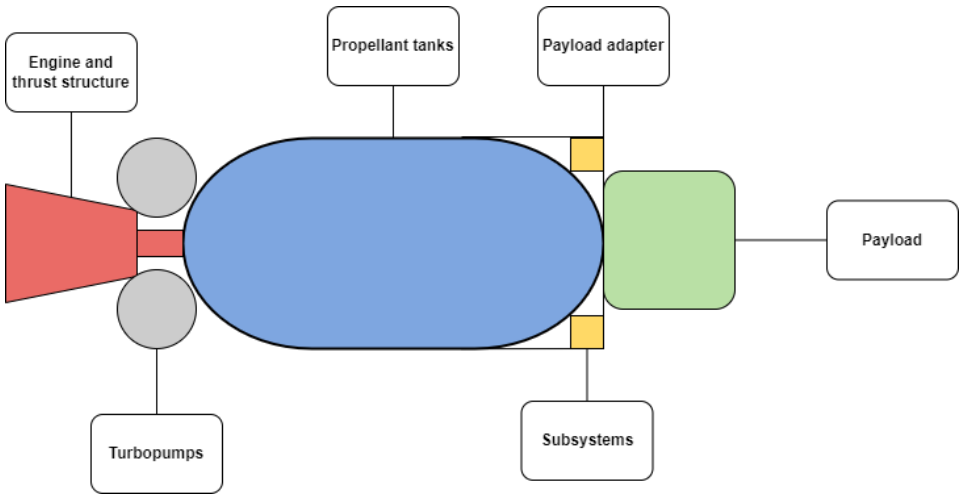

Figure 3.10: Upper stage geometry inspired by the work of Haex [17]

computed in metric units because it is based on the actual geometry of the tanks rather than a statistical estimating relation. m_{tank} in kg is converted to W_{tank} in lbs when computing the total propulsion system weight.

$$m_{tank} = m_{shell} K_{shell} \tag{3.46}$$

The rocket propulsion mass is then found by simply adding the two component masses.

$$W_{propulsion} = W_{eng} + W_{tank} \tag{3.47}$$

Lastly, the subsystem masses are computed, being the hydraulic system, avionics and electrical system masses which are computed as in Equation 3.48 and Equation 3.49.

$$W_{hydr} = 2.64\left[\left(\frac{(S_{ref} + S_{wfv})Q_{max}}{1000}\right)^{0.334} + (l_b + b_{span})^{0.5}\right] \tag{3.48}$$

$$W_{av} = 66.37 W_{GTOW}^{0.361} \qquad W_{elect} = 1.167\left(W_{GTOW}^{0.5} l_b^{0.25}\right) \tag{3.49}$$

As before, adding the component weight results in the subsystem total weight.

$$W_{sub} = W_{hydr} + W_{av} + W_{elect} \tag{3.50}$$

All of the component weights which form the gross take-off weight are now known except for the payload, which for the first stage is the upper stage gross take-off weight. Therefore, the output of the upper stage mass model, which shall be discussed shortly after, is required as input for the first stage mass model. With this input, the gross take-off mass of the first stage can be computed within the iterative loop discussed previously, until convergence.

$$W_{GTOW} = W_{propellant} + W_{str} + W_{sub} + W_{propulsion} + W_{payload} \tag{3.51}$$

3.3.3. Upper stage geometry model

Contrary to the first stage, the upper stage is a conventional rocket, albeit without a fairing. Therefore, the geometrical shape is much simpler as can be seen from Figure 3.10 and Equation 3.52 where the length is assumed to be fully determined by the payload length, propellant tank length and the engine length. This total length of the upper stage is constrained by the available length l_2 in the first stage, computed by Equation 3.33. The diameter of the upper stage is limited to the first stage diameter minus 10 cm, the same maximum diameter as the first stage propellant tanks, leaving 5 cm on either side between the first and upper stage.

$$l_2 = l_{payload} + l_{tanks,2} + l_{eng,2} \qquad l_{tanks,2} = l_2 - l_{payload} - l_{eng,2} \tag{3.52}$$

Table 3.8: Upper stage component masses to be estimated.

Component masses			
Rocket engine	$m_{eng,2}$	Valves	m_{valves}
Thrust structure	$m_{thr,2}$	Avionics	$m_{av,2}$
Propellant tanks	$m_{tanks,2}$	EPS	m_{EPS}
Turbo pumps	m_{pump}	Payload adapter	m_{pla}
Inter-tank structure	m_{inter}		

Now, the total upper stage length is constrained by the first stage, the payload length is determined by common payload dimensions for a certain payload mass, 0.97 m in this case, and the engine length can be computed by Equation 3.32 using the upper stage vacuum thrust given by Dawn Aerospace [15]. As a consequence, the propellant tank length is fully constrained and can be determined, which in combination with the upper stage diameter that is known, allows for the total available propellant storage volume to be computed. Knowing the available storage volume, the maximum propellant mass that can be stored in the upper stage can also be found together with the separate tank dimensions thanks to the O/F and propellant densities that are known. Using the same, common bulkhead configuration and definitions as in Figure 3.9, the total tank length is as stated on the left-hand side of Equation 3.53. putting all unknowns to one side, and the known lengths to the other, the right-hand side of Equation 3.53 is obtained.

$$l_{tanks,2} = l_{ox_2} + l_{f_2} - \frac{D_{t,2}}{2} \qquad l_{ox_2} + l_{f_2} = l_2 - l_{payload} - l_{eng,2} + \frac{D_{t,2}}{2} \tag{3.53}$$

Alternative expressions for the oxidiser and fuel tank lengths were already found in Equation 3.29 for the first stage and can be reused here for the upper stage. These equations involve V_{t,ox_2} and V_{t,f_2}, both of which can be expressed in terms of total propellant mass. In a similar fashion as Equation 3.27 and Equation 3.28 but now taken together and modified for the upper stage results in Equation 3.54. These expressions can then be plugged into Equation 3.29 (but modified for the upper stage) after which the equation is reshaped to end up with an expression for the maximum propellant mass that can be stored in the available length, Equation 3.55.

$$V_{t,ox_2} = 1.05\frac{m_{prop,2}O/F}{(1+O/F)\rho_{ox}} \qquad V_{t,f_2} = 1.05\frac{m_{prop,2}}{(1+O/F)\rho_f} \tag{3.54}$$

$$m_{prop,2} = \frac{\left((l_{ox_2} + l_{f_2}) - \frac{3}{2}D_{t,2}\right)\frac{\pi}{4}D_{t,2}^2 + \frac{\pi}{6}D_{t,2}^3}{1.05\left(\frac{O/F}{(1+O/F)\rho_{ox}} + \frac{1}{(1+O/F)\rho_f}\right)} \tag{3.55}$$

From this total propellant mass, the oxidiser and fuel masses and volumes are found which then lead to the computation of the tank dimensions, following the same procedure as the first stage.

3.3.4. Upper stage mass model

The upper stage mass model is much different than the first stage and requires the component masses listed in Table 3.8 to be computed and added to the payload and propellant mass.
First addressing the propulsion system components, the engine and thrust structure masses are estimated using Equation 3.56, only requiring the total vacuum thrust [3]. The propellant tank mass is calculated in the same way as for the first stage, explained from Equation 3.43 until Equation 3.46 except Equation 3.44, given that the tank dimensions have been determined in the upper stage geometry module and assuming the same shell mass correction factor.

$$m_{eng,2} = 1.104 \cdot 10^{-3} F_{t,vac} \tag{3.56}$$

$$m_{thr,2} = 2.55 \cdot 10^{-4} F_{t,vac} \tag{3.57}$$

Next, the assumption is made that turbo pumps are utilised as a pressurisation mechanism. Their mass is computed via Equation 3.58 [6].

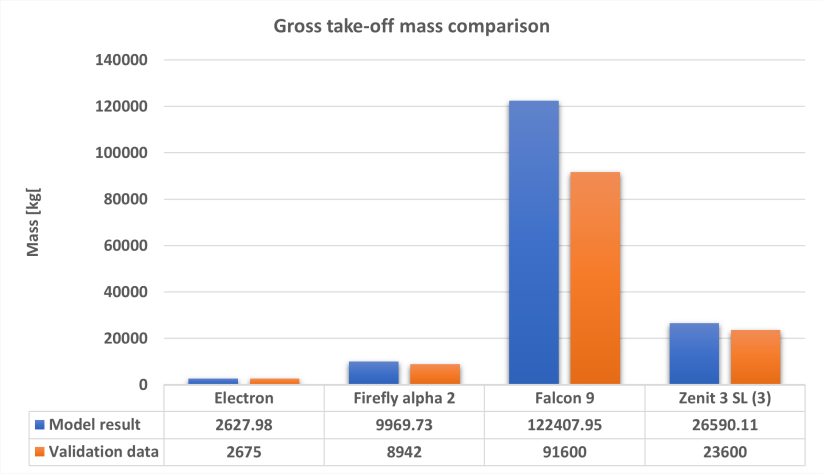

Figure 3.11: Gross take-off masses resulting from the mass model compared with validation data.

$$m_{pump} = C_{prop} C_{pump} \left(F_{t,vac} p_c\right)^{0.71} \qquad C_{prop} = 0.19 \quad C_{pump} = 1 \tag{3.58}$$

Because the tanks are configured in a common bulkhead design, there is no inter-tank structure which must be taken into account in the weight estimation and can be set to zero [11].
The subsystem component masses which involve the avionics, EPS and payload adapter masses are the final components to be estimated, which is done through Equation 3.59 and Equation 3.60 [11].

$$m_{av,2} = 0.25(246.76 + 1.3183 D_{upper} l_{upper}) \qquad m_{EPS} = 0.3321 m_{av} \tag{3.59}$$

$$m_{pla} = 0.00478 m_{payload}^{1.0132} \tag{3.60}$$

This results in a dry and gross take-off mass as stated in Equation 3.61 and Equation 3.62, the latter of which is used as input to the first stage mass model, as previously stated.

$$m_{dry,2} = m_{eng,2} + m_{thr,2} + m_{tank,2} + m_{pump} + m_{inter} + m_{valves} + m_{av,2} + m_{EPS} + m_{pla} \tag{3.61}$$

$$m_{GTOM,2} = m_{dry,2} + m_{payload} + m_{prop,2} \tag{3.62}$$

3.3.5. Mass model validation

As the mass model of the first stage is NASA's Hypersonic Aerospace Sizing Analysis, which is a widely used and already validated method, the mass model of the first stage does not need validation. It does need verification to ensure all computations are programmed correctly. This is done by comparing calculations of the mass model with computations done by hand and verifying correspondence. Using this method, the first stage mass model has been verified.

The upper stage mass model, on the other hand, makes use of mass estimating relations collected from different sources in literature and does require validation. Data is gathered on the upper stage of four launch vehicles: the Electron, Firefly Alpha 2, Falcon 9 v1.1 and the Zenit 3 SL which serve as reference vehicles for validation. First, the acquired input validation data is entered into the upper stage geometry model, after which the outputs of the geometry model are put into the upper stage mass model, together with the remaining validation input data. The resulting gross take-off and empty masses computed by the model are then compared to the actual mass budgets of the reference vehicles. Figure 3.11 and Figure 3.12 were constructed which show the comparison of the computed gross take-off masses and empty masses respectively and the reference vehicle data found in literature.
From Figure 3.12 it is apparent that in general the dry mass is estimated fairly accurately except for the Zenit 3 SL where the discrepancy is large. This may be attributed to the older and heavier materials that are used

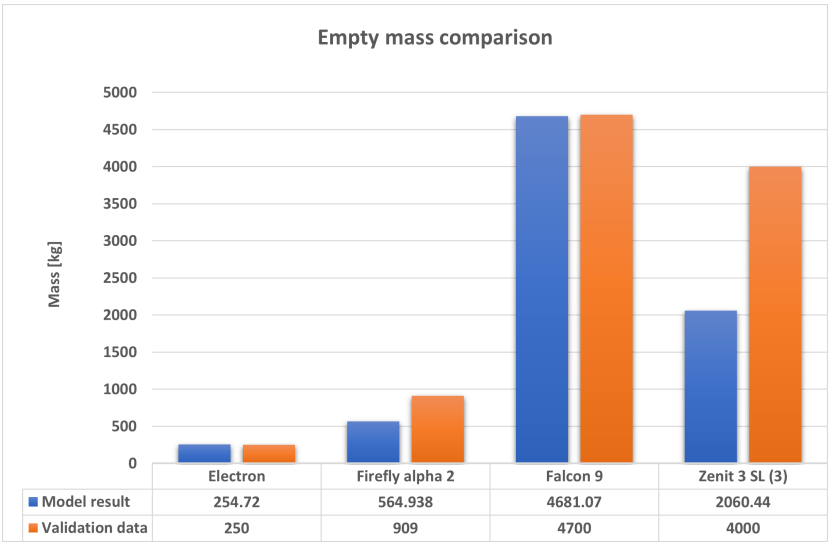

Figure 3.12: Empty masses resulting from the mass model compared with validation data.

in this vehicle compared to the other three which are modern launch vehicles using composite structures, known to be lighter. Also, the Falcon 9 upper stage dry mass is taken without fairing as this mass could be separately obtained. The Zenit 3 SL and Firefly Alpha 2 do include the fairing mass which also could explain the underestimation from the model, because the Mk-III upper stage does not use a fairing, a fairing mass is of course not included in the model. The gross take-off mass on the other hand indicates that the propellant mass is generally overestimated, except for the electron. This is because the upper stage model is very much focused on maximising the available propellant volume. For the reference vehicles, this may not be the case and other components are perhaps assumed to take more volume. Still, it can be said, especially for modern launch vehicles, that the upper stage mass model produces accurate results and can be used for further analysis.

3.4. Aerodynamic model

Crucial to analyse the vehicle's performance, is the aerodynamic model which determines the aerodynamic forces acting on the vehicle. The goal of this model is to obtain a lift and drag coefficient for each Mach number and angle of attack combination along the trajectory. Since the Mk-II geometry was assumed for the first stage of the Mk-III it is deemed logical to assume the performance in terms of aerodynamic coefficients to be the same as well. A text file was then provided by Dawn Aerospace containing the lift and drag coefficients for a range of Mach numbers and angle of attack combinations. The aerodynamic model consists of extracting these coefficients from the txt file, processing them and selecting the right coefficient for the corresponding input Mach number and angle of attack. The range of angles of attack over which the data spans is from 0° to 20° and is considered wide enough. The Mach number range however should be extended further as data is only provided until Mach 4. In addition, the spacing between the angles of attack is 4 degrees and between Mach numbers 0.1 at a minimum and 1.0 at a maximum, therefore the data should be interpolated in two dimensions to be able to provide accurate data for angles and Mach numbers which fall between data points.

Firstly the aerodynamic model reads the content of the txt file and creates a two-dimensional matrix containing the aerodynamic coefficients and two one-dimensional matrices containing the Mach numbers and angles of attack at which the aerodynamic measurements were done. Then, the coefficient data is interpolated in two dimensions using the scipy library which contains a 2D interpolation function that allows the user to specify the desired spacing of the interpolated data points.
Hereafter, the interpolated data is extrapolated with respect to the Mach number alone, up until Mach 6 which is expected to be the maximum velocity the first stage will experience. Again, the scipy library is used which has a curve-fitting function that fits a polynomial through a set of data points. Using this function, curves were fitted through the aerodynamic data of the supersonic regime (after the transonic regime). By extending these curves to Mach 6, the data could be extrapolated. After experimenting with different order polynomials, a third-order polynomial gave the best fit. Again the user can specify the spacing of the extrapolated data.

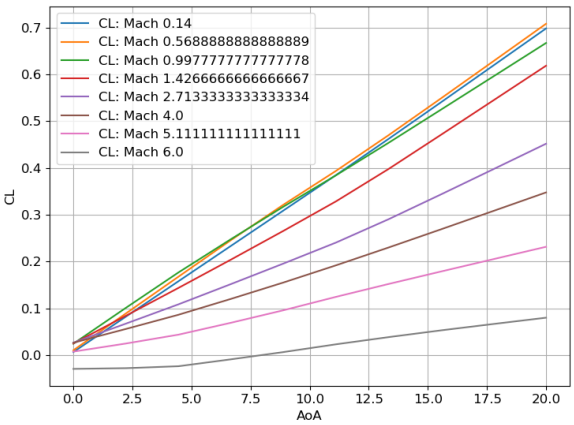

(a) Lift coefficient vs angle of attack for 0.14 < M < 6

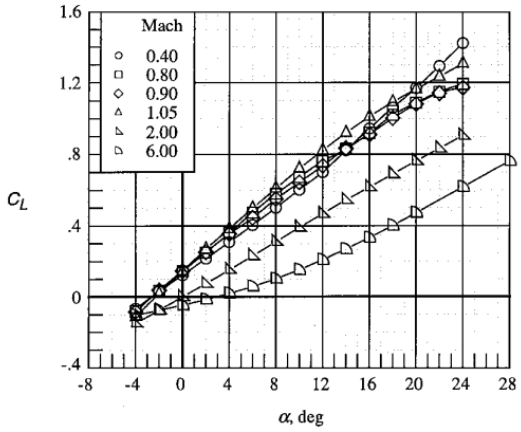

(b) Lift coefficient vs angle of attack for 0.4 < M < 6 [10].

Figure 3.13: Side-by-side comparison of the lift coefficient evolution of the aerodynamic model and the X-34 test vehicle.

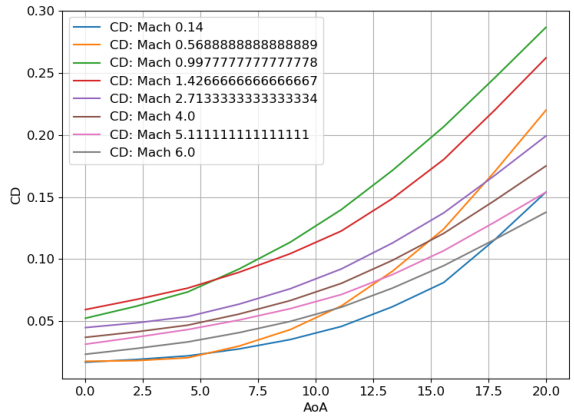

(a) Drag coefficient vs angle of attack for 0.14 < M < 6

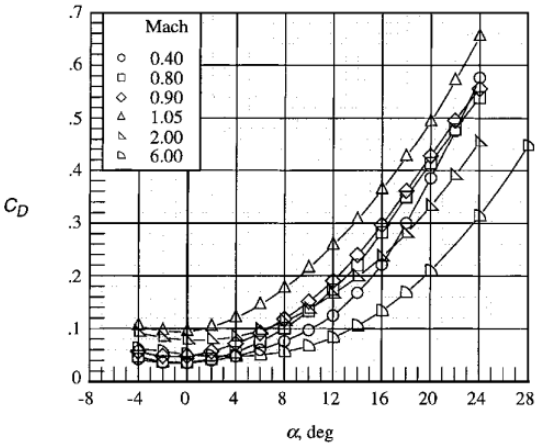

(b) Drag coefficient vs angle of attack for 0.4 < M < 6 [10].

Figure 3.14: Side-by-side comparison of the drag coefficient evolution of the aerodynamic model and the X-34 test vehicle.

The reason for not using the subsonic and transonic data to base the extrapolation on is that at these speeds completely different phenomena occur. If this data would be used, then the fitted curves would be skewed in a different shape leading to, unrealistic lift and drag coefficients. Lastly, but most importantly, two of the inputs of this model are the Mach number and angle of attack at which C_L and C_D are required. The model will find the data point closest to this combination of Mach number and angle of attack and return the coefficient values at this point.

3.4.1. Aerodynamic model validation

It is difficult to validate the aerodynamic model in numerical values as it is based on test data of the Mk-II and other reference vehicles will have a different geometry thus also a different aerodynamic performance. Still, the validity of the test data can be checked as well as the extrapolation procedure by comparing plots of the aerodynamic coefficients to those of other, comparable vehicles. One such vehicle which has a well-documented aerodynamic performance, is the X-34 test vehicle developed by Orbital Sciences. Brauckmann presented the aerodynamic data of a subscale model in a series of wind tunnel tests [10] which can be used to compare the general shape of the curves obtained by the aerodynamic model. In Figure 3.13 and Figure 3.14 one can find the side-by-side comparison of the lift and drag coefficients with respect to the angle of attack, for various Mach numbers. The general shape of the curves seems to match rather well and when looking closely, the C_L and C_D values are within the same order of magnitude as for the X-34. Considering the matching shapes and orders of magnitude, it can be said that the aerodynamic model produces trustworthy coefficients for a given Mach number and angle of attack combination up until Mach 6.

4

Modelling of the Vehicle Trajectory

Crucial to the design is the vehicle trajectory, which can make or break a vehicle's performance. In this chapter, the segments of which the trajectory consists will be discussed as well as how they are modelled. The latter includes which accelerations are assumed to be acting on the vehicle, the equations of motion that are solved, how the trajectory is controlled, i.e. the implemented guidance, how the airbreathing phases are set up and finally also the constraints to which the trajectory is submitted.

To model the vehicle's motion, its differential equations of motion need to be solved, which can be given in spherical coordinates within the Earth-Centered-Earth-Fixed rotational reference frame, the full form being provided by Mooij [29]. However, to simplify the simulation, the system was constrained to 3 degrees of freedom, bar the return to launch site manoeuvre, eliminating any sideslip, or yaw meaning that the only out-of-plane motion is caused by earth's rotation. This allows to have only the angle of attack as a control parameter of the vehicle attitude. The full equations of motion and corresponding kinematic equations are provided from Equation 4.1 until Equation 4.6, these are adapted accordingly to each phase of flight and environmental conditions. In Figure 4.1 a visual representation is given of the parameters involved to provide a better understanding of the system of equations to be solved.

$$\dot{V} = \frac{F_t \cos\alpha - D}{m} - g(r)\sin\gamma + \omega_E^2 r \cos\delta(\sin\gamma\cos\delta - \cos\gamma\sin\delta\cos\chi) \tag{4.1}$$

$$\dot{\gamma} = \frac{(F_t \sin\alpha + L)\cos\mu}{mV} + \left(\frac{V}{r} - \frac{g(r)}{V}\right)\cos\gamma + 2\omega_E \sin\chi\cos\delta + \frac{\omega_E^2 r\cos\delta(\cos\gamma\cos\delta + \sin\gamma\sin\delta\cos\chi)}{V} \tag{4.2}$$

$$\dot{\chi} = \frac{(F_t \sin\alpha + L)\sin\mu}{mV\cos\gamma} + \frac{V\cos\gamma\sin\chi\tan\delta}{r} + 2\omega_E(\sin\delta - \cos\chi\cos\delta\tan\gamma) + \frac{\omega_E^2 r\sin\delta\cos\delta\sin\chi}{V\cos\gamma} \tag{4.3}$$

$$\dot{r} = V\sin\gamma \tag{4.4}$$

$$\dot{\delta} = \frac{V\cos\gamma\cos\chi}{r} \tag{4.5}$$

$$\dot{\tau} = \frac{V\cos\gamma\sin\chi}{r\cos\delta} \tag{4.6}$$

Lastly, the vehicle mass is propagated by solving Equation 4.7 where q is the vehicle mass rate.

$$\dot{m} = -q \tag{4.7}$$

The trajectory is split up into two main segments, that of the first stage and that of the upper stage. The upper stage trajectory is decoupled from the first stage by defining separation conditions which serve as the initial state of the upper stage and as the final desired state of the first stage. The advantage of this is that

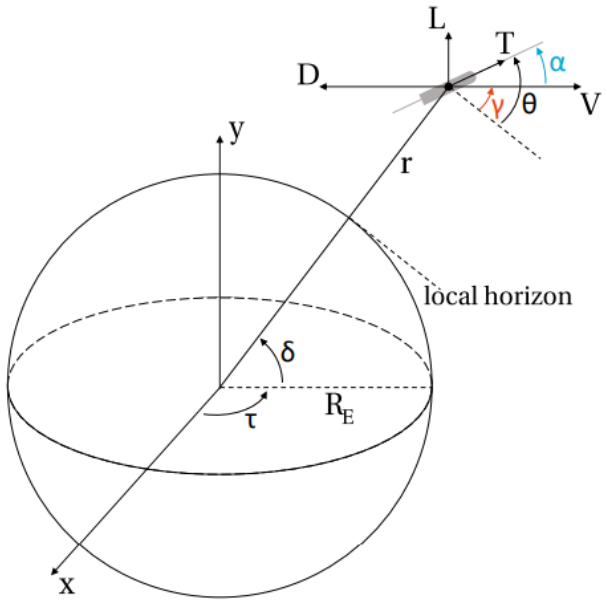

Figure 4.1: Illustration of vehicle state in the Earth-Centred-Earth-Fixed rotating reference frame (original figure adapted by Haex from the work of Balesdent[17][7]).

the influence of separation conditions on both stages can be investigated more easily and swiftly as only simulations for a single stage need to be run compared to one large simulation which is more computationally intensive. Also, this allowed for taking into consideration the preferences of Dawn related to the separation conditions in a simpler way. First, the upper stage trajectory will be discussed, followed by the first stage trajectory, then, the models are validated via a comparison of results to literature. The upper stage is discussed first because it is used as input to the first stage trajectory in the form of upper stage mass which depends on the trajectory and selected separation conditions.

4.1. Upper stage trajectory model

From the separation conditions, which are defined in terms of velocity, altitude, flight path and heading angle, the upper stage aims to inject a payload of 250 kg into a sun-synchronous orbit at 600 km altitude. If the vehicle is able to inject payload into this type of orbit, it is capable of answering most needs of the current launch vehicle industry within this payload category. There are two possible ways to reach this orbit from the separation conditions, which are a direct ascent to orbit and a direct ascent to a parking orbit, followed by a Hohmann transfer, both illustrated in Figure 4.2. The prior offers advantages mainly in terms of the time it takes to reach orbit and the control requirements. The latter however is more propellant efficient for a target orbit above 300 km, reducing upper stage mass [42]. For this reason, a direct ascent to a circular parking orbit at 200 km is selected, followed by a Hohmann transfer to the circular target orbit at 600 km altitude.

Having decided the type of transfer orbit, the mission profile and upper stage trajectory can be discussed in more detail. Starting from separation, the upper stage ignites its rocket engine for an amount of time, being the burn time. After burnout, the vehicle enters a ballistic arc or coasting period, as it is assumed that only gravity acts on the upper stage and all aerodynamic loads can be neglected. The culmination point or apogee of this ballistic arc must then reach 200 km in altitude such that a second burn can increase the velocity of the vehicle to the circular orbital velocity at this altitude, essentially injecting the Mk-III into its parking orbit. At this point, there should be enough propellant left in the upper stage to provide the ΔV required for the Hohmann transfer to the target orbit. For simplicity of modelling, it is assumed that the circularising burn and burns for the Hohmann transfer, are done in the form of impulsive shots, normal to the gravitational force vector, eliminating gravity losses.

To determine if an upper stage design has sufficient propellant on-board after its first burn, to circularise the

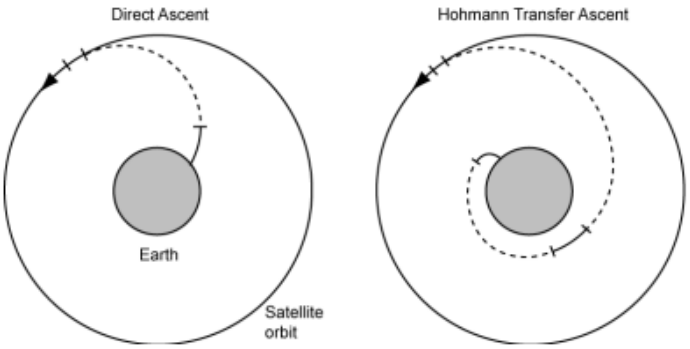

Figure 4.2: Comparison of a direct ascent to orbit and a Hohmann transfer ascent [42]

parking orbit and perform the Hohmann transfer, the required ΔV for these manoeuvres is to be computed as well as the necessary propellant for these manoeuvres. Using Keplerian orbital mechanics, the circular velocity at the parking orbit altitude is computed by Equation 4.8 and the needed velocity increment is found by subtracting the velocity at the culmination point of the ballistic arc as in Equation 4.9.

$$V_{circ,park} = \sqrt{\frac{\mu}{r_{park}}} \tag{4.8}$$

$$\Delta V_{circ,park} = V_{circ,park} - V_{culmination} \tag{4.9}$$

The velocity budget required for the Hohmann transfer consists of a first burn which injects the vehicle in an elliptical orbit with the perigee at the parking orbit altitude r_1 and the apogee at the target orbit altitude r_2 requiring ΔV_1 as in the left-hand side of Equation 4.10. Once at the apogee of this elliptical orbit, a circularising burn is performed which raises the perigee to the target orbit altitude, requiring ΔV_2 as in the right-hand side of Equation 4.10. The eccentricity of the transfer orbit is computed by Equation 4.11.

$$\Delta V_1 = V_{c_1}\sqrt{1+e} - V_{c_1} \qquad \Delta V_2 = V_{c_2} - V_{c_2}\sqrt{1-e} \tag{4.10}$$

$$e = \frac{r_2 - r_1}{r_2 + r_1} \tag{4.11}$$

The total ΔV budget required after reaching the parking orbit is then obtained via Equation 4.12.

$$\Delta V_{tot} = \Delta V_{circ,p} + \Delta V_1 + \Delta V_2 \tag{4.12}$$

Using the Tsiolkovsky rocket equation, the propellant mass required for these manoeuvres is found which is used to verify if a vehicle design has enough propellant left after the first burn and reaching the required altitude. No gravity or steering losses are taken into account because of the assumption of tangential impulsive shots.

$$\Delta V_{tot} = I_{sp} g_0 \ln \frac{m_{initial}}{m_{dry}} \tag{4.13}$$

4.1.1. Upper stage guidance

To control the powered upper stage ascent trajectory, the angle of attack is modulated by using a parametric control law as proposed by Haex and Balesdent [17][7] which provides an input desired flight path angle, compares it to the actual flight path angle and determines the vehicle's angle of attack that needs to steer the vehicle towards the desired flight path angle. In mathematical terms, such a control law can be expressed as in Equation 4.14, where K_c is the gain factor which is assigned a value of 5 in the work of Haex for best results, which was confirmed during the work of this thesis [17]. The desired flight path angles are given as input to the trajectory model in the form of control nodes which are equally spaced in time along the powered ascent phase. These control nodes are trajectory design variables to be optimised which is elaborated further upon in Chapter 5.

$$\alpha = K_c(\gamma_{des} - \gamma) \tag{4.14}$$

4.1.2. Upper stage constraints

As for most launch vehicle designs, there are constraints within which the trajectory should remain, this could be to ensure the vehicle integrity or to simply meet the mission requirements. The most obvious constraints are the intermediate and final target orbits which the design should be able to reach. A parking orbit between 195 and 205 km is deemed acceptable, the target orbit however is taken at exactly 600 km altitude.

The maximum longitudinal and lateral accelerations acting on the upper stage are set at 100 m/s^2 (10 g) and 40 m/s^2 (4 g) as determined during the literature review [30]. The third and final constraint to the upper stage is due to the design choice made by Dawn to have an upper stage without a fairing. Without a fairing to protect the payload, the maximum aerothermal flux experienced by the upper stage is limited to 1135 W/m^2 to avoid damaging the payload. Three different expressions are used to compute the aerothermal flux, one for hypersonic continuum flow and one for free molecular flow stated in Equation 4.15, and one transition function between the two different flow regimes provided in Equation 4.16 [23]. Note that R is the object nose radius, taken to be 0.05 m as a conservative estimation.

$$\dot{q}_{st,cont} = \frac{110285}{\sqrt{R}} \frac{\rho_\infty}{\rho_{SL}} \left(\frac{V_\infty}{V_{circ}} \right)^{3.15} \qquad \dot{q}_{st,fm} = \frac{1}{2} \alpha_T \rho_\infty V_\infty^3 \tag{4.15}$$

$$\dot{q}_{trans} = \dot{q}_{cont} \left(1 - e^{\frac{\dot{q}_{fm}}{\dot{q}_{cont}}} \right) \tag{4.16}$$

4.2. First stage trajectory model

The first stage's goal is to take off horizontally, climb and accelerate to the required separation conditions, launch the upper stage and return to the take-off location. The latter is selected to be Rotterdam The Hague Airport which is the closest airport to the offices of Dawn Aerospace in Delft. This divides the first stage trajectory analysis into four segments: take-off, ascent, return to the launch site and landing, each of which will be discussed separately.

4.2.1. Take-off

Because the Mk-III takes off horizontally, just like an aircraft it can be modelled as such. The take-off phase starts when the engines ignite until lift-off is reached. For this segment, the equations of motion are a little bit different than those described above at the top of this chapter. For the take-off only the translational motion in the velocity direction is considered which is defined by the thrust, drag, vehicle weight, generated lift and friction drag as illustrated in Figure 4.3 which results in the equation of motion as in Equation 4.17 where the last term represents the friction drag. For the friction factor, a value between 0.02 and 0.05 is often proposed depending on the runway surface and vehicle tires, for now, a value of 0.03 is assumed. During the take-off, the angle of attack is kept at zero, until the lift-off velocity is reached at which the vehicle rotates to increase its angle of attack and lift coefficient, such that enough lift can be generated to lift off. This angle of attack is limited by the landing gear and is taken to be 15 degrees.

$$\dot{V} = \frac{T - D}{m} - \frac{\mu(W - L)}{m} \tag{4.17}$$

4.2.2. Ascent

The moment that the Mk-III lifts off from the ground the ascent phase starts which has a slightly different profile for every concept considered. The baseline design, using only rocket propulsion is the simplest as it only continuously utilises its rocket engine up until the separation conditions are reached. On the other hand, the ramjet concept is firstly accelerated by the rocket engines until at a certain Mach number, the ramjets ignite and take over until the designated propellant for the airbreathing engines is burned. Thereafter the rocket engines are reignited and propel the spaceplane to the desired altitude and velocity for separation. Different than for the two other concepts, the turbojet design uses its airbreathing engines from the start of the take-off phase until all of the designated fuel is burned. At this point, the rocket engines are ignited to continue the ascent. The equations of motion to be solved are as those given from Equation 4.1 until Equation 4.6, keeping the bank angle at zero degrees during the entire ascent.

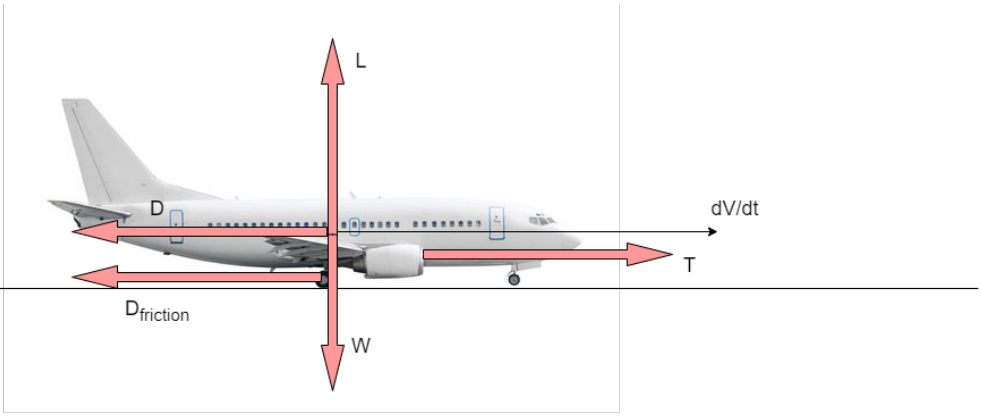

Figure 4.3: Schematic of the relevant forces and acceleration acting on the vehicle during take-off.

4.2.3. Return to launch site

After reaching the separation conditions and launching the upper stage, the first stage enters an unpowered ballistic trajectory which sees the vehicle decelerating until the culmination point before it returns and accelerates towards the earth, eventually re-entering the atmosphere. To complete the return to launch site, multiple options exist for the baseline and airbreathing concepts. For the prior, Haex already identified and compared three possible return methods based on the work of Hellmann, in-plane pitch over, aeroturn and glideback [19].

In-plane pitch over requires the spaceplane to pitch up or down and turn 180° right after upper stage separation, followed by a boost burn to increase the downrange. Because this manoeuvre is executed before re-entry and the velocity is decreased by the boost burn, this type of return reduces the thermal loads experienced during re-entry, albeit at the cost of a more complex control system. An aeroturn is only initiated after re-entry and makes use of the aerodynamic surfaces of the spaceplane to turn it towards the launch site. Once the turn is completed, a return boost is done to increase the downrange of the vehicle. This method is much more demanding on the thermal protection system as the vehicle is not decelerated before re-entry, unlike the in-plane pitch-over. Lastly, the glide back can be seen as the same manoeuvre as the aeroturn but without the return boost [17][19]. The comparison done by Haex showed that a powered return method for the Mk-III is not required and not even necessarily beneficial in terms of gross take-off mass compared to the passive return method which is the glide back. Therefore, for design simplicity, a glide back return manoeuvre is chosen as the return method for the baseline design.

Because of the higher specific impulse of the airbreathing engines, they can be operated for a prolonged period of time compared to a rocket engine, without requiring excessive amounts of propellant, hence, the airbreathing concepts allow for a flyback return method rather than a boost back method such as the aeroturn and in-plane pitch over. The turning manoeuvre for the flyback also makes use of the aerodynamic surfaces of the spaceplane via banking until the desired heading is reached, after which the airbreathing engines can be restarted. The altitude and velocity at which the airbreathing engines are started depends on the type of airbreathing engine. Successful return to launch site is achieved when the vehicle is able to reach the longitude and latitude from the start of the ascent phase before touching down.

4.2.4. Guidance

For any launch vehicle, proper guidance is crucial to ensure that the vehicle follows the desired (optimal) trajectory. For the Mk-III, both the ascent and the return flight need to be guided, the prior only involving a change in angle of attack to fly the desired flight path profile, whereas the latter includes both the angle of attack and bank angle to perform the return manoeuvre adequately.

Ascent guidance

As mentioned before and similar to the upper stage, the first stage ascent is guided by modulating the angle of attack in order to change the vehicle's flight path angle towards a desired value which is done by using the parametric control law provided in Equation 4.14. Six control nodes, spaced equally along the ascent trajectory provide a desired flight path angle for the vehicle to follow at those times. Between those time stamps,

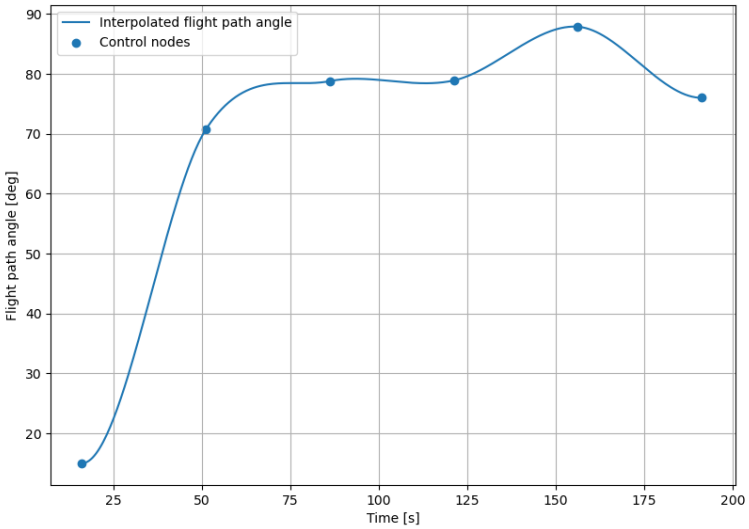

Figure 4.4: Example of the parametric control law with control nodes containing the desired flight path angles and the resulting interpolated flight path angle profile.

the desired flight path angle is interpolated using a cubic hermite spline interpolator as proposed by Dirkx and Mooij aiming to eliminate potential problems occurring due to derivative discontinuities at the control nodes [13]. The flight path angle values at these control nodes are the trajectory design variables to be optimised by the optimiser discussed in chapter 5. An example of the control nodes and resulting interpolated flight path angle profile can be seen in Figure 4.4. By trial and error, the best control performance was found for a gain factor K_c of 1.75 for the first stage control, which is slightly higher than what Haex proposed.

Return guidance

Both the baseline and airbreathing concepts, make use of the aerodynamic surfaces of the spaceplane to perform the return manoeuvre and will therefore also use the same return guidance. This does not only involve the angle of attack but also the bank angle which turns the vehicle until reaching the heading that directs the spaceplane towards the launch site. For the aerodynamic surfaces to make a significant impact on the trajectory, the dynamic pressure must be sufficiently high, which is why the banking manoeuvre is initiated from below a certain threshold altitude. Once this altitude is reached, the Mk-III initiates its turn by taking a maximum bank angle of 40° until the difference between the desired heading and current heading, drops below a threshold value. Once below the threshold heading difference, the bank angle is decreased linearly until 0°. This way of modulating the bank angle, also allows for corrections to be made if the vehicle were to deviate from the desired heading angle for some reason. In mathematical terms, the bank angle modulation is as provided by Equation 4.18.

$$\mu = \begin{cases} 0° & h > h_{thr} \\ \pm 40° & h < h_{thr} \text{and} |\Delta\chi| > 9° \\ 40° \dfrac{(\chi - \chi_{des})}{9} & h < h_{thr} \text{and} |\Delta\chi| < 9° \end{cases} \tag{4.18}$$

The bank angle guidance law is only useful if χ_{des} is provided. Luckily, χ_{des} or in other words the bearing angle can be computed rather straightforward by inserting Equation 4.19 in Equation 4.20. Note that the ls subscript stands for launch site [1].

$$Y = \cos\delta_{ls} \sin(\tau_{ls} - \tau) \qquad X = \cos\delta \sin\delta_{ls} - \sin\delta \cos\delta_{ls} \cos(\tau_{ls} - \tau) \tag{4.19}$$

$$\chi_{des} = \text{atan2}(Y, X) \tag{4.20}$$

For the angle of attack profile during the return flight, a simpler guidance model is selected where first the angle of attack is maximised to 20° in order to decelerate the vehicle as much as possible and limit the downrange before completing the turnaround. Once the turn manoeuvre has been completed the angle of

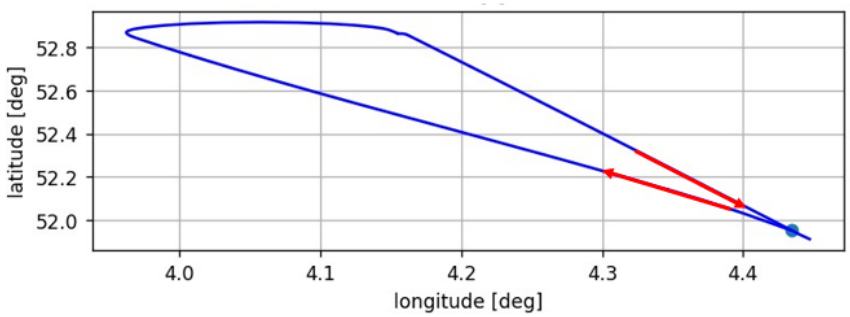

Figure 4.5: Longitude vs latitude from take-off until landing, with launch site indicated by the blue dot.

attack is decreased to the value which results in the highest lift-over-drag ratio for the current Mach number to maximise the gliding range of the vehicle. In Figure 4.5 one can see what a turn looks like in terms of the longitude and latitude of the vehicle thanks to the described return guidance.

4.2.5. Trajectory constraints

Constraints are applied to the first stage trajectory as well, the most important one being the target separation conditions. These are the altitude, velocity and separation flight path angle that must be reached in order for the upper stage to successfully reach the desired orbit. These constraints are imposed as inequality constraints which eliminate any trajectory designs that are too far off the desired separation conditions. For trajectory designs which approach the desired separation conditions, an inequality constraint in the form of the specific energy of the burnout point is applied which eliminates solutions with a lower specific energy than that of the desired separation conditions. The specific energy is computed as in Equation 4.21 and what this type of constraint does, is that it does not immediately eliminate a solution when it for example reaches a smaller velocity at the end of the burn but goes 5 km higher than the specified desired separation altitude. If the specific energy at burnout is equal to or higher than the specified separation conditions, the design could still provide acceptable initial conditions for the upper stage. The other, second most important constraint is the return to launch site constraint which enforces the first stage to reach the launch site after its ascent and deployment of the upper stage. This constraint is also applied as an inequality constraint that eliminates solutions that do not reach the original launch site location.

$$E_{sp} = \frac{1}{2}V^2 + gh \tag{4.21}$$

Less strict constraints include the maximum dynamic pressure, angle of attack range, maximum bending load, maximum accelerations and finally the maximum stagnation heat flux, all applied as inequality constraints in the optimisation procedure as will be discussed in the next chapter bar the angle of attack which is directly applied to trajectory model. A maximum dynamic pressure constraint was already identified by Van Kesteren at 90 kPa for launch vehicle design [22]. In the same work, a bending load was also defined as the angle of attack in radians, times the dynamic pressure, with the maximum allowable value at 18000 Pa $\cdot$ rad. The maximum allowable acceleration in the longitudinal and lateral direction is taken as $100\text{m}/\text{s}^2$ and $40\text{m}/\text{s}^2$ respectively as taken by Haex from the Electron payload user's guide [17]. Lastly, as already mentioned, the angle of attack is limited directly in the trajectory model meaning that no trajectory design involves an angle of attack out of bounds and it is not applied as an inequality constraint in the optimisation scheme. The range of allowable angles of attack for the first stage is between 0 and 20 degrees simply because this is the range for which aerodynamic data is available for the Mk-III.

Although there is not really a constraint put on the maximum experienced stagnation point heat flux during re-entry, it would be smart to keep an eye on it and make sure it does not exceed the values found for other launch vehicles such as the Space Shuttle which had a maximum stagnation point heat flux of 200 kW/m^2. In the work presented by Dirkx and Mooij on the design of re-entry vehicles, a rather simple approximation of the heat flux at the stagnation point was found which is formulated in Equation 4.22 where the left-hand side originates from the work of Chapman and the right-hand side from Anderson [12] [5]. Here, R_N is the nose radius and N_1 and N_2 take the values of 0.5 and 3, respectively, when assuming laminar conditions. When using the cold wall approximation $\frac{T_w}{T_{aw}}$ becomes zero. Note that Haex presented a more accurate and

Table 4.1: Validation vehicle and trajectory in and outputs from the study done by Maddock et al. [26]. *(*) derived value*

First stage		Upper stage	
Dry mass [kg]	11343	Dry mass [kg]	1853.6
Payload mass [kg]	12996	Payload mass [kg]	500.0
Gross take-off mass [kg]	70872	Gross take-off mass [kg]	12996
Max vacuum thrust [kN]	1164.3	Max vacuum thrust [kN]	129.61
Specific impulse [s]	330.31	Specific impulse [s]	352.0
Wing reference area [m^2]	40.0*	Separation velocity [m/s]	2900.0
Initial velocity [m/s]	250.0	Separation altitude [m]	70000
Initial altitude [m]	11000	Separation flight path angle [deg]	27.0
Initial flight path angle [deg]	10.81	Target orbit altitude [km]	600.0

complex method of Fay and Ridell, but for now, the shown method is deemed sufficiently accurate and is simple to implement.

$$q_{c,s} = k\rho^{N_1}V^{N_2} \qquad k = \frac{1.83 \cdot 10^{-4}}{\sqrt{R_N}}(1 - \frac{T_w}{T_{aw}}) \tag{4.22}$$

4.3. Trajectory model validation

To make sure that the created trajectory model is trustworthy and produces correct results, validation of it is needed and extremely important. Although it is rather difficult to find suitable literature which can be used for validation by comparison of outcomes, mostly because of limited documentation which makes it hard to reproduce results. Nevertheless, one study has well-documented trajectory outcomes and inputs as well. This study was also used in two previous theses for validation and was done by Maddock et al. [26]. The vehicle considered in this paper is a rocket-powered two-stage-to-orbit launch vehicle which utilises horizontal launch and landing whilst aiming for a target orbit of 600 km, a very similar concept as the Mk-III considered in this thesis. One might question the validity of using this study as it did not include any designs using airbreathing propulsion, however, if the trajectory model (and optimisation procedure) can be validated for the baseline design, then it is deemed to be valid for the airbreathing concepts as well if their optimised trajectory shapes comply to what is expected by experienced engineers from Dawn Aerospace. No study could found be where an airbreathing launch vehicle was modelled and the results were well documented, hence the chosen validation method. For the upper stage trajectory, this is of no importance as this is a conventional rocket, similar to the one modelled by Maddock et al.

Given in the table below is the data from the vehicle and trajectory obtained in the study done by Maddock et al. which are necessary as input for the trajectory model created above such that the outcomes of both models can be compared to one another and the validity of the trajectory model built in this thesis can be confirmed. Note that the wing reference area is not mentioned in the paper itself and the value seen here was derived by Haex based on the overall vehicle size.
The vehicle described by the parameters in Table 4.1 is created and the trajectory parameters are inserted in the trajectory models. Considering the upper stage first, the validation model included throttling of the engine thrust which was not done in the model built in this thesis and also no direct information was provided on the thrust level along the trajectory. By using the plotted vehicle mass evolution over time provided in the validation paper, an estimation could be made on the mass flow variation with time, which allows the thrust profile to be recreated because the specific impulse is known and the upper stage is assumed to suffer negligible pressure losses. As can be seen from Figure 4.6 this results in an optimised upper stage which closely matches the validation case. both trajectories are able to reach the target orbit although the simulated results have a slightly higher final velocity and a less steep increase in velocity during the first main burn. Still, the difference can be considered negligible, and the validity of the upper stage trajectory can be confirmed by these results.

When running the first stage optimisation model, larger differences can be seen in Figure 4.6 where the full lines are the first stage trajectories. For this part of the trajectory, it seemed that no throttling was applied to the rocket engine thrust which allowed for a more straightforward comparison. From the left-hand side of

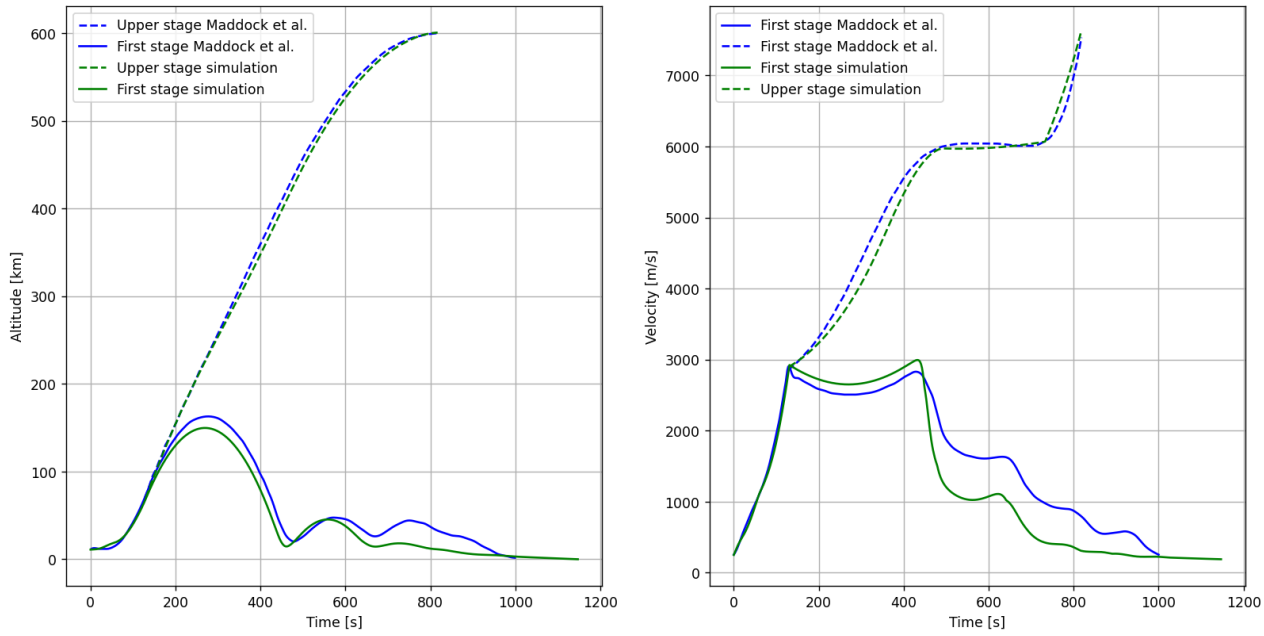

Figure 4.6: Comparison of the trajectory model results for the input data tabulated in Table 4.1 and the results obtained by Maddock et al. [26].

Figure 4.6, the main differences are that the first stage has a lower culmination point of the ballistic arc whilst having a slightly higher burnout velocity (as seen in the plot on the right side). When analysing the flight path angles at burnout, it turned out that for the simulation, it was slightly below that of the validation model, it is known that the initial flight path angle of a ballistic arc is extremely influential on the following trajectory and mostly even on the culmination altitude [46]. In the same plot, the simulation results also show a much longer and more shallow gliding flight after re-entry, this can be explained by the fact that no aerodynamic data is available on the validation vehicle and the aerodynamic coefficients of the Mk-II were used instead. It is most likely that the maximum L/D of the Mk-II is higher than that of the vehicle designed by Maddock et al. leading to an improved and prolonged gliding flight.

The right-hand side of Figure 4.6 which compares velocity versus time, shows a higher separation or burnout velocity for the simulation results, again a possible explanation is the aerodynamic performance of the vehicles being difficult to compare due to a lack of information on the validation vehicle. A higher drag coefficient of the validation vehicle than the Mk-II would explain the slight difference in velocity. Similar to the altitude, a discrepancy in velocity profile can be seen during the return flight as well which indicates that the simulated vehicle slows down much more rapidly than the validation vehicle which might be opposing to the argument of a worse drag performance just mentioned. However, this is not the case, the difference is most likely due to a different return guidance. The return guidance implemented in the trajectory model described in this chapter maintains a maximum angle of attack for maximum drag, which is 20° whereas in the validation study, the angle of attack remains largely below 10° even, only increasing towards 20° at the end of the return phase.

Considering that most of the discrepancies shown between the results obtained by Maddock et al. and the trajectory model built for this report are rather small and that the larger discrepancies can be given a logical explanation, the trajectory model can be accepted to be valid and working. However, as already mentioned the study only included a rocket-powered design and no airbreathing engines. To provide the final argument which confirms the model validity for airbreathing engines as well, discussions were held with an expert from Dawn Aerospace with years of experience, about the expected trajectory outcomes for the airbreathing designs. Briefly summarised, it was expected that the airbreathing trajectories would initially follow a less steep ascent, maximising the thrust-producing capabilities of the airbreathing engines which lie in the denser layers of the atmosphere as here the air is dense enough. From the results, which shall be presented in chapter 6 this was indeed the case, fully confirming that the trajectory model can be trusted to provide sensible results.

5

Numerical Modelling and Optimisation

The previous two chapters elaborately discussed equations, methods, design choices and assumptions to base the vehicle and trajectory models on, the actual tools to numerically model and optimise those models however, have not been touched upon yet and will be done in this chapter. The first and most important tool is the one with which all the numerical modelling is done: TU Delft Astrodynamic Toolbox or TUDAT in short, this tool will be discussed first. Hereafter, the selected optimisation tool is explained, how it works and how it converges to an optimised solution of the design problem which is discussed lastly. The design problem section will mostly provide an overview of the variables optimised by the optimisation scheme.

5.1. TUDAT

As the name suggests, TUDAT is a tool developed by research staff and graduate students at the Faculty of Aerospace Engineering of Delft University of Technology and is essentially a set of C++ libraries [37]. This set of libraries contains a multitude of functions that can be used to model, simulate and design trajectories of spacecraft and launch vehicles by providing atmospheric models of planets within our solar system, propagators, integrators, ephemerides of celestial bodies, thrust models, rotation models and so on. Because the functionality of TUDAT is in C++, which is not the most user-friendly programming language, Tudatpy was developed to provide an interface in the more common Python language that allows the functionality of TUDAT to be accessed [37]. An additional benefit of using TUDAT is that it also includes a library full of built-in optimiser schemes called Pagmo, but more on that later.

5.1.1. Integration and propagation

Because the vehicle's equations of motion consist of a system of differential equations, an integrator is required to solve those equations. Many integrators exist and plenty of them are already pre-built in TUDAT such that the type of integrator just has to be selected and configured instead of building one from scratch. Available integrator types are the variable and fixed step size Runge-Kutta integrators, the Bulirsch-Stoer integrator, and the Adams-Bashforth-Moulton integrator. From the work of Haex who performed a thorough analysis of the type of integrator to be used, it was determined that the Runge-Kutta-Fehlberg method also referred to as RKF45, is a robust scheme with sufficient precision and one that does not require an exorbitant amount of computational power, resulting in the selection of this integrator type during the numerical simulations.

After solving the equations of motion, the vehicle state is to be adapted based on those solved equations, for this a propagator is used. Again, multiple propagator types are available in TUDAT, Cowell's method being the most straightforward one. This method defines the 3-dimensional positional state and its derivative, the velocity, of the vehicle in Cartesian coordinates as in Equation 5.1 where $\mathbf{x}$ is the vehicle state vector [17].

$$\mathbf{x} = \begin{bmatrix} \mathbf{r} \\ \dot{\mathbf{r}} \end{bmatrix} ; \dot{\mathbf{x}} = \begin{bmatrix} \dot{\mathbf{r}} \\ \dot{\mathbf{v}} \end{bmatrix} \tag{5.1}$$

5.2. Numerical optimisation

Before starting this section on numerical optimisation in general and the selected algorithm, the reader should be aware that this thesis is not focused on optimisation itself and as a consequence, the discussion on optimisation methods will be rather short and largely based on the gathered literature by Haex and the work of Balesdent who both wrote theses with multi-disciplinary design optimisation of launch vehicles as the central topic. If the reader is interested in a more in-depth explanation or more information on the topic, he or she is kindly referred to Haex and Balesdent [17][7].

Optimisation, in short, is the procedure of finding the most optimal solution to a given problem, within launch vehicle design this could be to find a design with a maximum payload mass for a given target orbit, or a design with minimum gross take-off mass for given payload and target orbit. Within the field of numerical optimisation, two types of optimisation algorithms can be distinguished, gradient-based algorithms and gradient-free algorithms. Numerous studies in recent years on optimal launch vehicle design by Balesdent [7], van Kesteren [22], Vandamme [39] and Haex [17], all used gradient-free algorithms which results in the tendency to also use such an algorithm for this study. After an extensive literature review by Haex on gradient-free optimisation algorithms, a differential evolution algorithm was chosen because of its excellent convergence and robustness characteristics and will be used in this study.

5.2.1. Differential evolution algorithm

The selected algorithm is the differential evolution 1220 which is a modified version of the differential evolution algorithm. This type of algorithm is bio-inspired and can be classified as a population-based, evolutionary optimisation algorithm, that, as the name suggests, makes use of Darwin's principle of survival of the fittest and was developed by Storn in 1997 [2]. How this algorithm operates and attempts to find the most optimal solution, can be summarised in five steps as presented by Ponnuthurai [35]:

1. **Initialisation:** A random population of a specified amount of individuals is created where every individual is a design vector consisting of a combination of the optimisation variables within the solution space.
2. **Mutation:** Every candidate individual is used to create a mutant vector by combining randomly selected individuals from the population.
3. **Crossover:** Mutant vectors are then combined with the original individuals by using some type of cross-over process. Cross-over can be done based on randomly selected individuals or the best-performing individuals, using binomial or exponential operations. This creates a set of trial vectors or trial individuals.
4. **Selection:** Following the crossover, the fitness level of the trial vectors is determined based on the objective function, in the case of this thesis, this will be the gross take-off mass that is minimised. If the fitness of the trial vector is better than the fitness of the parent, it replaces this parent in the new generation. When done for the entire population, this results in a generation with improved (or at least equal) fitness.
5. **Repeat:** This process, from mutation until selection is repeated for a user-defined amount of generations, leading to a final population that is converged to the optimal solution of the specific problem.

The main difference between the modified DE1220 algorithm and the original DE algorithm is the self-adaptive nature of DE1220 making it more consistent over different types of problems [17].

Besides the fact that the DE1220 algorithm is an excellent optimisation scheme, it is also available in PyGMO. PyGMO is a library in Python, based on the C++ PaGMO library developed at ESA that contains numerous algorithms to solve all sorts of optimisation problems [37]. This library is available and within, and can be easily integrated with the Tudatpy environment, making it an excellent choice to take an optimisation algorithm from.

5.3. Optimisation problem

The goal of the optimisation problem is to find a vehicle and trajectory design which results in the lowest gross take-off mass although many studies optimise for dry mass. The reason why this is not done in this study is that it is expected for the dry mass to be heavier for airbreathing concepts than for the baseline concept, due to the addition of airbreathing engines and the main idea behind airbreathing engines is to save on propellant and mainly oxidiser mass which would result in a reduced gross take-off mass.

Discussing the trajectory optimisation of the upper stage first, the optimisation design vector is as provided in Equation 5.2, containing the burn time, available propellant mass for the Hohmann transfer and trajectory flight path angles at three control nodes along the first burn.

$$\mathbf{x}_{des,up} = \begin{bmatrix} t_b & m_{Hohm} & \gamma_1 & \gamma_2 & \gamma_3 \end{bmatrix} \tag{5.2}$$

For the first stage, the optimisation design vector differs slightly for the different concepts, the baseline containing the ascent burn time, the rocket sea-level rocket thrust and five control nodes equally spaced along the ascent trajectory. Note that the sixth control node is the initial flight path angle and is fixed. For the ramjet design, 4 additional optimisation variables are introduced, the ramjet inlet area, the ramjet ignition Mach number, basically at which Mach number the ramjet is ignited and airbreathing operation starts and finally the ascent and return fuel masses for the airbreathing engines. The latter two design variables require some additional clarification as one might expect a design variable such as the rocket burn time t_b for the airbreathing engines as well instead of fuel masses. The reason for this is due to the variable fuel mass flow of the airbreathing engines that depends on altitude and velocity such that the required fuel mass can not be estimated beforehand meaning that the vehicle mass can not be computed which is very important for the trajectory model. This is solved by assuming a certain fuel mass to be taken on board, designated for the airbreathing engines which operate until this fuel is burned. Also, the return fuel mass is introduced for the powered return of the airbreathing concepts. The turbine concept does not include the inlet area or the initial Mach number variables simply because an already existing turbine engine is used and it operates from take-off until the designated airbreathing fuel is fully burned. To limit the design space, smaller test runs were performed of which the convergence behaviour was analysed in combination with what was expected beforehand based on literature such as the work of Haex [17] and expertise by Dawn Aerospace. This allowed for a more accurate definition of the lower and upper boundaries of the design variables.

$$\mathbf{x}_{des,base} = \begin{bmatrix} t_b & F_t & \gamma_1 & \gamma_2 & \gamma_3 & \gamma_4 & \gamma_5 \end{bmatrix} \tag{5.3}$$

$$\mathbf{x}_{des,ram} = \begin{bmatrix} t_b & m_{f,ascent} & m_{f,return} & A_i & M_{ab} & F_t & \gamma_1 & \gamma_2 & \gamma_3 & \gamma_4 & \gamma_5 \end{bmatrix} \tag{5.4}$$

$$\mathbf{x}_{des,turb} = \begin{bmatrix} t_b & m_{f,ascent} & m_{f,return} & F_t & \gamma_1 & \gamma_2 & \gamma_3 & \gamma_4 & \gamma_5 \end{bmatrix} \tag{5.5}$$

5.3.1. Application of constraints in the optimisation problem

Already mentioned in Chapter 4, were the trajectory constraints applied to the model within which the optimisation problem should find an optimal solution. To converge towards a solution within these constraints and ”guide” the optimiser towards solutions that meet the requirements, penalty functions are applied to the fitness value of individuals. Depending on how much an individual deviates from the target orbit, separation conditions or required downrange, a proportionate penalty value is added to that individual’s fitness, resulting in convergence around the desired target orbit, separation conditions or reaching the landing site. For trajectory constraints such as maximum acceleration, maximum bending load and maximum dynamic pressure, fixed value penalties are added for each instance of a constraint violation to ’push’ the individuals towards trajectories that comply with the constraints. The values or proportionality of the penalties were determined based on trial and error during test runs. A penalty value of 250 kg was added for every time step the trajectory exceeded the dynamic pressure and bending load constraints, 500 kg was added for every violation of the maximum acceleration. The shortage in downrange in meters was taken and multiplied by 0.2 which was then added to the fitness value. The same was done for the discrepancy in separation altitude and velocity, with proportionality factors of 2.5 and 200 respectively. For the upper stage optimisation, the difference in parking orbit altitude and desired target orbit in meters was added to the fitness value and the shortage in ΔV budget for the Hohmann transfer was multiplied by 50.

6

Results and Discussion Thereof

All of the previous chapters, separately, do not provide many answers to the research questions introduced in Chapter 1, together however results can be produced which can answer those research questions which is what is presented in this chapter. Firstly, the baseline design shall be discussed which shall serve as a reference design for comparing the airbreathing designs with. Thereafter, the optimisation results of the ramjet and turbine engine concepts are given. The chapter is concluded with a summary of the findings of the airbreathing designs and how they compare to the baseline design which will form the basis for answering the research questions in Chapter 8.

6.1. Baseline design

The baseline design of the Mk-III is divided into the upper stage design which shall be used for all concepts no matter the propulsion type used, and the first stage design which is of course only specific to the baseline. The results of both optimised stages are presented here.

6.1.1. Upper stage

Previously discussed in Chapter 4 it was mentioned that the upper stage was decoupled from the first stage by using a fixed separation point which leaves endless possibilities of combinations of altitude velocity and flight path angle to take as separation conditions. It speaks for itself that a higher and faster separation point results in a lighter and smaller upper stage but increases the demands on the first stage, not only because it needs to reach a higher altitude and velocity but also because of the increased thermal loads and increased downrange it needs to cover towards the launch site. On the other hand, lower and slower separation conditions reduce these demands on the first stage but increase the mass and size of the upper stage, hence a balanced separation point had to be chosen.

From the start Dawn Aerospace immediately made their preference very clear to have separation conditions as low and slow as possible as this would decrease the thermal requirements on the vehicle drastically during re-entry, therefore three separation altitudes were considered, one of them proposed by Dawn themselves: 80 km, 90 km and 100 km. For 80 km, Dawn proposed a separation velocity of 1175 m/s, to which the same separation Mach number was added as to the other separation altitudes, Mach 5. This separation velocity was chosen because first of all, it is already a significant velocity and secondly because this velocity is not as demanding on the vehicle in terms of thermal and aerodynamic loads. Thirdly, at this separation velocity, the vehicle does not exceed Mach 6 during re-entry which also helps reduce the thermal loads. An additional request by Dawn was for the separation flight path angle to be 60 degrees, however, it quickly became clear from analysis of the first stage, that this would result in not being able to meet the return to launch site requirement and a staging flight path angle higher than 70 degrees would be necessary. This finding is supported by the work of Haex and Sonneveld who also obtained a staging flight path angle above 70 degrees [17][34]. Initially, it was expected that separation at 90 km and Mach 5 would be the best compromise, for a separation angle of 60 degrees this was indeed the case but for the higher separation angles, this superiority quickly disappeared as can be seen from the upper stage characteristics tabulated in Table 6.1. Here it can be seen that the upper stage gross mass for separation at 80 km and 90 km does not differ by a significant

Table 6.1: Upper stage designs for various separation conditions

h_s [km]	v_s [m/s]	γ_s [deg]	γ_1 [deg]	γ_2 [deg]	γ_3 [deg]	M_{GTOM} [kg]	M_p [kg]	M_{dry} [kg]	l_{upper} [m]
80	1175	79	79.4	65.6	28.4	7674	7094	580	6.17
80	1405	79	74.7	43.3	20.1	6675	6104	571	5.84
90	1377	79	65.3	55.1	41.2	6614	6044	570	5.82
100	1431	79	65.5	50.8	17.9	6760	6189	572	5.87

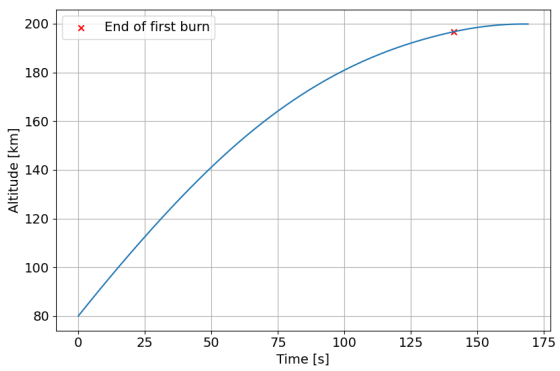

(a) Altitude vs time plot.

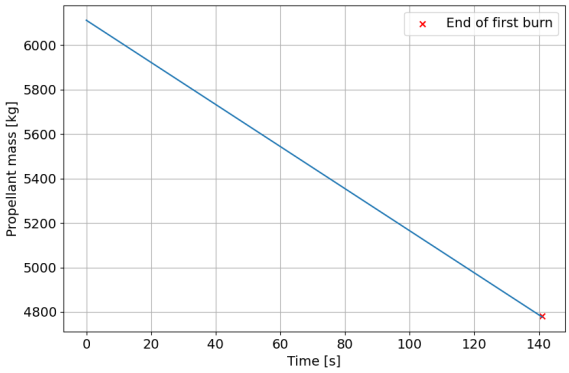

(b) Propellant mass evolution over time during the first burn.

Figure 6.1: Altitude and mass profiles over time for the optimal upper stage trajectory starting from 80 km at Mach 5.

amount and when keeping in mind that the demands on the first stage in terms of altitude to be reached would be lessened significantly, separation at 80 km and Mach 5 becomes the preferred option. The cause of this small difference in mass is two-fold: gravity losses and steering losses. First, because the burn time is so short, the flight path angle during the burn remains higher leading to more gravity losses. Adding to this, a higher initial flight path angle requires more steering in the form of an angle of attack which deviates further from zero than for the lower separation point, meaning higher steering losses. This also explains why separation at 100 km at Mach 5, which would normally result in a lighter upper-stage design, has such a large mass, and many steering and gravity losses.
In Figure 6.1, the altitude and propellant mass profiles over time are presented which nicely show the vehicles capability of reaching the parking orbit, still having 4780 kg of propellant mass on board to perform the Hohmann transfer whereas only 4754 kg was required.

6.1.2. First stage

With the selected separation conditions and upper stage design, all necessary input is at hand to run the optimiser for the baseline first stage. A population of design vectors containing different combinations of burn time, rocket thrust and control node flight path angles is generated and evolved a number of times until convergence is reached. Of course, the final result depends on the initial population that is generated randomly meaning that this procedure had to be repeated a couple of times, from this set of optimal solutions, the best-performing one was selected. The mission profile is listed below and the detailed vehicle design is tabulated in Table 6.2. Note that the burnout conditions slightly exceed the separation conditions stated above which only confirms that the first stage is able to put the upper stage into the required initial state.

- **Payload:** 250 kg
- **Target orbit:** Sun-Synchronous orbit at 600 km altitude.
- **Parking orbit:** Circular orbit at 199.8 km altitude
- **Burnout conditions:**
  - Burnout velocity: 1414 m/s
  - Burnout altitude: 81.6 km
  - Burnout flight path angle: 79°
- **RTLS**

Table 6.2: Detailed first and upper stage designs for the baseline concept

First stage		Upper stage	
Gross take-off mass [kg]	41571	Gross take-off mass [kg]	6675
Dry mass [kg]	7592	Dry mass [kg]	321
Payload mass [kg]	6775	Payload mass [kg]	250
Propellant mass [kg]	27304	Propellant mass [kg]	6104
Sea level thrust [kN]	420	Vacuum thrust [kN]	30
Sea level specific impulse [s]	265	Vacuum specific impulse [s]	320
ΔV [m/s]	2780	ΔV [m/s]	7718
Diameter [m]	1.94	Diameter [m]	1.84
Length [m]	24.25	Length [m]	5.84

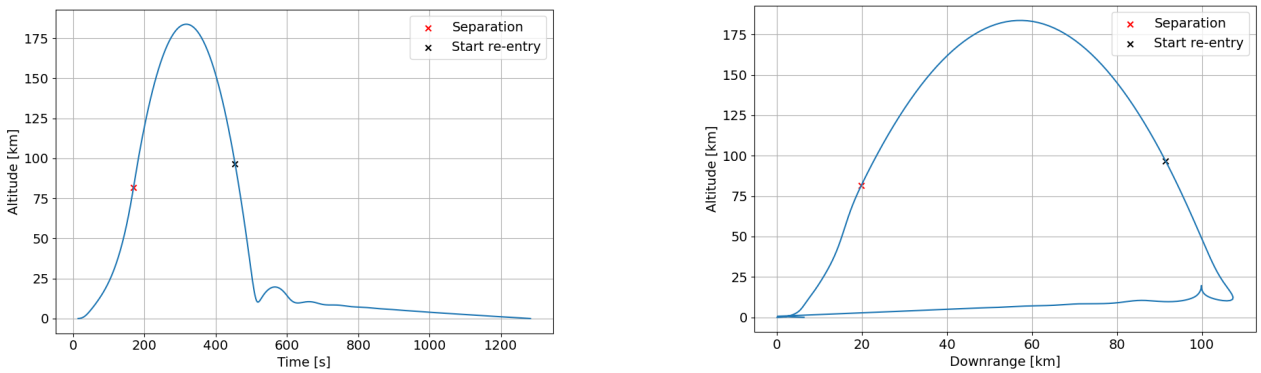

(a) Altitude vs time plot.

(b) Altitude vs downrange plot.

Figure 6.2: Altitude versus time and altitude versus downrange plots for the optimal baseline first stage design.

- Launch site: Rotterdam The Hague Airport
- Return method: Glideback

From Figure 6.2 until Figure 6.4 the trajectory characteristics of the baseline first stage are plotted where Figure 6.2 focuses on the altitude and downrange of the trajectory, Figure 6.2b proving that the vehicle is able to reach the launch site. For this however, as already mentioned in Subsection 6.1.1, a rather high separation angle is required, otherwise the vehicle is not able to glide back to the launch site. One way in which the separation angle could be reduced towards the desired angle by Dawn is to improve the gliding performance of the vehicle, i.e. a higher maximum lift-over-drag ratio. Figure 6.3 presents the Mach number and velocity of the first stage over the entire trajectory, where the maximum velocity is reached during re-entry at around 1710 m/s or Mach 5.6. This is relatively low compared to other launch vehicles such as the validation vehicle designed by Maddock et al. which reaches speeds of 2500 m/s and above. A consequence of this is lower thermal loads acting on the vehicle and less constraining requirements on the thermal protection system. One might wonder what the cause of the oscillating behaviour of the flight path angle and angle of attack profiles, are, these are caused by the change in angle of attack from the maximum drag case to a value for maximum lift-over-drag ratio. For maximum L/D, much more lift is generated and the vehicle starts ascending again, before eventually descending again due to the decrease in velocity because of drag, followed again by acceleration. This motion quickly dampens to a nearly constant flight path angle whilst the Mk-III is heading towards the launch site.

6.2. Ramjet concept

As the ramjet concept came on top of the trade-off in Chapter 2, it was considered to be the most promising one and therefore will be discussed first. Before, jumping into the results, it is important to note that during the optimisation of the ramjet-powered design, the inlet area of a single engine was constrained to be a maximum one-quarter of the total cross-sectional area of the fuselage (0.74 m^2). Such a large inlet, being equal to half of the fuselage cross-section when combining the two ramjet engines, is considered to be the limit for the geometrical design, otherwise, the Mk-III will become a flying inlet.

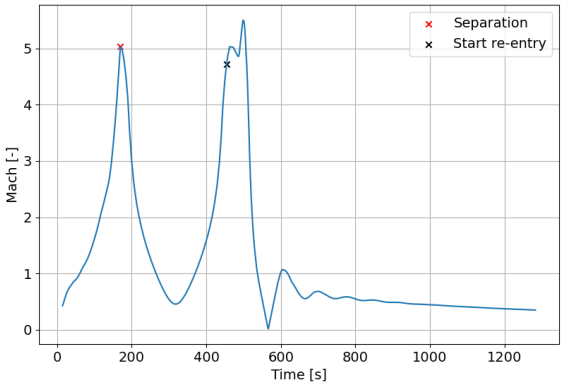

(a) Mach vs time plot.

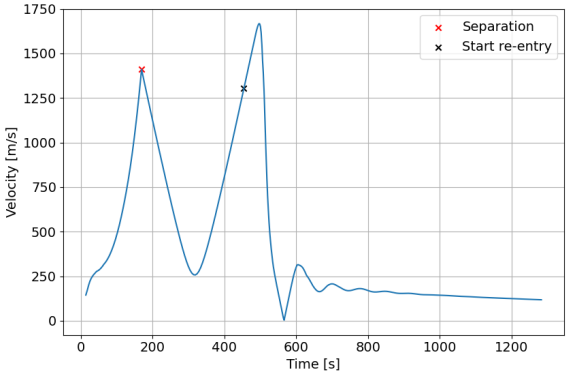

(b) Velocity vs time plot.

Figure 6.3: Mach number and velocity versus time for the optimal baseline first stage design.

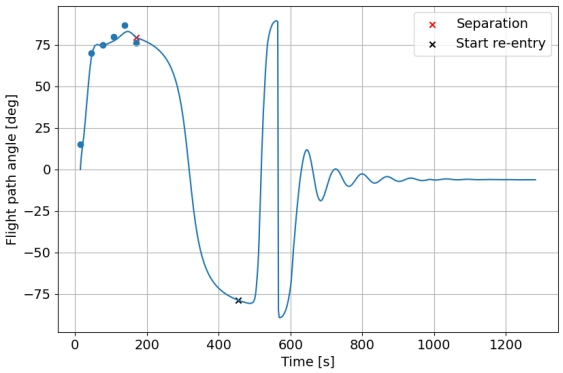

(a) Flight path angle profile over time.

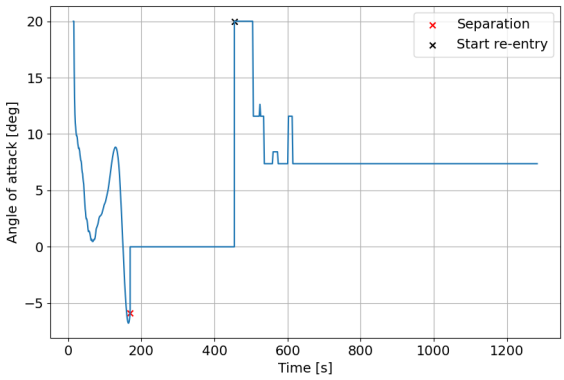

(b) Angle of attack profile over time .

Figure 6.4: Flight path angle and angle of attack profiles of the optimal baseline firs stage over time.

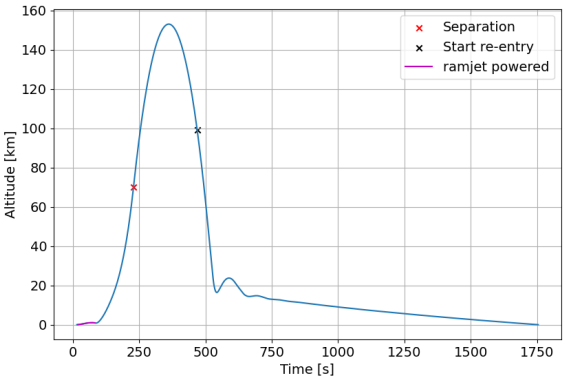

(a) Altitude vs time plot.

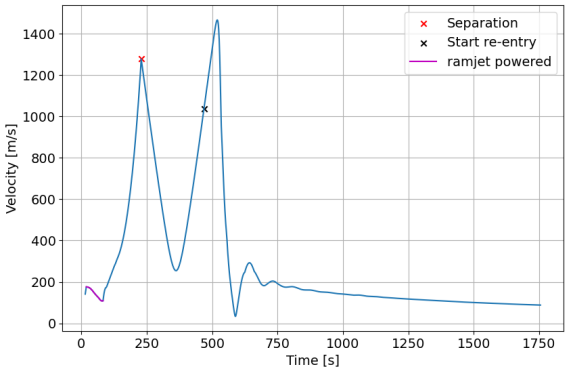

(b) Velocity vs time plot

Figure 6.5: Altitude and velocity versus time plots for a ramjet-powered design.

6.2.1. Optimised design

When running the optimisation, a surprising tendency was found, one which limits the duration of the ramjet-powered phase in order to obtain a 'feasible' design that meets all the requirements. This 'feasible' design is merely the baseline design to which the mass of a ramjet engine is added, such that a first stage trajectory as shown in section 6.1 is obtained. When diving deeper into the results of designs which do include a significant ramjet-powered ascent phase, it becomes clear why this is the case. The trajectory shown in Figure 6.5, is the one for a ramjet-powered design with a maximum inlet area, that uses 1000 kg of fuel during the ramjet phase (corresponding to about 30 seconds). From these graphs, it can be seen that the velocity immediately decreases when the ramjet is ignited and eventually the altitude starts to drop instead of steadily increasing. This is a clear indication that for the allowable inlet area, the ramjets cannot provide sufficient thrust to overcome the aerodynamic drag at high-subsonic, trans- and supersonic velocities. A design where a significant portion of the ascent is powered by ramjets subject to this inlet area constraint will reach the target altitude and velocity unless the rocket engines are going to deliver more thrust and burn significantly more fuel than in the baseline design, leading to a much larger gross take-off mass. This is supported by the fact that the vehicle, for which the trajectory is shown below, has an equal gross take-off mass as the baseline design, but burns out at 70 km and 1270 m/s instead of 81.6 km and 1414 m/s indicating that a significant amount of additional propellant mass would be required to achieve the desired constraints.

6.2.2. Concept potential

What if the inlet area constraint would be increased to double the original value, 1.47 m^2 that is, would then the ramjets be able to produce enough thrust and would this concept then provide an advantage over the baseline concept? Simply put, the answer to both of these questions is yes. The optimiser re-run, but with the increased inlet area constraint, resulting in a first stage vehicle of which the characteristics are tabulated in Table 6.3 and the trajectory variables are plotted from Figure 6.6 until Figure 6.7. The designed vehicle has a gross take-off mass that is 2329 kg less than the baseline, whilst having a dry mass that is 307.4 kg heavier. In total, the ramjet design consumes 2052 kg of fuel more than the baseline design but it saves 4788 kg in oxidiser mass meaning that in total 2736 kg of propellant mass was saved, which is a very promising result. One might also wonder why the inlet area is not almost equal to the constraint value, this is because otherwise the maximum dynamic pressure constraint is violated, as well as the maximum bending load constraint.

Using Figure 6.6b, the initial hypothesis that the trajectory during the airbreathing phase would be flatter, can be confirmed. Compared to the baseline design, the trajectory remains more shallow before steeply ascending whereas, for the baseline, it immediately shoots up towards 70° and higher. The reason behind this is that the trajectory is accommodating for the ramjet required dense air to provide sufficient thrust to keep accelerating the vehicle. In Figure 6.9a it can be seen how the airbreathing phase has a much lower mass rate than the rocket-powered phases before and after, this alone is already a benefit but adding to it, is that this occurs in the densest layers of the atmosphere, resulting in far less aerodynamic losses to be compensated for by the less efficient rocket engines, comparing to the baseline design.

Table 6.3: Detailed first and upper stage designs for the ramjet concept with increased ramjet inlet area.

Ramjet powered first stage			
Gross take-off mass [kg]	39242	A_i [m^2]	1.28
Dry mass [kg]	7899.4	h_s [km]	80.5
Payload mass [kg]	6675	V_s [m/s]	1413
Rocket propellant mass [kg]	21917	γ_s [deg]	78
Ramjet fuel mass [kg]	2651	Diameter [m]	1.94
Sea level rocket thrust [kN]	205.5	Length [m]	24.25
Sea level specific impulse [s]	265		

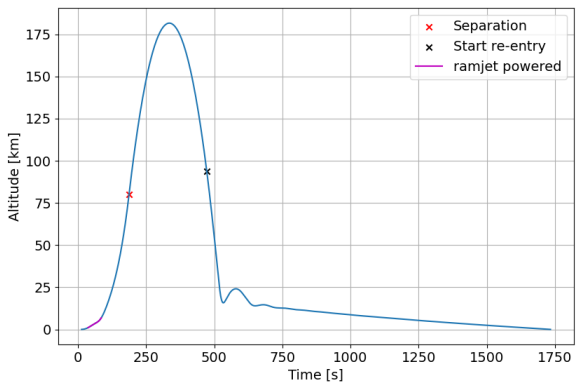

(a) Altitude vs time plot.

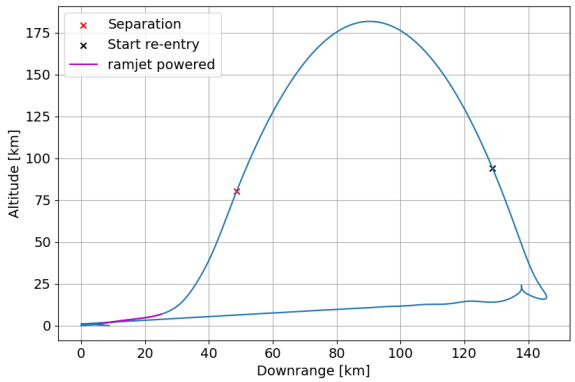

(b) Altitude vs downrange plot.

Figure 6.6: Altitude versus time and altitude versus downrange plots for one of the most optimal ramjet designs (with increased inlet area).

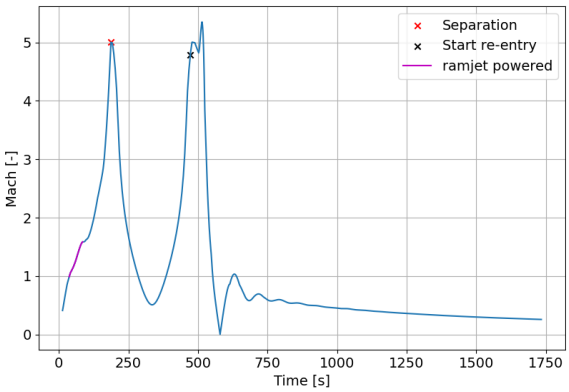

(a) Mach vs time plot.

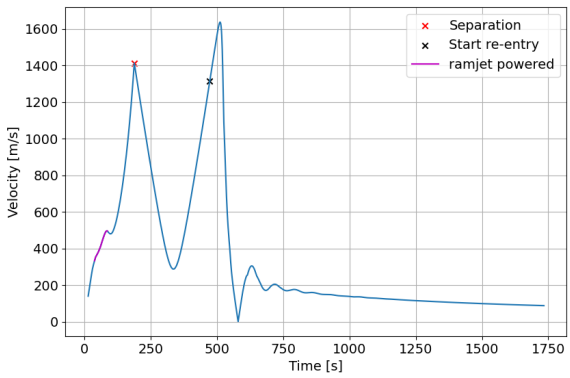

(b) Velocity vs time plot.

Figure 6.7: Mach number and velocity versus time for one of the most optimal ramjet designs (with increased inlet area).

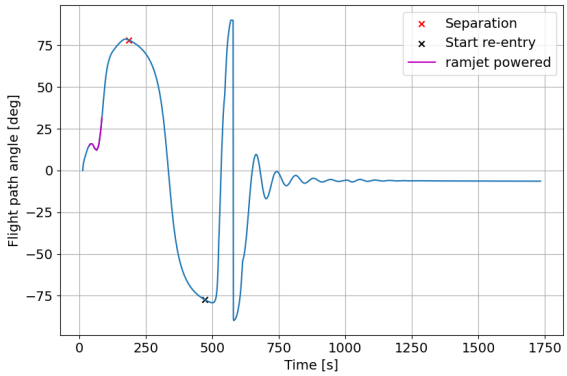

(a) Flight path angle profile over time.

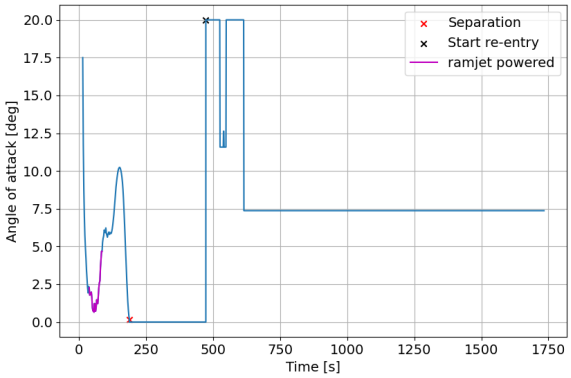

(b) Angle of attack profile over time .

Figure 6.8: Flight path angle and angle of attack profiles for one of the most optimal ramjet designs (with increased inlet area) over time.

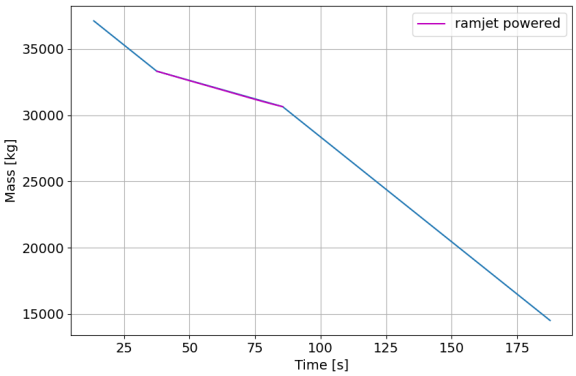

(a) Mass evolution over time

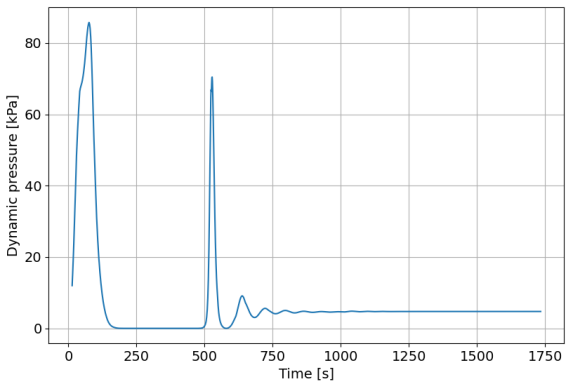

(b) Dynamic pressure over time.

Figure 6.9: Mass evolution during the ascent and trajectory dynamic pressure for one of the most optimal ramjet designs (with increased inlet area) over time.

6.3. Turbine engine concept

To briefly recap on the turbine engine concept, two existing F100 P&W-229 engines are used which propel the Mk-III during take-off and the initial ascent before transitioning to the fully rocket-powered phase. From the optimisation of this concept, there were no designs found within the design space that were able to reach the desired separation conditions and reach the launch site afterwards. Contrary to the ramjet concept, returning to the launch site, was not the most challenging part, instead, reaching the separation point was. Reaching the desired staging conditions would only be possible if the rocket engines were more powerful than for the baseline design and burn for more than 225 seconds, leading to vehicle designs with a higher take-off mass than 55000 kg, making this concept significantly heavier, eliminating any advantages it could have had over the baseline design. Also, this would make the airbreathing phase of the ascent almost irrelevant compared to the rocket-powered phase, showing that the optimised design tends towards not using the turbine engines at all.

Two main causes can be identified resulting in this concept being unfeasible. The first one is the sheer lack of thrust that the selected turbine engines are able to provide, they are simply not capable of significantly accelerating the vehicle. The vehicle actually begins to decelerate not long after take-off. The second cause is the added mass of the turbine engines, each engine weighs about 1500 kg, which results in dry mass that is 3000 kg heavier, or an increase of nearly 40% compared to the baseline. Combining this with the first cause, basically means that the rocket engines, have to do the same job as they have to do in the baseline design, just now for a much heavier vehicle. In addition, because the performance of turbine engines deteriorates with altitude, their segment during the ascent, which starts at sea level, will be much flatter than for a rocket engine, meaning that more time will be spent in the densest layers of the atmosphere, leading to large aerodynamic losses.

Nevertheless, one can not ignore that the high specific impulse of the turbine engines drastically improves the return performance when comparing it to the ramjet and baseline concepts as can be seen in Figure 6.10 where the altitude of one of the most optimal turbine engine designs is plotted versus the downrange. Here, only 701 kg of fuel mass was used during the return to cover a downrange of nearly 200 km compared to 110 km for the gliding flight. Still, this design has a total vehicle mass of more than 50000 kg and only reaches a separation altitude and velocity of 68 km and 1100 m/s respectively. It is evident that for not much fuel mass compared to the total mass, the vehicle downrange can be increased a lot. During the descent, the lack of thrust of the turbine engines is not such a big problem and neither is the added mass as the latter does not affect gliding performance, only L/D does. On the other hand, the high efficiency allows the turbine engines to provide thrust over a prolonged period of time leading to the large return downrange this concept is able to cover. Note that this design also experiences the oscillatory behaviour as already observed for the baseline design, which not coincidentally, is initiated the moment that the turbine engines start providing thrust which increases vehicle velocity, leading to an increased lift, resulting in the vehicle going up again until not enough thrust can be generated anymore and the vehicle decelerates again. Also here, the oscillation dampens out to a constant descent rate. The crossing of lines on the left side of Figure 6.10 is merely the vehicle turning back after reaching the launch site, because of the implemented guidance, this just means that the vehicle is able to fly a couple of kilometres further than necessary to reach the launch site.

6.3.1. Concept potential

Before completely discarding this concept, it is worth analysing if there is any potential that could make it worth exploring if some constraints of conditions were to change. Firstly, and most obvious, is a different turbine engine which would provide more thrust at a smaller mass penalty. The F100 engine was chosen because there was plenty of information available and has a reasonably high performance but that does not take away the fact that it is a rather old engine. There are certainly new turbine engines available with a higher T/W of which data is classified making it virtually impossible to include in the design. A lighter but more powerful engine could perhaps accelerate the first stage sufficiently and save enough propellant mass to offset the added engine mass. Another important factor is the vehicle drag which was already discussed in the previous section but is also applicable to the turbine engine concept. The vehicle experiences significant drag during the simulations and if this were to be decreased by an optimised aerodynamic shape, less thrust would be needed to accelerate the vehicle whilst in the dense layers of the atmosphere, potentially allowing the Mk-III to be initially powered by turbine engines.

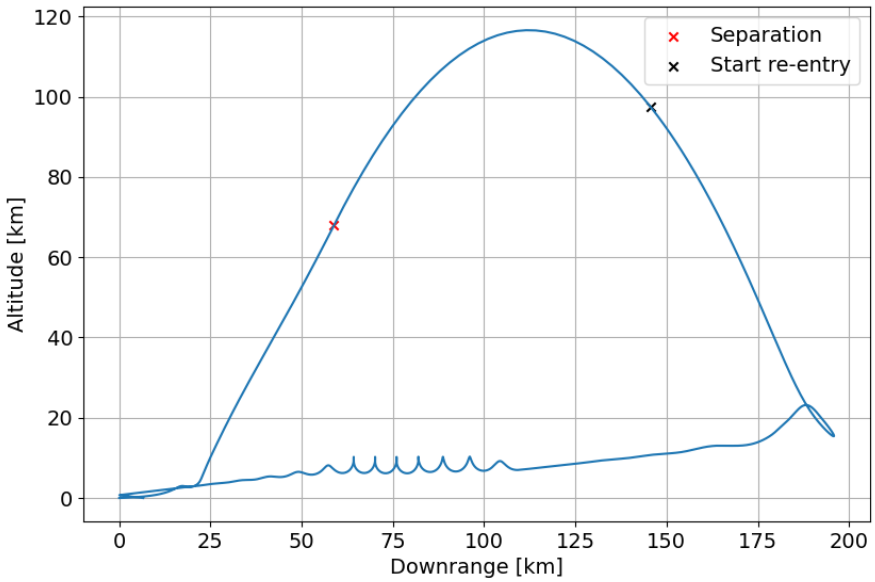

Figure 6.10: Altitude versus downrange for one of the most optimal turbine engine concept designs.

Now, instead of focusing on the weak points which would need to be improved, the idea arose to focus on the strong point of the turbine engine concept: the return flight. With its superior performance during the return flight, the turbine engine could perhaps be used solely here, to make the very challenging RTLS requirement significantly easier, hopefully resulting in a more efficient trajectory and perhaps also allowing for a lower separation flight path angle as desired by Dawn Aerospace. Having two heavy turbine engines during the ascent without using them there would probably still make this idea impossible, but what if only one engine would be installed on the Mk-III? This would halve the added mass and the thrust that the engine is able to provide, while the latter could still be sufficient to drastically increase the return range compared to the baseline model. This configuration was created in the vehicle and trajectory models and the optimiser was run, keeping the fuel mass designated for the airbreathing engine during ascent at 0. This, however, also did not result in any feasible design without exceeding a gross mass of 50000 kg.

6.4. Summary of the discussed results

This chapter began by presenting the different separation conditions and their corresponding upper stage designs that were considered to reach a sun-synchronous orbit at 600 km via a direct ascent to a parking orbit at 200 km, followed by a Hohmann transfer, whilst carrying 250 kg of payload. Based on the high separation flight path angle that would be required for the first stage to reach the launch site and the resulting lack of significant difference in total mass, the upper stage with separation at 80 km and Mach 5 was selected over the upper stage starting from 90 km. This resulted in an upper stage of 6775 kg, measuring 5.84 m in length and 1.84 in diameter. Based on this upper stage, all first stage concepts were designed.

The baseline concept is the original Mk-III design which relies solely on rocket engines for reaching the desired separation conditions. It served as a basis to develop the airbreathing concepts and is used to compare those with. After running the optimisation scheme on the baseline vehicle and trajectory models, an optimal or near-optimal design weighing 41571 kg was found which launches the upper stage at 81 km altitude and 1414 m/s. In addition, the first stage was able to return to the launch site after performing a banking manoeuvre resulting in a steady turn of 180° and had 6 kilometres in reserve as was seen from the bottom left side of Figure 6.2b where the vehicle seems to turn again after reaching the landing site which is simply because the computed downrange is always positive whereas in reality the vehicle actually flies over the launch site and would be able to land 6 kilometres further. The detailed designs of both the first and the upper stages were tabulated in Table 6.2.

After concluding on the baseline design, the most promising airbreathing concept, according to the trade-off at least, was optimised. The resulting trajectory of the ramjet concept was as expected, flatter during the

airbreathing phase, in order maximally benefit from the dense air for thrust generation. Although the potential of this concept, propelling the launch vehicle through the dense layers of the atmosphere more efficiently, could clearly be seen, the constraint on the maximum inlet area is a serious deal-breaker. The ramjet inlets would have to be excessively large compared to the cross-section of the Mk-III before they are capable of producing enough thrust to provide an actual benefit over the pure rocket-powered design. When for a moment neglecting this issue, a ramjet design was found that was able to save 2736 kg in propellant mass compared to the baseline design. The gross take-off mass was reduced slightly less because the ramjet concept dry mass is larger, but still, 2329 kg in gross mass could be saved which shows the potential of a ramjet-powered launch vehicle. A possible solution to the excessive inlet area, without changing the requirements, would be to improve the aerodynamic design of the Mk-III in terms of drag during the trans- and supersonic regimes. This would lead to less thrust being required to accelerate the vehicle, perhaps allowing the ramjet inlet area to be decreased to a reasonable size.

Finally, an attempt was made to determine the feasibility of the runner-up of the trade-off which was the turbine engine configuration. From the optimisation results, it quickly became clear, that this concept is unfeasible, if not, highly impractical mainly due to the mass penalty of the added engines and the lack of those. The dry mass increases by almost 40% due to these engines which is simply too much and does not allow the vehicle to reach the desired separation conditions without requiring excessively powerful rocket engines and much more propellant than for the baseline design, defeating the main reason why airbreathing engines were considered at all. However, the turbine engine concept did have a far superior performance during the return flight, being able to cover almost 200 km whilst using only a little over 700 kg of fuel. Based on this performance, the idea came to install just one turbine engine and have it operate only during the return flight in an attempt to benefit from the strong points of this concept whilst minimising the weak points. This resulted in a feasible design, but one that still had a worse performance in terms of take-off mass than the baseline concept at a gross mass of over 50000 kg. The main factor which could make this concept more feasible is the turbine engine model. If lighter engines, providing more thrust would be available, they could be also used effectively during the ascent. This would dramatically improve the potential of this concept, but there are no such engines today for which data is not classified, making it hard to measure the realistic improvements that are possible.

Concluding on the airbreathing designs, both concepts have complementary strong points, the ramjet concept performs better during the ascent given that the inlet area can be large enough, whereas for the turbine engine concept, an excellent return performance can be seen. Combining the advantages of both of these concepts where the ramjet can make the ascent trajectory more efficient and the turbojet can make the return trajectory less constraining, allowing for a more shallow separation flight path angle, thus, also a lighter upper stage, might give airbreathing propulsion a real change of improving launch vehicle performance. The concept which was placed third in the trade-off based on a lack of development, aims to do this. If progress is made in the development of high-performing turbine-based combined cycle engines, a new era for launch vehicle design might kick off, but this would require a lot of development costs to be made. Despite, the lack of thrust of the ramjet engines because of geometrical constraints and the dangerously high dynamic loads when large enough, the ramjet concept is still considered to have more potential than the turbine engine concept when considering both separately. But for now, rocket engines are still the best option to propel the first stage of the Mk-III given the constraints put on the vehicle and trajectory design.

7

Sensitivity Analysis

In order to identify the parameters that are most influential on the simulation results and also investigate the robustness of the found near-optimal designs, a sensitivity analysis was conducted. This involved changing individual parameters in the upper stage, baseline first stage and ramjet first stage designs and analysing which result this had compared to the original design. This procedure did not involve the turbine engine design, mainly because of this concept showed the lowest feasibility and potential, making it not worth investigating further. The sensitivity of the upper stage design is determined with respect to the staging flight path angle which was already identified as rather influential, and with respect to the parking orbit altitude. The changes in baseline design results are studied because of uncertainty in the mass estimation model of the first stage. Also, the rocket engine-specific impulse is varied to quantify the resulting changes. For the ramjet model, the impact of an improved or decreased aerodynamic performance in terms of both lift and drag coefficient is analysed as it was mentioned in Chapter 6 that an improved aerodynamic shape would drastically improve the feasibility and potential of this concept. Finally, the flight path values at the control nodes are varied for both the baseline and ramjet concepts to see what uncertainty in these would do to the results.

7.1. Upper stage

Keeping the initial altitude and velocity constant, the separation flight path angle was varied by ± 3° ± 6° and ±9° resulting in the upper stage designs tabulated in Table 7.1. The results show that the model behaves as expected, with higher separation flight path angles resulting in larger trajectory corrections, requiring more propellant mass resulting in a heavier vehicle. In the case that separation would occur at an angle three degrees higher than the design, 3% more propellant mass would be required than what is designed for which is an acceptable result. It is not expected that the separation conditions would deviate by a much larger angle as this would mean that there is a serious malfunction somewhere in the vehicle's control system.

Table 7.1: Sensitivity of the upper stage design characteristics to a varying separation flight path angle.

γ_s [deg]	γ_1 [deg]	γ_2 [deg]	γ_3 [deg]	M_{GTOM} [kg]	M_p [kg]	M_{dry} [kg]	l_{upper} [m]
85	69.2	58.1	35.1	7069	6495	574	5.98
82	65.4	49.9	9.7	6860	6289	572	5.90
79	**74.7**	**43.3**	**20.1**	**6675**	**6104**	**571**	**5.84**
76	65.9	44.2	21.1	6534	5965	569	5.80
73	69.0	48.1	29.0	6405	5837	568	5.75
67	60.6	57.4	35.4	6216	5651	566	5.68

The effects of a different parking orbit for the upper stage have not been treated at all, since the original one at 200 km was selected without a quantitative analysis. If for some reason, the parking orbit should be higher or lower than the current one, it is important that this does not have too much of a negative impact on the upper stage design. In Table 7.2, the optimised upper stage designs are shown for four different parking orbits, 50 km above, 50 km below, 10 km above and 10 km below the original one. What can be seen from this is that both

the significantly higher and lower parking orbits require more propellant than the original one. The prior is most likely because it requires a more vertical flight, inducing lots of gravity losses, and the latter because of the steering losses to flatten the trajectory. The other two parking orbits do not show very significant changes in upper stage characteristics, although it is observed that the optimal parking orbit altitude given the separation conditions and target orbit is a little lower than the original one. For a fully optimised design it is recommended to find the optimal parking orbit which shall be somewhere around 190 km.

Table 7.2: Sensitivity of the upper stage design characteristics to a changing parking orbit altitude.

h_{park} [km]	γ_1 [deg]	γ_2 [deg]	γ_3 [deg]	M_{GTOM} [kg]	M_p [kg]	M_{dry} [kg]	l_{upper} [m]
250	72.6	59.8	6.2	7437	6860	576	6.09
210	73.5	41.4	12.7	6710	6139	571	5.85
200	**74.7**	**43.3**	**20.1**	**6675**	**6104**	**571**	**5.84**
190	63.8	44.1	21.3	6630	6060	570	5.82
150	47.9	32.0	5.6	7029	6455	573	5.96

7.2. Baseline design first stage

In Chapter 3, the Hypersonic Aerospace Sizing Analysis tool was used to determine the mass of the first stage which is a validated and proven mass estimation method. still, it is not perfect and deviations exist. The authors of HASA state that the estimation method can differ by about ±10 %, hence it makes sense to see what the impact of such a mass variation is on the vehicle's performance [18]. As only the dry mass components were computed using the HASA tool, this mass was varied as shown in Table 7.3. The results here show that, logically for a reduced dry mass, the vehicle performance increases, although it increases by a significant amount, mainly the final burnout velocity. This however also results in the downrange constraint not being met as can be seen by the negative downrange margin. For an increase in dry mass of 10%, the baseline concept is not able to reach the separation conditions anymore whilst keeping all other parameters the same. Also here, the largest difference can be seen in the final burnout velocity. If the eventual dry mass would be larger than initially estimated, a more powerful rocket engine is necessary to reach the desired separation conditions.

Table 7.3: Sensitivity of the first stage trajectory to the error margin in the mass estimation method.

ΔM_{dry} [-]	h_f [km]	V_f [m/s]	γ_f [deg]	ΔR [km]	M_{GTOM} [kg]	M_{dry} [kg]	ΔV [m/s]
+ 10.0 %	78.04	1328	79	14.1	42415	8436	2683
+ 0.0 %	81.60	1414	79	5.3	41571	7592	2780
- 10.0 %	86.85	1522	79	-8.3	40744	6765	2883

To see what the robustness is of the baseline first stage trajectory design, the control nodes are varied by a fixed and equal amount at every node as in Table 7.4. Then, it is investigated if the design is still able to meet the requirements and if not, which are not met. When all nodes are varied both by adding up to five degrees or subtracting five degrees, the vehicle remains capable of bringing the upper stage to the desired altitude and velocity, meaning that this part of the design is rather robust. It becomes tricky when attempting to return to the launch site when the flight path angles at the control nodes are decreased. This behaviour is logical as the trajectory is flattened and the return range to be covered becomes larger. It was also found that the most influential parameter on this requirement, was the final control node, as this one is the most determining factor for the final flight path angle. This final flight path angle is as already mentioned before the biggest determining factor of the horizontal distance covered during the ballistic arc. All other control nodes could be varied by a significant amount and the vehicle will still reach the separation conditions but the final node must be carefully selected in order to reach the launch site again.

Table 7.4: Sensitivity of the first stage trajectory results to varying control node inputs from -5 to +5 degrees per control node.

$\Delta\gamma$ [deg]	γ_0 [deg]	γ_1 [deg]	γ_2 [deg]	γ_3 [deg]	γ_4 [deg]	γ_5 [deg]	h_f [km]	V_f [m/s]	γ_f [deg]	ΔR [km]
+5	20	64.1	84.8	87.8	89.5	82	81.8	1404	85	37.9
+2.5	17.5	61.6	82.3	85.3	87.0	79.5	81.7	1407	82	29.4
+0	15	59.1	79.8	82.8	84.5	77	81.6	1414	79	5.3
-2.5	12.5	56.6	77.3	80.3	82.0	74.5	80.8	1418	76	-18.9
-5	10	54.1	74.8	77.8	79.5	72	80.2	1427	73	-43.7

7.3. Ramjet design first stage

The reasoning behind analysing the sensitivity of the ramjet design to the aerodynamic performance was already provided in the introductory paragraph of this chapter. As mentioned there, an improved, or decreased aerodynamic performance could make the ramjet concept more promising or completely impractical. Whilst varying the lift and drag coefficients by 5 and 10%, the impact on the ramjet design which included the increased inlet area constraint, is analysed in terms of final burnout altitude, velocity and the downrange margin. In Table 7.5 it is shown that for a 5% increase in drag, the design immediately becomes incapable of meeting the separation requirements both in terms of altitude and velocity. The effects of an increased or decreased drag are also larger than those for changed lift coefficients. If, as proposed in Chapter 6, the aerodynamic drag would be reduced, the ramjet concept would get a large boost in performance, allowing it to reach higher altitudes and velocities for the same design, or allowing the inlet area to be reduced to an acceptable value. Notably is that only for a decrease in lift coefficient of 10%, the downrange margin becomes negative and the Mk-III does not fulfil the return requirement whereas for all other negative changes in lift and drag, return to launch site is still feasible.

Table 7.5: Sensitivity of the first stage trajectory to changing aerodynamic characteristics oft the vehicle.

ΔC_L [-]	ΔC_D [-]	h_f [km]	V_f [m/s]	γ_f [deg]	ΔR [km]	R [km]
+0.0%	+0.0%	80.05	1413	78	8.8	154.8
+5.0%	+0.0%	80.66	1420	78.1	21.8	168.5
-5.0%	+0.0%	79.00	1402	78.1	1.7	145.4
+10.0%	+0.0%	81.36	1428	78.1	35.3	183.3
-10.0%	+0.0%	77.60	1386	78.2	-5.2	145.3
+0.0%	+5.0%	77.23	1377	78.2	11.3	149.3
+0.0%	-5.0%	82.08	1430	77.8	16.8	168.8
+0.0%	+10.0%	74.01	1334	78.2	13.6	143.6
+0.0%	-10.0%	87.36	1506	77.7	11.8	179.8

Lastly, as for the baseline design, the trajectory control nodes are varied for the ramjet concept as well to see what the impact would be of increased and decreased input flight path angles. For the ramjet design, the control nodes were changed by only 2.5 degrees as this turned out to be already sufficient for the ramjet design to not meet the separation requirements, indicating that the trajectory is highly optimised and slight deviations would already cause mission failure. This lack of robustness is not in favour of the ramjet concept and further adds to the case of why it remains inferior to the baseline design.

Table 7.6: Sensitivity of the first stage ramjet concept trajectory results in varying control node inputs from -2.5 to +5 degrees per control node.

$\Delta\gamma$ [deg]	γ_0 [deg]	γ_1 [deg]	γ_2 [deg]	γ_3 [deg]	γ_4 [deg]	γ_5 [deg]	γ_6 [deg]	h_f [km]	V_f [m/s]	γ_f [deg]	ΔR [km]
+2.5	12.5	19.4	18.3	64.3	79.4	85.6	80.5	81.6	1383	80.56	36.7
+0.0	10	16.9	15.8	61.8	76.9	83.1	78	80.05	1413	78	8.83
-2.5	7.5	14.4	13.3	59.3	74.4	80.6	75.5	74.68	1381	75.56	-0.19

8

Conclusion and recommendations

During the development of the Mk-III, a winged, semi-reusable, two-stage-to-orbit launch vehicle that takes off and lands horizontally of which the first stage returns to the launch site, the idea arose to utilise airbreathing engines on the first stage to improve the vehicle performance in terms of gross take-off mass. During this thesis, the feasibility of such a concept was investigated and how much of an improvement would it be compared to a conventional rocket-powered vehicle if feasible, or what the main causes would be that make this concept infeasible. The conclusions of this research are presented in this chapter by answering the research questions which were formulated at the start. Thereafter, some further recommendations are made on what could be interesting to study for an improved understanding of this entire topic.

8.1. Conclusion

A primary research question was introduced in Chapter 1, embodying the main goal of this research. This question was further broken down into sub-questions which add up and together form an answer to the primary research question. Here, each of the sub-questions is treated until they are combined to formulate an answer to the primary research question at the end of this section.

Research Sub-Question 1: *What is the best type of airbreathing concept considering the requirements of the Mk-III?*

In the literate review conducted prior to this thesis, all airbreathing engine types that were not immediately considered infeasible were identified: Turbine engines, ramjets, scramjets, dual-mode scramjets, turbine-based combined cycle engines and rocket-based combined cycle engines. Based on their characteristics, and four performance criteria being, TRL, T/W, I_{sp} and range of operations, they were compared to one another and traded off by using an analytical hierarchy process presented in Chapter 2. From this trade-off, it was the ramjet engine that was the clear victor, the second option is the turbine engine, closely followed by the TBCC engine. although the TBCC engine could have a superior performance over the two other options, the low TRL has too much of a negative impact on this concept. Both the ramjet and the turbine engine concepts are proceeded with such that they both can be compared. As will become clear from the next research questions, the trade-off correctly determined that the ramjet concept is better performing than the turbine engine concept.

Research Sub-Question 2: *Can airbreathing propulsion be integrated in the Mk-III whilst meeting the original mission requirements?*

To provide an answer to this sub-question it was first important to determine the mission requirements, these are two-fold. The upper stage must reach the target sun-synchronous orbit at 600 km altitude starting from set separation conditions. The first stage, on the other hand, needs to bring the upper stage to those separation conditions, release it there and return to the launch site afterwards. Different separation conditions were compared based on their resulting optimised upper stage designs, from these, a separation altitude, velocity and flight path angle of 80 km, 1405 m/s and 79° respectively, were chosen, resulting in an upper stage weighing 6675 kg. These separation conditions and upper stage mass were then used for all first stage concepts.

Table 8.1: Detailed first stage design for the ramjet concept with increased ramjet inlet area.

Ramjet powered first stage			
Gross take-off mass [kg]	39242	A_i [m^2]	1.28
Dry mass [kg]	7899.4	h_s [km]	80.5
Payload mass [kg]	6675	V_s [m/s]	1413
Rocket propellant mass [kg]	21917	γ_s [deg]	78
Ramjet fuel mass [kg]	2651	ΔR [kg]	8.8
Sea level rocket thrust [kN]	205.5	Diameter [m]	1.94
Sea level specific impulse [s]	265	Length [m]	24.25

The vehicle and trajectory models described in Chapter 3 and Chapter 4 for both the ramjet and turbine engine concept, were put into a differential evolution optimisation algorithm as presented in Chapter 5. The optimisation results for the turbine engine concept did not show any signs of feasibility for the current vehicle design and selected engines. This was mainly attributed to the lack of thrust and added mass of the two selected F100-PW-229 engines as they were not capable of accelerating the vehicle sufficiently and still added 3000 kg of dry mass to the vehicle. The separation conditions would only be reached if a huge amount of propellant was burned resulting in designs weighing above 55000 kg. The only area in which this concept performed exceptionally well, was in meeting the RTLS requirement as the turbine engines significantly increase the return range.

For the ramjet concept, the initial optimisation results also did not result in any design that included a significant ramjet-powered phase, that was able to meet the requirements. The optimiser results even converged towards solutions which minimised ramjet contribution. Rather similar to the turbine engine concept, this was because the ramjets not being able to produce enough thrust within the inlet area constraint set at one-quarter of the fuselage cross-section, per engine. In an attempt to find a ramjet-powered design that was able to meet the requirements, the limit inlet area was doubled and the optimiser was run again. This time, a design was found that was able to reach the target altitude and velocity and is capable of returning to the launch site, the vehicle characteristics of which, are tabulated in Table 8.1. Nevertheless, an inlet area of 1.28 m^2 is questionably large to implement in the geometrical design. To achieve a design, with a feasible ramjet inlet area, the aerodynamic performance of the Mk-III would need to be improved in terms of drag such that the generated thrust by a smaller engine is enough to significantly accelerate the vehicle. The sensitivity analysis in Chapter 7 showed a significant improvement in performance when reducing the drag by 5%.

Research Sub-Question 3: *Will an airbreathing concept reduce the Mk-III take-off mass?*

Before designing the airbreathing concepts discussed above, a baseline design using only rocket engines was created and optimised, with which a comparison could be made. In Table 8.2 an optimised baseline design is presented which reaches 81.6 km and 1414 m/s at burnout, meeting the separation conditions and is capable of returning to the launch site, having a margin of 5.3 km. As no feasible airbreathing design was found that was able to meet all requirements, stayed within set constraints and was not excessively heavy, an airbreathing concept will not reduce the take-off mass of the Mk-III. However, if the ramjet concept with increased inlet area would be geometrically feasible, it would definitely decrease the take-off mass as can be seen by comparing the results in Table 8.1 and Table 8.2. The ramjet concept is able to save 2736 kg in propellant mass leading to a reduced take-off mass of 2329 kg because it has a heavier dry mass.

Primary Research Question: *Would it be feasible to integrate airbreathing propulsion in the Dawn Mk-III, aiming to decrease the gross take-off mass whilst fulfilling the mission requirements?*

Through the design and optimisation of two concepts using different types of airbreathing engines, an attempt was made to assess the overall feasibility of airbreathing propulsion on the Mk-III. From this analysis, neither a turbine engine concept nor a ramjet concept was able to fulfil the mission scenario within the set constraints which also immediately eliminates the use of the second part of the primary research question. However, when removing the geometrical constraint put on the ramjet inlet area, the potential of the ramjet concept is clear as day as the gross take-off mass is reduced by 2329 kg whilst fulfilling all requirements. If the ramjet inlet area required to produce sufficient thrust could be decreased, by for example reducing the

Table 8.2: Detailed first and upper stage designs for the baseline concept

First stage		Upper stage	
Gross take-off mass [kg]	41571	Gross take-off mass [kg]	6675
Dry mass [kg]	7592	Dry mass [kg]	321
Payload mass [kg]	6775	Payload mass [kg]	250
Propellant mass [kg]	27304	Propellant mass [kg]	6104
Sea level thrust [kN]	420	Vacuum thrust [kN]	30
Sea level specific impulse [s]	265	Vacuum specific impulse [s]	320
ΔV [m/s]	2780	ΔV [m/s]	7718
Diameter [m]	1.94	Diameter [m]	1.84
Length [m]	24.25	Length [m]	5.84

vehicle drag, a ramjet-powered Mk-III vehicle would be feasible and beneficial over a rocket-powered design. Regardless, this is currently not the case and airbreathing propulsion cannot be integrated into the Mk-III whilst meeting the mission requirements, let alone decrease the gross take-off mass.

8.2. Recommendations

During this research, there were multiple interesting side-quests that could be worth exploring and studying, perhaps even providing a basis for new studies on the Mk-III and airbreathing propulsion applied to launch vehicles. In addition, some aspects are listed that were not addressed during this thesis because they were considered out of the research scope.

Separation: During this thesis the assumption was made that the first stage simply brings the upper stage to a certain altitude and velocity. The actual procedure of separation and the effects it has on the states of both vehicles was not addressed. Also, the separation method was neglected, the upper stage is housed inside the first stage which requires some mechanism or procedure to get it out of the vehicle, how this will be done is unknown.

First stage aerodynamic optimisation: Because the Mk-III is still conceptional, the aerodynamic characteristics of its predecessor were taken. This vehicle was not optimised for trans- and supersonic velocities and improvements could be made especially in terms of experienced drag. It would be worth studying the geometric shape of the Mk-III to reduce drag and offer more potential for the ramjet concept.

Control law: Currently a rather simple control law is applied to guide the first and upper stages during their ascent. A more sophisticated control method such as a PID controller might reduce losses during the ascent trajectories and help improve the design.

Turbine engine design: As an already existing turbine engine was selected which provides a relatively high performance and has enough data available, chances are very high that this engine is not optimal for use on the Mk-III. A more modern turbine engine with higher thrust and lower drag would offer more chances of the turbine engine concept becoming feasible. Alternatively, a turbine engine could be designed specifically for the Mk-III.

Geometric design: One of the main unanswered questions in this thesis was the feasibility of the large ramjet inlet areas. It is necessary that a more detailed geometric design of the vehicle is available such that estimations can be made on the maximum allowable ramjet inlet area rather than assuming one.

References

[1] J Acharya. *What is bearing angle and calculate between two Points*. URL: https://www.igismap.com/what-is-bearing-angle-and-calculate-between-two-points/ (visited on 07/24/2023).

[2] M.F. Ahmad et al. “Differential evolution: A recent review based on state-of-the-art works”. In: *Alexandria Engineering Journal* 61.5 (2022), pp. 3831–3872. ISSN: 1110-0168. DOI: https://doi.org/10.1016/j.aej.2021.09.013. URL: https://www.sciencedirect.com/science/article/pii/S111001682100613X.

[3] D.L. Akin. *Mass Estimating Relations*. 2016. URL: https://spacecraft.ssl.umd.edu/academics/791S16/791S16L08.MERsx.pdf.

[4] *Analytical Hierarchy Process Trade-off Tool Users Manual*. Version 2.7. 2017.

[5] J.D. Anderson Jr. *Hypersonic and High-Temperature Gas Dynamics, Second Edition*. 2006. ISBN: 978-1-60086-195-6.

[6] B.T.C. Zandbergen. *Thermal Rocket Propulsion (version 2.08)*. Delft: Faculty of Aerospace Engineering, 2020.

[7] M Balesdent. “Multidisciplinary Design Optimization of Launch Vehicles”. PhD thesis. Ecole Centrale de Nantes (ECN), Nov. 2011. URL: https://theses.hal.science/tel-00659362.

[8] T. Benson. *Propulsion System Analysis*. URL: https://www.grc.nasa.gov/www/k-12/Missions/Jim/Project1ans.htm (visited on 09/01/2023).

[9] J Bradford, John Olds, and J Wallace. “CONCEPT ASSESSMENT OF A HYDROCARBON FUELED RBCC-POWERED MILITARY SPACEPLANE”. In: (Mar. 2023).

[10] Gregory J. Brauckmann. “X-34 Vehicle Aerodynamic Characteristics”. In: *Journal of Spacecraft and Rockets* 36.2 (1999), pp. 229–239. DOI: 10.2514/2.3453.

[11] F. Castellini. “MULTIDISCIPLINARY DESIGN OPTIMIZATION FOR EXPENDABLE LAUNCH VEHICLES”. POLITECNICO DI MILANO, 2012.

[12] D.R. Chapman. *An Analysis of the Corridor and Guidance Requirements for Supercircular Entry into Planetary Atmospheres*. 1959. URL: https://ntrs.nasa.gov/api/citations/20190002210/downloads/20190002210.pdf.

[13] D Dirkx and E. Mooij. *Video Tutorials - Code and Topics: Lunar ascent details*. 2023.

[14] Michel Doublier and Marcel Pouliquen. “Airbreathing Combined Engines for Space Transportation Systems”. In: *SAE Transactions* 97 (1988), pp. 121–127. ISSN: 0096736X. URL: http://www.jstor.org/stable/44470310 (visited on 03/31/2023).

[15] *ESPA User’s guide: The EELV Secondary Payload Adapter*. Tech. rep. 2018.

[16] O. Biblarz G.P. Sutton. *Rocket Propulsion Elements*. Hoboken, New Jersey: Wiley, 2017.

[17] T. Haex. *Dawn Aerospace Mk-III: An exploration of cost driven mission scenarios of a winged Two Stage to Orbit semi-Reusable Launch Vehicle integrated in the common airspace*. University of Technology Delft, 2020.

[18] Gary Harloff and Brian Berkowitz. “HASA: Hypersonic Aerospace Sizing Analysis for the preliminary design of aerospace vehicles”. In: (Dec. 1988).

[19] B.M. Hellman. *Comparison of Return to Launch Site Options for a Reusable Booster Stage*. Georgia Institute of Technology, 2005. URL: https://smartech.gatech.edu/bitstream/handle/1853/8026/SSEC_SB3_doc.pdf.

[20] P. ten Houte de Lange. “Dawn Aerospace Mk-III Thermal Analysis”. University of Technology Delft, 2022.

[21] *Introducing the Dawn Mk-II Aurora*. URL: https://www.dawnaerospace.com/spacelaunch (visited on 08/25/2023).

[22] M.W. van Kesteren. “Air Launch versus Ground Launch: a Multidisciplinary Design Optimization Study of Expendable Launch Vehicles on Cost and Performance”. Delft University of Technology, 2013.

[23] T. Lips and B. Fritsche. “A comparison of commonly used re-entry analysis tools”. In: *Acta Astronautica* 57.2 (2005), pp. 312–323. ISSN: 0094-5765. URL: https://www.sciencedirect.com/science/article/pii/S0094576505000767.

[24] Wesley Lord, Douglas Macmartin, and T. Tillman. “Flow control opportunities in gas turbine engines”. In: June 2000. DOI: 10.2514/6.2000-2234.

[25] R. Chase M. Tang. “The Quest for Hypersonic Flight with Air-Breathing Propulsion”. In: Ohio, U.S.A., 2008. URL: https://arc.aiaa.org/doi/abs/10.2514/6.2008-2546.

[26] C.A. Maddock et al. “Conceptual design analysis for a two-stage-to-orbit semi-reusable launch system for small satellites”. In: *Acta Astronautica* 152 (2018), pp. 782–792. URL: https://doi-org.tudelft.idm.oclc.org/10.1016/j.actaastro.2018.08.021.

[27] J.D. Mattingly, W.H. Heiser, and D.T. Pratt. *Aircraft Engine Design*. American Institute of Aeronautics and Astronautics, Inc, 2002. ISBN: 1-56347-538-3.

[28] Unmeel B. Mehta and Jeffrey V. Bowles. “Two-Stage-to-Orbit Spaceplane Concept with Growth Potential”. In: *Journal of Propulsion and Power* 17.6 (2001), pp. 1149–1161. DOI: 10.2514/2.5886. URL: https://doi.org/10.2514/2.5886.

[29] E. Mooij. *The motion of a vehicle in a planetary atmosphere*. Delft University of Technology Faculty of Aerospace Engineering, 1994. ISBN: 90-5623-003-4.

[30] M. Peeters. *A Hybrid Propulsion Concept for the MK-III*. Delft University of Technology, 2023.

[31] N. Relang and et al. “Design of Supersonic and Hybrid engine based Advanced Rocket (SHAR)”. In: *IOP Conference Series: Materials Science and Engineering* 1226 (). DOI: 10.1088/1757-899X/1226/1/012031.

[32] A.F. El-Sayed. *Fundamentals of Aircraft and Rocket Propulsion*. Springer London, 2016. ISBN: 978-1-4471-6796-9. DOI: https://doi.org/10.1007/978-1-4471-6796-9.

[33] M. Snead. “Assessing the practicality of scramjet-powered, single-stage aerospaceplanes”. In: (2008). URL: https://www.thespacereview.com/article/1092/1 (visited on 03/31/2023).

[34] V. Sonneveld. *Aerodynamic Design and Analysis of a Two Stage to Orbit Winged semi-Reusable Launching Vehicle*. University of Technology Delft, 2021.

[35] P. N. Suganthan. “Differential Evolution Algorithm: Recent Advances”. In: *Theory and Practice of Natural Computing*. Berlin, Heidelberg: Springer Berlin Heidelberg, 2012, pp. 30–46. ISBN: 978-3-642-33860-1.

[36] *TECHNOLOGY READINESS LEVEL (TRL)*. 2020. URL: https://sci.esa.int/web/sci-ft/-/50124-technology-readiness-level (visited on 03/30/2023).

[37] *Tudat Space*. 2022. URL: https://docs.tudat.space/en/latest/#.

[38] *Ultimate Load*. URL: https://www.skybrary.aero/articles/ultimate-load (visited on 06/07/2023).

[39] J.M.V. Vandamme. “Assisted-Launch Performance Analysis: Using Trajectory and Vehicle Optimization”. Delft University of Technology, 2012.

[40] J. Vandenkerckhove. “Comparison between ejector-ramjets and turbo-ramjets for T.S.T.O. propulsion”. In: *5th International Aerospace Planes and Hypersonics Technologies Conference*. DOI: 10.2514/6.1993-5095. URL: https://arc.aiaa.org/doi/abs/10.2514/6.1993-5095.

[41] R. Varvill et al. “SABRE TECHNOLOGY DEVELOPMENT: STATUS AND UPDATE”. In: 2019. URL: https://www.eucass.eu/doi/EUCASS2019-0307.pdf.

[42] K.F. Wakker. *FUNDAMENTALS OF ASTRODYNAMICS*. Institutional Repository Library Delft University of Technology Delft - The Netherlands, 2015. ISBN: 978-94-6186-419-2.

[43] R.J. Weber. *Propulsion for hypersonic transport aircraft*. 1965. URL: https://www.icas.org/ICAS_ARCHIVE/ICAS1964/Page%5C%20977%5C%20Weber.pdf.

[44] H.J. Welna and C.E Campbell. *Preliminary Free-jet Performance of XRJ43-MA-3 Ram-jet Engine at a Mach Number of 2.70*. National Advisory Committee for Aeronautics, 1955.

[45] H.J. Welna and D.H. Reilly. *Preliminary Evaluation of Flight-Weight XRJ47-W-5 Ram-jet Engine at a Mach number of 2.75*. National Advisory Committee for Aeronautics, 1955.

[46] H. Wittenberg et al. *Lecture Notes AE4-870A:Rocket Motion*. 2014.

[47] O. Younossi and et al. *Military Jet Engine Acquisition*. 2002. URL: https://www.rand.org/content/dam/rand/pubs/monograph_reports/2005/MR1596.pdf.

A

Analytical hierarchy process

Intensity	Definition	Explanation
1	Equal	Two items contribute equally to the objective
3	Moderate	Experience and judgment slightly favor one item over another
5	Strong	Experience and judgment strongly favor one item over another
7	Very strong	An item is strongly favored and its dominance demonstrated in practice
9	Extreme	The evidence favoring one activity over another is of the highest possible order of affirmation
2,4,6,8	Intermediate values	When compromise is needed

Figure A.1: Subjective scale meaning of numbers as presented by Dutch Space [4].

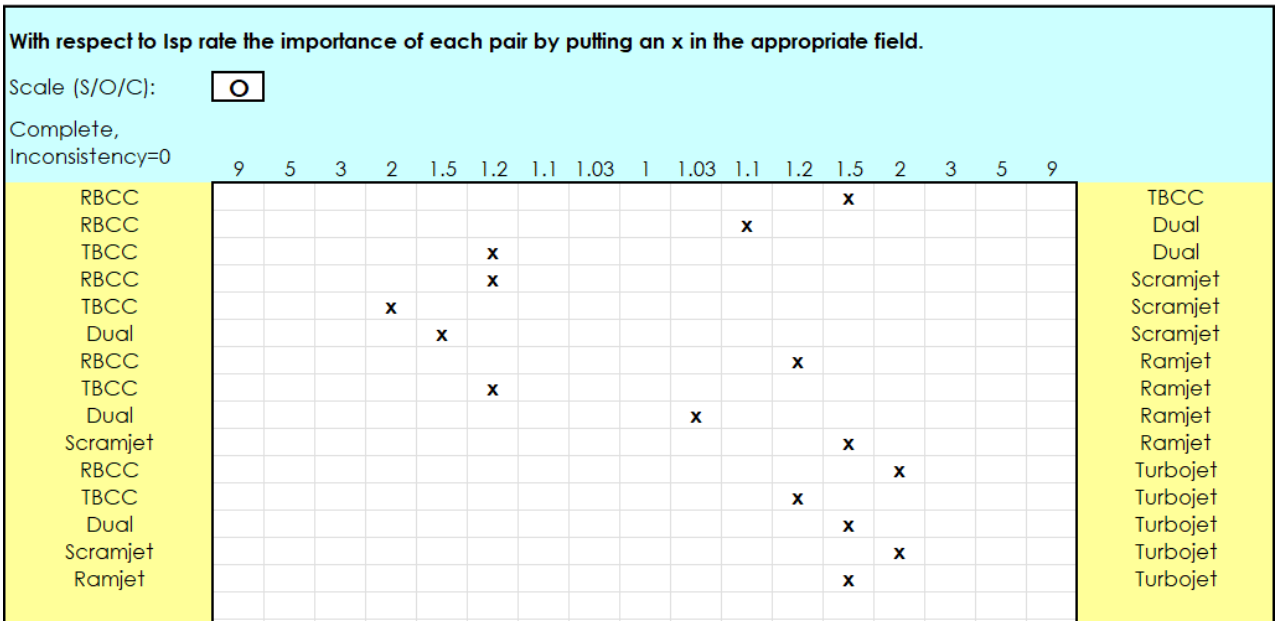

Figure A.2: Screenshot of the concept evaluation with respect to I_{sp}.

With respect to Range rate the importance of each pair by putting an x in the appropriate field.

Scale (S/O/C): O

Complete, Inconsistency=0.00

	9	5	3	2	1.5	1.2	1.1	1.03	1	1.03	1.1	1.2	1.5	2	3	5	9	
RBCC									x									TBCC
RBCC							x											Dual
TBCC							x											Dual
RBCC		x																Scramjet
TBCC		x																Scramjet
Dual		x																Scramjet
RBCC							x											Ramjet
TBCC							x											Ramjet
Dual									x									Ramjet
Scramjet																x		Ramjet
RBCC				x														Turbojet
TBCC				x														Turbojet
Dual				x														Turbojet
Scramjet														x				Turbojet
Ramjet				x														Turbojet

Figure A.3: Screenshot of the concept evaluation with respect to range of operations.

With respect to T/W rate the importance of each pair by putting an x in the appropriate field.

Scale (S/O/C): O

Complete, Inconsistency=0

	9	5	3	2	1.5	1.2	1.1	1.03	1	1.03	1.1	1.2	1.5	2	3	5	9	
RBCC			x															TBCC
RBCC				x														Dual
TBCC													x					Dual
RBCC		x																Scramjet
TBCC					x													Scramjet
Dual				x														Scramjet
RBCC					x													Ramjet
TBCC														x				Ramjet
Dual													x					Ramjet
Scramjet															x			Ramjet
RBCC			x															Turbojet
TBCC												x						Turbojet
Dual					x													Turbojet
Scramjet													x					Turbojet
Ramjet				x														Turbojet

Figure A.4: Screenshot of the concept evaluation with respect to T/W.

Table A.1: Sensitivity analysis with varying weighting criteria

Case 1: TRL 75% less weighting			Case 2: Isp 75% less weighting			Case 3: Range 75% less weighting		
Rank	**Concept**	**Score**	**Rank**	**Concept**	**Score**	**Rank**	**Concept**	**Score**
1	RBCC	0.20	**1**	Ramjet	0.21	**1**	Turbojet	0.20
2	Ramjet	0.20	**2**	TBCC	0.18	**2**	Ramjet	0.20
3	TBCC	0.19	**3**	RBCC	0.18	**3**	TBCC	0.17
4	Dual mode	0.17	**4**	Turbojet	0,18	**4**	RBCC	0.16
5	Turbojet	0.16	**5**	Dual	0.15	**5**	Dual	0.14
6	Scramjet	0.09	**6**	Scramjet	0.12	**6**	Scramjet	0.13
Case 4: T/W 75% less weighting			**Case 5: TRL double weighting**			**Case 6: Isp double weighting**		
Rank	**Concept**	**Score**	**Rank**	**Concept**	**Score**	**Rank**	**Concept**	**Score**
1	Ramjet	0.20	**1**	Ramjet	0.21	**1**	Turbojet	0.20
2	TBCC	0.19	**2**	Turbojet	0.21	**2**	Ramjet	0.19
3	Turbojet	0.19	**3**	TBCC	0.18	**3**	TBCC	0.19
4	RBCC	0.15	**4**	Scramjet	0.16	**4**	RBCC	0.16
5	Dual	0.15	**5**	RBCC	0.13	**5**	Dual	0.15
6	Scramjet	0.12	**6**	Dual-mode	0.12	**6**	Scramjet	0.11
Case 7: Range double weighting			**Case 8: T/W double weighting**			**Case 9: TRL half and Isp twice weighting**		
Rank	**Concept**	**Score**	**Rank**	**Concept**	**Score**	**Rank**	**Concept**	**Score**
1	Ramjet	0.20	**1**	Ramjet	0.20	**1**	Turbojet	0,19
2	TBCC	0.19	**2**	RBCC	0.19	**2**	Ramjet	0.19
3	RBCC	0.18	**3**	Turbojet	0.17	**3**	TBCC	0.19
4	Dual	0.17	**4**	TBCC	0.17	**4**	RBCC	0.17
5	Turbojet	0.16	**5**	Dual	0.15	**5**	Dual	0.16
6	Scramjet	0.10	**6**	Scramjet	0.11	**6**	Scramjet	0.10
Case 10: TRL half and range double weighting			**Case 11: TRL half and T/W double weighting**			**Case 12: Isp half and TRL double weighting**		
Rank	**Concept**	**Score**	**Rank**	**Concept**	**Score**	**Rank**	**Concept**	**Score**
1	Ramjet	0.20	**1**	Ramjet	0.20	**1**	Ramjet	0.21
2	TBCC	0.19	**2**	RBCC	0.20	**2**	Turbojet	0.21
3	RBCC	0.19	**3**	TBCC	0.18	**3**	TBCC	0.18
4	Dual mode	0.17	**4**	Turbojet	0.17	**4**	Scramjet	0.16
5	Turbojet	0.16	**5**	Dual	0.16	**5**	RBCC	0.12
6	Scramjet	0.09	**6**	Scramjet	0.10	**6**	Dual	0.12
Case 13: Isp half and range double weighting			**Case 14: Isp half and T/W double weighting**			**Case 15: Range half and TRL double weighting**		
Rank	**Concept**	**Score**	**Rank**	**Concept**	**Score**	**Rank**	**Concept**	**Score**
1	Ramjet	0.21	**1**	Ramjet	0.21	**1**	Ramjet	0.21
2	TBCC	0.19	**2**	RBCC	0.19	**2**	Turbojet	0.20
3	RBCC	0.18	**3**	TBCC	0.17	**3**	TBCC	0.18
4	Turbojet	0.16	**4**	Turbojet	0.17	**4**	Scramjet	0.15
5	Dual	0.16	**5**	Dual	0.15	**5**	RBCC	0.13
6	Scramjet	0.10	**6**	Scramjet	0.11	**6**	Dual	0.12
Case 16: Range half and Isp double weighting			**Case 17: Range half and T/W double weighting**			**Case 18: T/W half and TRL double weighting**		
Rank	**Concept**	**Score**	**Rank**	**Concept**	**Score**	**Rank**	**Concept**	**Score**
1	Turbojet	0.20	**1**	Ramjet	0.20	**1**	Ramjet	0.21
2	Ramjet	0.19	**2**	Turbojet	0.18	**2**	Turbojet	0,21
3	TBCC	0.18	**3**	RBCC	0.18	**3**	TBCC	0.17
4	RBCC	0.15	**4**	TBCC	0.17	**4**	Scramjet	0.16
5	Dual	0.15	**5**	Dual	0.14	**5**	RBCC	0.13
6	Scramjet	0.12	**6**	Scramjet	0.12	**6**	Dual	0.12
Case 19: T/W half and Isp double weighting			**Case 20: T/W half and range double weighting**					
Rank	**Concept**	**Score**	**Rank**	**Concept**	**Score**			
1	Turbojet	0.20	**1**	Ramjet	0.20			
2	TBCC	0.19	**2**	TBCC	0.20			
3	Ramjet	0.19	**3**	RBCC	0.18			
4	RBCC	0.15	**4**	Dual	0.17			
5	Dual	0.15	**5**	Turbojet	0.16			
6	Scramjet	0.12	**6**	Scramjet	0.10			